D2.1 Good practice criteria for multi-hazard forecasting (including a multidisciplinary calibration) and application limits, as enablers for risk reduction through restoration, exportable to other coasts

12/07/23

WP2

Lead beneficiary: LIM/UPC

Author/s: M. Espino, L. Garrote, D. Santillan, X. S.-Artús, V. Gracia, M. Liste, M. Mestres, M. Grifoll, M. Balsells, J. Staneva, B. Jacob, W. Chei, J. Pein, L. Villa, P. Dissanayake, M. de Vries, I. Federico, S. Causio, O. Boutron, C. Briere, R. Caillibote & A. S-Arcilla

REST-COAST

Large Scale RESToration of COASTal Ecosystems through Rivers to Sea Connectivity

This project receives funding from the European Union's Horizon 2020 research and innovation programme, under Grant Agreement 101037097

Prepared under contract from the European Commission
Grant agreement No. 101037097
EU Horizon 2020 Coordination and Support Action

Project acronym:	**REST-COAST**
Project full title:	**Large Scale RESToration of COASTal Ecosystems through Rivers to Sea Connectivity**
Start of the project:	01.10.2021
Duration:	54 months
Project coordinator:	Prof. Agustín Sánchez-Arcilla, Universitat Politècnica De Catalunya (UPC)
Type:	Restoring biodiversity and ecosystem services
Call:	H2020-LC-GD-2020-3
Deliverable title	Good practice criteria for multi-hazard forecasting (including a multidisciplinary calibration) and application limits, as enablers for risk reduction through restoration, exportable to other coasts
Deliverable n°	D2.1
Nature of the deliverable:	Report
Dissemination level:	Public
WP responsible:	WP2
Lead beneficiary:	LIM/UPC
Citation:	Espino, M., L. Garrote, D. Santillan, X. S.-Artús, V. Gracia, M. Liste, M. Mestres, M. Grifoll, M. Balsells, J. Staneva, B. Jacob, W. Chei, J. Pein, L. Villa, P. Dissanayake, M. de Vries, I. Federico, S. Causio, O. Boutron, C. Briere, R. Caillibote & A. S-Arcilla (2023). *Good practice criteria for multi-hazard forecasting (including a multidisciplinary calibration) and application limits, as enablers for risk reduction through restoration, exportable to other coasts*. Deliverable D2.1. EU Horizon 2020 REST-COAST Project, Grant agreement No 101037097
Due date of deliverable:	Month n°21
Actual submission date:	Month n°21

Deliverable status:

Version	Status	Date	Author(s)
0.0	Template	15 March 2023	Manuel Espino (UPC)
1.0	First Draft	30 June 2023	M. Espino, X. S.-Artús, V. Gracia, M. Liste, M. Mestres, M. Grifoll, M. Balsells, A. S-Arcilla (UPC), L. Garrote, D. Santillan (UPM), J. Staneva, B. Jacob, W. Chei, J. Pein, L. Villa (HZG), P. Dissanayake, M. de Vries (DEL), I. Federico, S. Causio (CMCC), O. Boutron (TDV), C. Briere, R. Caillibote (EGIS)

Table of Contents

Preface

The Rest-Coast Project (Large scale RESToration of COASTal ecosystems through rivers to sea connectivity) is an EU Horizon 2020 research project (Grant agreement No. 101037097) whose overall goal is to address with effective and innovative tools the key challenges faced by coastal ecosystem restoration across Europe. The approach chosen for this project will deliver a highly interdisciplinary contribution, with the demonstration of improved practices and techniques for hands-on ecosystem restoration across several pilot sites, supported by the co-design of innovative governance and financial arrangements, as well as an effective strategy for the dissemination of results.

Summary

REST_COAST/WP2 is introducing ESS into coupled hydro-morpho-eco models with parameterizations for closure submodels and ESS, already suited to work under present and future climate conditions, using data from recent campaigns and from this project. The prepared coupled and nested models enable an objective assessment of impacts and hazards in the simulated domains, considering ESS synergies and tradeoffs within the highly non-linear behaviour of these systems. The delivery of ESS is being assessed under present conditions in terms of proxies that can be used for quick assessments of performance and as a basis for economic and management decisions.

In particular, Task 2.1 has prepared nested domains for downscaling Copernicus forecasts, with 3 domains for most Pilots and sea level rise rates according to the selected scenarios and horizons and including local subsidence, resulting in hazard predictions for RSLR rates up to about 10 mm/yr. Hazard estimates thus consider the increase of sediment transport due to sea level rise as a function of bed sediment composition with mixed mud, fines and coarse sediments depending on the Pilot. The simulations are based on calibrated hydro-morpho-eco models that include interactions to consider the delivery of ESS with/without restoration in hazard propagation. The best models for each Pilot have been selected (in terms of calibration and local expertise/control), featuring structured and unstructured grids (e.g. COAWST + X-Beach for Ebro and Shyfem + WW3 for Venice). These modelling suites form the basis for multi-hazard predictions and the ongoing development of the EWS with ESS, where restoration performance will be assessed with indicators derived from WP1 to WP5 and calculated with WP2 simulations.

The validated modelling suites are being applied to develop EWSs driven by Copernicus products, where the partners have a long-track record of contributions to model/product development. These EWS serve to simulate multi-hazards in the Pilots, with/without ESS and for present and future climatic conditions. The resulting simulations form the basis for an on-going multi-variable error assessment to promote the uptake by stakeholders and to steer adaptation pathways, providing predictions and projections that will substantiate governance transformations (by comparing simulated what if scenarios) and socioeconomic engagement (by making explicit the shared benefits of restored ESS and comparing them to traditional interventions or do-nothing options).

Here we report the work on risk reduction supported by modelling from the Pilots that have started this development, which are the Pliots involved in D2.1 and Task 2.1. In Task 2.2. and D2.2 there will be another two Pilots in this modelling work for multi-hazard assessments and risk reduction. Because of that, Pilots at earlier stages in modelling-based risk assessments, are not reported here, but they are following these

advances to support their work in developing adaptation pathways and governance transformation, as well as advancing in their capabilities to develop an integrated modelling framework.

List of abbreviations

CMCC. Centro Euro-Mediterraneo sui Cambiamenti Climatici

COR. Consorzio coordinamento delle ricerche al Sistema lagunare di Venezia (CORILA)

CORE-PLAT. COastal REstoration PLATform

D. Deliverable

DEL. Deltares

EGIS. EGIS Water and Maritime

ESS. Ecosystem services

EU. European Union

FSK. NLWKN-Forschungsstelle Küste

HZG. Helmholtz-Zentrum Geesthacht

LIM. Laboratori d'Enginyeria Marítima /Univ. Politècnica de Catalunya

Mst. Milestone

NbS. Nature-based Solutions

NN. NetworkNature

T. Task

TDV. Tour du Valat

UPC. Universitat Politècnica de Catalunya

UPM. Universidad Politécnica de Madrid

WP. Work Package

1. General introduction

WP2 is preparing a risk assessment simulation tool for multi-hazard forecasting, based on calibrated hydro-morpho-eco coupled models with ESS parameterised as a function of restoration scale and climatic conditions. The coupled models, calibrated for present conditions and critically analysed for future climates, notably relative sea-level-rise and changes in storminess, are being used to consistently simulate impacts across timescales (from storms to decades), considering the socio-economic data and projections available at the Pilots to co-design limits for alarm levels. Here the partners have agreed on the future scenarios (RCPs 4.5 and 8.5), horizons, and storm return periods (5, 50 and 100 years) to be used, in order to produce comparable analyses (Mst 8). The resulting risk estimations, with explicit error intervals based on in-situ/satellite data, aim to provide:

1. Warnings for present conditions (Task 2.1) and future scenarios (Task 2.2) with model application limits and co-designed thresholds for the dashboard being developed in WP6. This work is the basis of the ongoing work to prepare good practice criteria for multi-hazard forecasting, with application limits (D2.1) for the Pilots.
2. Maps displaying risk levels in space, considering existing infrastructures and ESS to modulate risk propagation (Task 2.3) and suited to incorporate adaptation pathways (WP4) for assessing risk reduction with/without ESS to promote a proactive approach to restoration.
3. Probabilistic characterizations of main drivers and responses in the risk assessment to estimate hazards for single and multi-variable combinations, considering existing knowledge plus conventional/conditional statistics (Task 2.4).

Pilot analyses will enrich the global assessment of risk reduction through wetland restoration, improving the model calibration for the coastal archetypes considered in the Pilots. From the combined results, WP2 will provide simulated data to derive good practice criteria for multi-hazard forecasting, exportable to any coastal site.

REST-COAST modelling encompasses a number of state-of-the-art models already calibrated for the Pilots and which are being further validated within the project. These models comprise unstructured and structured meshes for waves, currents, morphodynamics and nutrient /pollutant dispersion and transport. The bathymetries for the pilots are based on improved combinations of aerial photographs, lidar data and EMODNET bathymetry. The model runs are driven by CMEMS products and include, at different levels depending on the Pilot, some of the ecosystem services considered. The simulation of what-if scenarios has been harmonised for the Pilots and comprise present and future conditions (RCP 8.5 and RCP 4.5 scenarios and storms with commonly agreed 5, 50 and 100 year return periods).

2. Multi-hazard forecasting (including a multidisciplinary calibration) and application limits Ebro Delta Pilot (LIM, UPM)

2.1. Introduction

The Ebro River is the second largest river in the Iberian Peninsula and generates a deltaic system in the southern area of Catalonia, on the Spanish Mediterranean coast, which extends around 25 kilometres offshore and forms two enclosed bays (Fangar to the north and Alfacs to the south). The Ebro valley was a closed basin until its opening to the Mediterranean Sea ca. 5.3 M years ago (transition between the Miocene and Pliocene). During the 20th and 21st centuries there has been a relative stabilization of the deltaic morphology, largely caused by the anthropic hydrological modifications carried out in the basin.

Nowadays we can distinguish three types of sedimentary environments in the Ebro Delta: the deltaic plain, the coastal environments and the marine environments.

- The deltaic plain comprises most of the emerged lands and includes two types of sedimentary environments: river environments and lake and marsh environments. The former are represented by the river channels and the natural specks that surround them (dykes), formed by soils of medium granulometry and for silt. The lacustrine and marshy environments are located in the regular or permanently flooded wetlands.

- Coastal and transitional environments are sedimentary environments with fluvial influence in which there is a more or less intense retreat of sediments by marine agents (waves and storms). These environments are basically represented by the deltaic front, formed by the crescent-shaped sand bars and associated with the deltaic progression. The materials which form them have a fairly homogeneous granulometry, basically sandy. The beaches, the coastal bars and the arrows are holomarine coastal formations, originated from the deltaic river front, which are removed by the sea, or from the erosion of the ancient deltaic lobes.

- Marine environments can be classified into bay, beach and platform environments.

  - The beach environment develops in the bodies of sea water that are confined by the coastal fringe, even though they are connected in accordance with the open sea by the permanent rivers.

  - The prodelta environment is located in coastal submerged environments and constitutes the transition between fluvial-marine and marine sediments. It is mainly made up of terrestrial materials with a significant content of organic matter of terrestrial origin.

  - The continental shelf environment is located in the open sea, at a depth of more than 100 m, and is a relict sedimentary environment, associated with the last post-glacial eustatic descents.

All aquatic ecosystems of the delta are influenced by water coming from rice fields. About 65% of the delta's area is dedicated to rice cultivation. From April to October, a quantity of 45 m3·s-1 of river water is diverted to the irrigation canals for continuous irrigation (Ibàñez et al., 1997). The river water is rich in nutrients (Ibàñez et al., 1995), but farmers add large amounts of fertilizer to enhance rice production, as well as several types of pesticides, mainly during spring and early summer (Ibàñez et al., 1997). Water coming from the rice fields is carried by drainage canals to the sea through the bays.

The Ebro river and deltaic plain are the main focus of UPM, while LIM is working on Coastal and Marine environments, currently focusing on the Trabucador barrier beach (South hemidelta).

2.2. Ebro river and deltaic plain simulation domain

We simulate the erosion process, sediment transport, and sediment deposition in the Ebro Delta pilot case through numerical modeling, using the freely-available two-dimensional (2-D) Iber code (Cea et al. 2007; Bladé et al. 2014), which solves the 2-D hydrodynamic equations coupled to the sediment transport equations, amongst others. In the following sections, we first describe the hydrodynamic equations and the erosion model, followed by a description of the Pilot site in terms of model configuration data (topography, hydrodynamic parameters, and boundary conditions) and, finally, we calibrate the hydrodynamic numerical model with controlled flood observations.

2.2.1. Description of the numerical model for fluvial simulation (Iber)

Iber solves the 2-D Depth-Integrated Shallow-Water Equations (SWE) using a finite volume scheme. This scheme can handle unstructured meshes, irregular topographies, friction losses, and wet-dry fronts (Cea et al. 2007). The 2D SWEs are derived from the Navier–Stokes equations by assuming quasi-hydrostatic flow and incompressibility of water. The 2D mass conservation equation in a Cartesian coordinate system is given by:

$$\frac{\partial h}{\partial t} + \frac{\partial hU_x}{\partial x} + \frac{\partial hU_y}{\partial y} = 0, \tag{1}$$

and the momentum balance equations in conservative form with source terms in a Cartesian coordinate system are:

$$\begin{aligned} &\frac{\partial}{\partial t}(hU_x) + \frac{\partial}{\partial x}\left(hU_x^2 + g\frac{h^2}{2}\right) + \frac{\partial}{\partial y}(hU_xU_y) \\ &\quad = -gh\frac{\partial z_b}{\partial x} + \frac{\tau_{s,x}}{\rho} - \frac{\tau_{b,x}}{\rho} + \frac{\partial}{\partial x}\left(\nu_t h\frac{\partial U_x}{\partial x}\right) + \frac{\partial}{\partial y}\left(\nu_t h\frac{\partial U_x}{\partial y}\right), \end{aligned} \tag{2}$$

and

$$\begin{aligned} &\frac{\partial}{\partial t}(hU_y) + \frac{\partial}{\partial y}\left(hU_y^2 + g\frac{h^2}{2}\right) + \frac{\partial}{\partial x}(hU_yU_x) \\ &\quad = -gh\frac{\partial z_b}{\partial y} + \frac{\tau_{s,y}}{\rho} - \frac{\tau_{b,y}}{\rho} + \frac{\partial}{\partial x}\left(\nu_t h\frac{\partial U_y}{\partial x}\right) + \frac{\partial}{\partial y}\left(\nu_t h\frac{\partial U_y}{\partial y}\right). \end{aligned} \tag{3}$$

In the previous equations, h is the water depth, U_i is the depth average velocity along the i direction, ρ is the density of the water, z_b is the channel-bottom height, g is the acceleration of gravity, $\tau_{b,i}$ is the bed friction along the i direction, $\tau_{s,i}$ is the free-water surface friction along the i direction (i.e., wind traction), and ν_t is the turbulent eddy viscosity. In the following simulations, we neglect molecular and eddy viscosities, wind traction, as well as Coriolis acceleration. The bed friction terms, $\tau_{b,i}$, read:

$$\tau_{b,i} = \rho g h\frac{n^2U_i^2}{h^{4/3}} \tag{4}$$

where i = x, y, and n is the Manning coefficient.

The Iber erosion and sediment transport module solves the non-cohesive sediment transport equations with uniform granulometries, in a non-stationary regime. The hydrodynamics, sediment transport processes, and river morphology interplay in mobile-bed simulations. Iber software couples these three processes. Iber simulates sediment transport as bedload and suspended load.

The sediment transport process is simulated through the 2D Exner equation (Anderson 2002; Mudd & Furbish 2004; Paola & Voller 2005). The equation provides the bed elevation evolution in response to the erosion and sedimentation and is given in the form of bedload and suspended load:

$$(1-\phi)\frac{\partial z_b}{\partial t}+\frac{\partial q_{b,x}}{\partial x}+\frac{\partial q_{b,y}}{\partial y}+(E-D)=0, \tag{5}$$

where ϕ is the porosity, $q_{b,i}$ is the bedload discharge along the i direction, E is the entrainment deposition term of suspended sediment on the bed, and D is the deposition term of suspended sediment on the bed.

We simulate the bedload solid flow rate due to the bedload transport using the van Rijn equation (Van Rijn 1984a), as it provides satisfactory results compared with laboratory experiments (Santillan et al. 2020). The equation reads:

$$q_b^*=\frac{0.053}{D^{*0.3}}\left(\frac{\tau^*}{\tau_{crit}^*}-1\right)^{2.1}, \tag{6}$$

where q_b^* is the dimensionless bedload solid volumetric flow rate, D^* is the dimensionless diameter of solid particles, τ^* is the dimensionless shear stress acting on the particles, and τ_{crit}^* is the dimensionless critical shear stress. The dimensionless bedload solid volumetric flow rate, q_b^*, is:

$$q_b^*=\frac{q_b}{\sqrt{(s-1)gD^3}}, \tag{7}$$

where q_b is the bedload solid volumetric flow rate, s is the ratio between the densities of the particles and water, $s=\rho_S/\rho$, and D is the characteristic diameter of sediments, usually taken as the median diameter $D=D_{50}$.

The dimensionless diameter of solid particles is given by:

$$D^*=D\left(\frac{g(s-1)}{\nu^2}\right)^{1/3}, \tag{8}$$

being ν the kinematic viscosity of water, and the dimensionless shear stress is:

$$\tau^*=\frac{\tau_b}{\rho(s-1)gD}, \tag{9}$$

being τ_b the bed friction shear stress, given by Eq. (4).

The dimensionless critical shear stress τ_{crit}^* is given by the Soulsby-Whitehouse equation (Soulsby & Whitehouse 1997), based on the experiments of Shield (1936). It is given by:

$$\tau_{crit}^*=\frac{0.3}{1+1.2D^*}+0.055\left(1-e^{-0.02D^*}\right). \tag{10}$$

Iber simulates the suspended sediment transport with the depth-averaged convection-diffusion equation for the sediment concentration. The model accounts for the turbulent diffusion and the equilibrium suspended concentration, and is given by:

$$\frac{\partial hC}{\partial t}+\frac{\partial hU_xC}{\partial x}+\frac{\partial hU_yC}{\partial y}=\frac{\partial}{\partial x}\left(\left(\Gamma+\frac{\nu_t}{S_c}\right)h\frac{\partial C}{\partial x}\right)+\frac{\partial}{\partial y}\left(\left(\Gamma+\frac{\nu_t}{S_c}\right)h\frac{\partial C}{\partial y}\right)+\frac{\partial D_{s,x}}{\partial x}+\frac{\partial D_{s,y}}{\partial y}+(E-D), \tag{11}$$

where C is the depth-averaged concentration of suspended solids, Γ is the molecular diffusion coefficient for suspended solids, S_c is the Schmidt number, which relates the moment turbulent diffusion coefficient with the suspended turbulent diffusion coefficient, and $D_{s,i}$ is the suspended sediment dispersion along the i direction due to the non-homogeneous vertical velocity profile and sediment concentration.

The Entrainment/Deposition term, $(E-D)$, models the bedload grains that become suspended (entrainment) and deposited from suspended sediments to the bed layer. We simulate the Entrainment/Deposition term with the Van Rijn formula (van Rijn, 1987), given by:

$$E-D=\alpha\omega_s(C^*-C), \tag{12}$$

where α is a coefficient that relates the mean suspended particle concentration and the river bedload concentration, ω_s is the fall velocity of the suspended sediments, C^* is the depth-averaged suspended load concentration at equilibrium conditions, and C is the depth-averaged suspended load concentration.

The fall velocity of the suspended sediments for sand particles is computed using Van Rijn (1984b) recommendations. For particles smaller than about 0.1 mm, ω_s is given by

$$\omega_s = \frac{(s-1)gD_{50}^2}{18\nu}, \tag{13}$$

for suspended sand particles in the range 0.1 to 1 mm, the fall velocity is:

$$\omega_s = 10\frac{\nu}{D_{50}}\left\{\left(1+\frac{0.01(s-1)gD_{50}^3}{\nu^2}\right)^{0.5}-1\right\}, \tag{14}$$

and for particles larger than 1 mm, the following equation is used:

$$\omega_s = 1.1[(s-1)gD_{50}]^{0.5}. \tag{15}$$

The depth-averaged suspended load concentration at equilibrium conditions, C^*, reads (Van Rijn 1984b):

$$C^* = \frac{1}{\alpha}0.005\frac{T^{1.5}}{{D^*}^{0.3}}, \tag{16}$$

where T is the transport stage parameter given by:

$$T = \frac{(U^*)^2-(U^*_{crit})^2}{\left(U^*_{crit}\right)^2}, \tag{17}$$

in which U^*_{crit} is the critical bed-shear velocity, that according to Shields (1936) is:

$$U^*_{crit} = \sqrt{\frac{\tau^*_{crit}}{\rho}}, \tag{18}$$

and bed-shear velocity, U^*, reads (Van Rijn 1984b):

$$U^* = \frac{\sqrt{g}}{C'}\overline{U}, \tag{19}$$

in which $C' = 18\log(12R_b/3D_{90})$ is the Chézy-coefficient related to grains, R_b is the hydraulic radius related to the bed according to Vanoni-Brooks (1957), and $\overline{U}$ is the mean flow velocity.

The system of Partial Differential Equations are solved using a first-order finite volume scheme based on the Monotonic Upwind Scheme for Conservation Laws (Van Leer 1979).

2.2.2. Description of model configuration data: topography, hydrodynamic parameters, boundary conditions

The Ebro River is strongly regulated with dams, of which the Mequinenza-Ribarroja-Flix reservoir system retains a large part of the sediment flow in the Ebro River (Figure 2.2.1). Therefore, this reservoir system must be included in the numerical domain to model the sediment transport to the Delta site. The modelling objectives are: (1) to study the alternatives to restore, at least in part, the sediment flow, (2) to estimate the quantity of sediments that can be mobilized, (3) to determine how long the sediments would take to research the Delta site, and (4) to know how the sediment would be delivered to the Delta system.

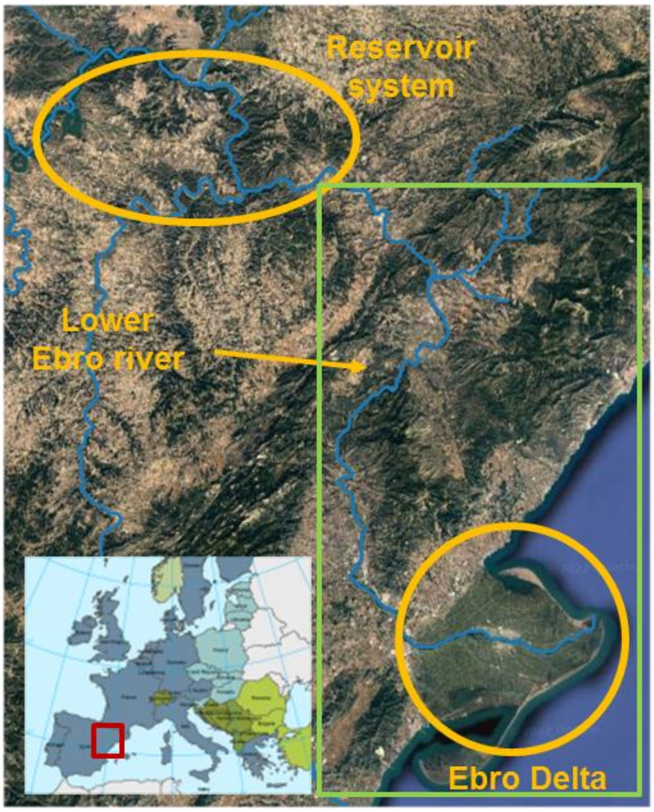

Figure 2.2.1: Ebro Delta pilot site

The topography of the simulated stretch is depicted in Figure 2.2.1. The fluid flow and sediment transport from the Flix reservoir, located about 100 km from the river mouth and 41.1 meters above the mean sea level, up to the Delta site, was simulated. This dam is the last barrage in the Ebro River.

A Triangulated Irregular Network (TIN) model of the river with 0.4-meter tolerance, maximum side of 300 meters, and minimum side of 15 m was generated using a 1 m-resolution Digital Terrain Model (DTM) of the Ebro basin provided by the Spanish National System for Flood Risk. This TIN includes 100 km of the Ebro River topography and is composed of about 2,489,643 triangles (Figure 2.2.2, left). Figure 2.2.2, right shows two snapshots of the topography. The TIN was used to generate a coincident unstructured mesh composed of about 2,489,643 triangular elements, in which each triangle of the TIN model is a finite volume in the numerical model.

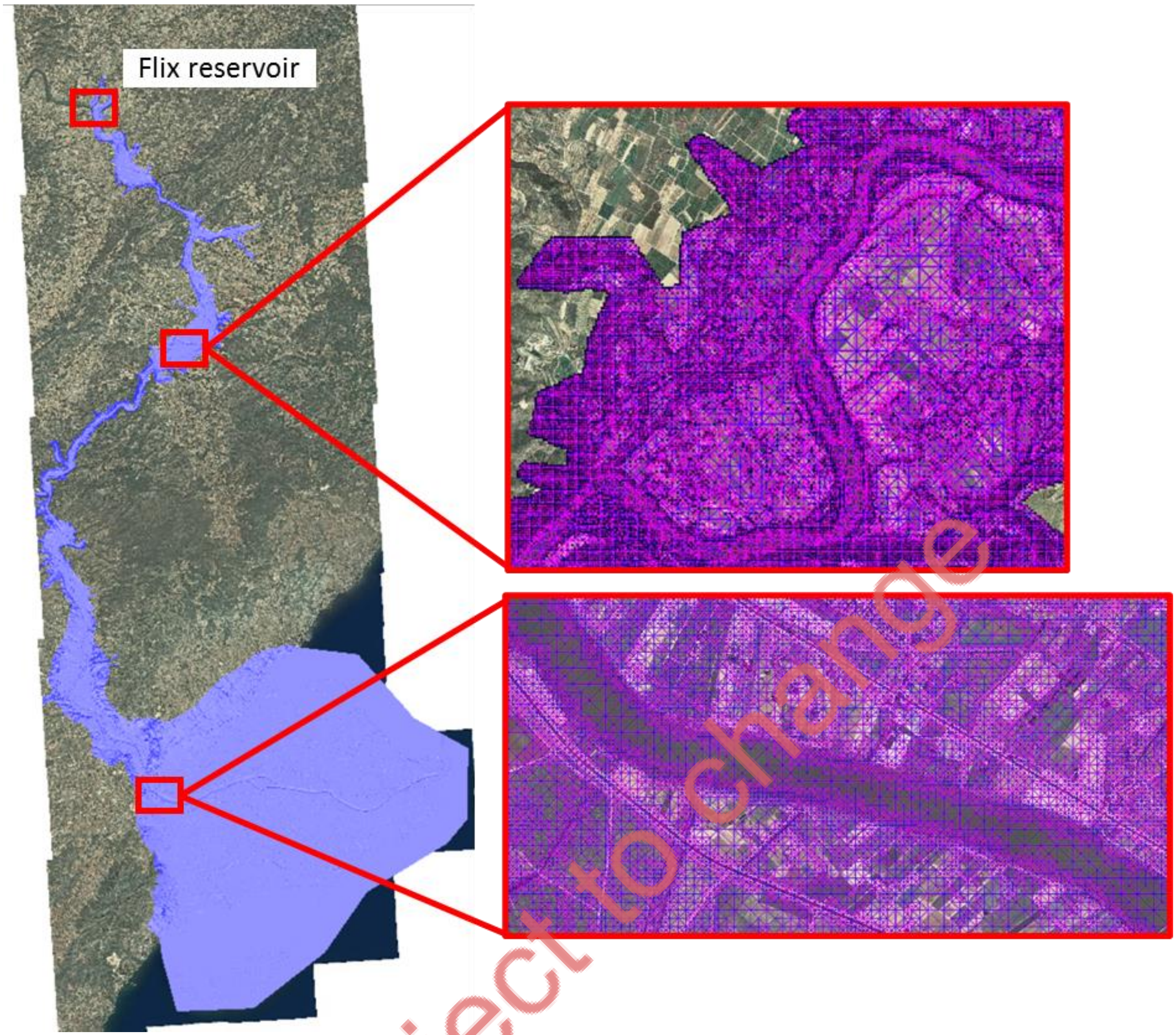

Figure 2.2.2: Domain of the numerical simulations in the Ebro Delta pilot site

The boundary hydrodynamics conditions of the numerical model are (1) imposed flow rate in Flix in subcritical regime, and (2) outlet boundary condition in critical regime imposed on the sea.

2.2.3.Hydrodynamic calibration of the model with controlled flood observations

The rugosity of the model, given by Manning's coefficient, has been calibrated with the observed flood event on May 5th, 2022. This event also allows testing the performance of the hydrodynamic module. The Ebro Automatic Hydrological Information System (SAIH) provides 30-minute flow rate observations at two points of the river: Ascó and Tortosa -see Figure 3 (a). Moreover, during the flood event, 180 m^3/s were abstracted from the river in Xerta through an irrigation channel. The observed flow rate in Ascó and Tortosa gauge stations are plotted in Figure 2.2.3 (b) and Figure 3 (c), respectively.

(a) Location of Ascó and Tortosa flow-rate gauge stations

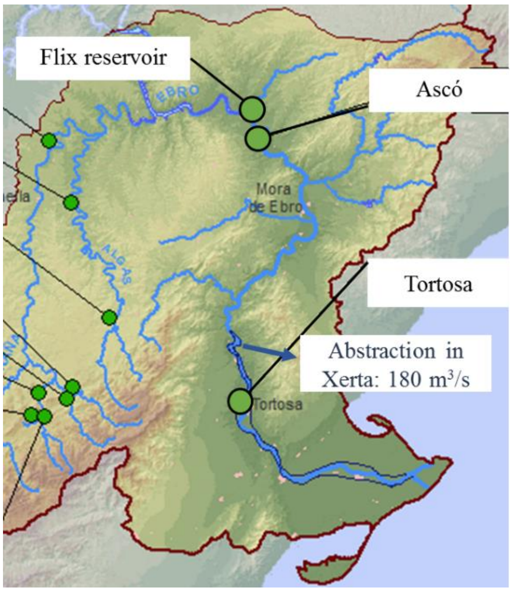

(b) Observed flow rate in Ascó flow-rate gauge station

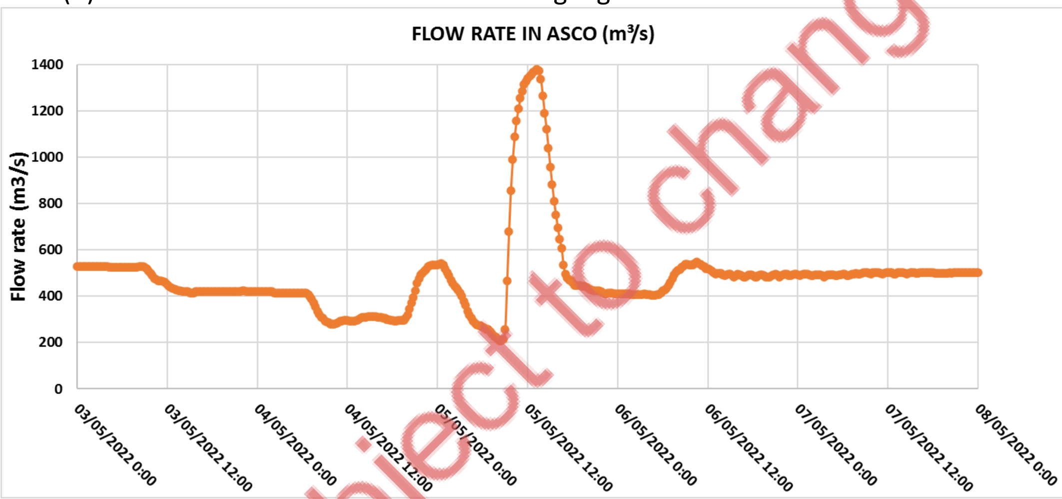

(c) Observed flow rate in Tortosa flow-rate gauge station

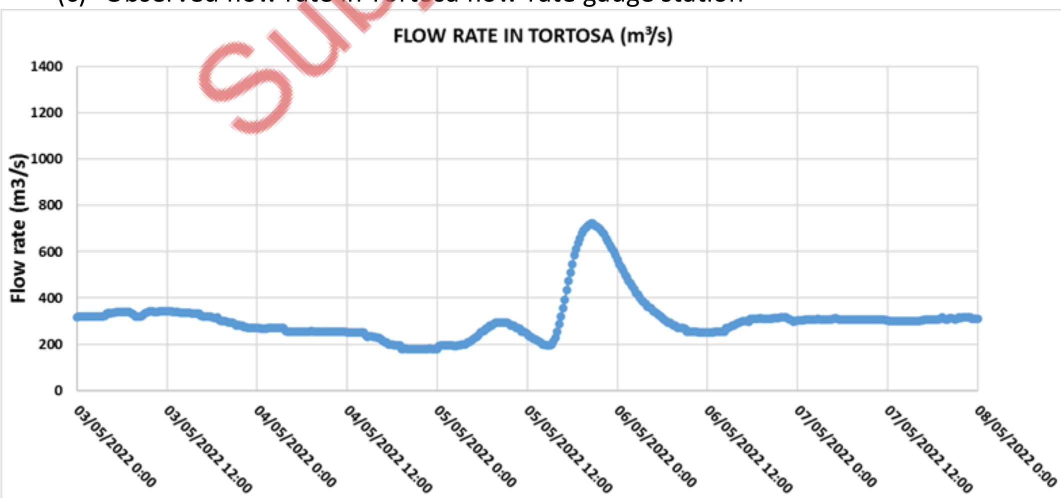

Figure 2.2.3: River Ebro flow-rates at the Ascó and Tortosa gauge stations.

The boundary conditions of the numerical model are, thus, (1) imposed flow rate in Ascó in subcritical regime given by the observed data plotted in Figure 3 (b), and (2) outlet boundary condition in critical regime imposed on the sea. Several numerical simulations were run with different values of Manning's coefficient, and the modelled flow rate in Tortosa was compared to the measured rates. The best agreement between the simulated and the observed flow rates were obtained with a Manning's coefficient of 0.027. The results are depicted in Figure 2.2.4. The model can capture the flood-wave propagation along the river in terms of time and flood peak downstream of the inlet. Figure 2.2.5 shows the river's water depth at 5:30 p.m. on 5th May 2022.

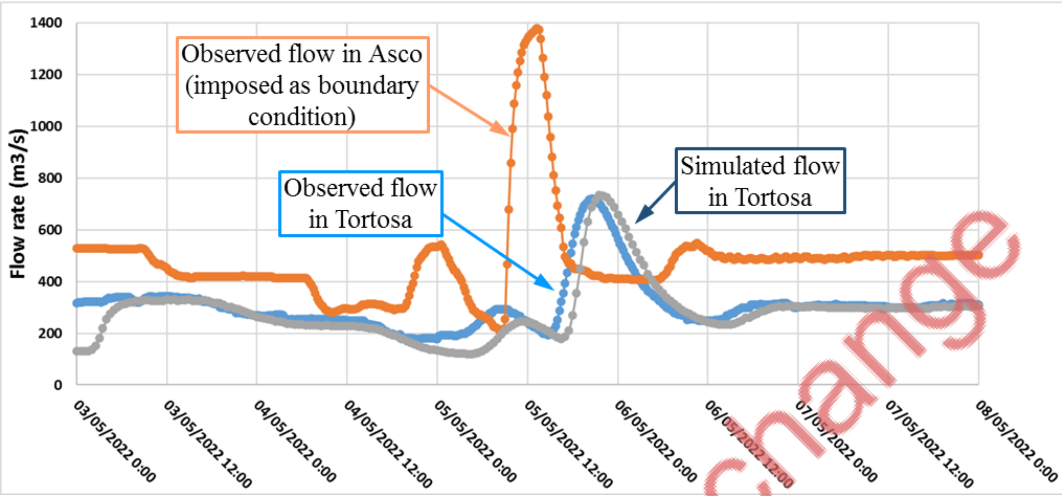

Figure 2.2.4: Observed and simulated flow rate in Tortosa.

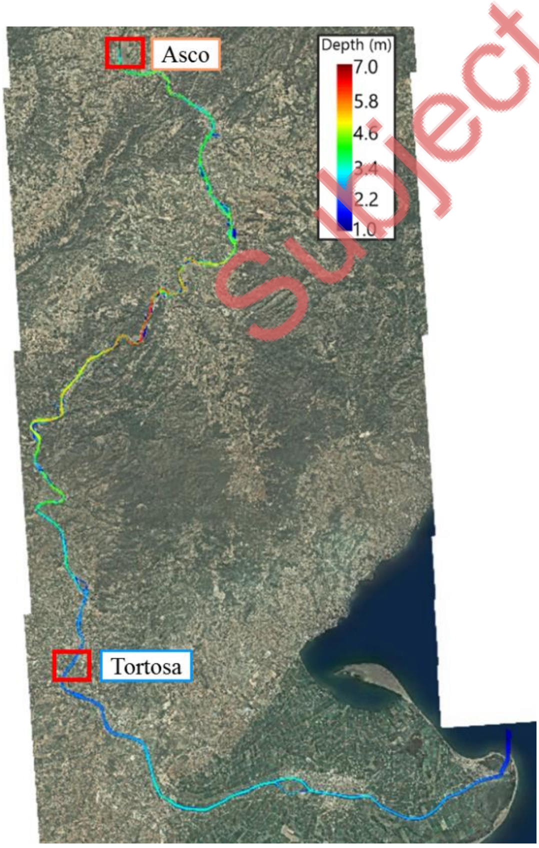

Figure 2.2.5: Water depth at 5:30 p.m. on 5th May 2022.

2.2.4. Approach to the characterization of sediment transport (based on historical observations)

Ibañez et al. (1996) studied the changes in the hydrological and sediment transport produced by large dams on the lower Ebro River and its estuary. They provided estimates of annual suspended sediment transport for several mean river flows, based on the data obtained from Gorria's experiments (Gorria, 1877), and listed in Table 2.2.6. Two flow regimes were adopted, i.e., the mean water flow, with high frequency over the hydrological year, and the annual flood regime, with low frequency over the hydrological year.

Table 2.2.6: Annual suspended sediment transport from Gorria's data (Gorria, 1877) and Ibañez et al. (1996)

Flow regime	Mean flow (m^3/s)	Frecuency (days/year)	Concentration of suspended sediment (g/l)
Mean water	710	256	0.9
Annual flood	1764	11	7.2

The performance of the model was assessed by simulating both flow regimes, and evaluating whether the code can reproduce the data in Table 2.2.6. In the following section, the parameters of the sediment transport model are included, the concentration of suspended sediments at several time steps are presented, and the performance of our model is analyzed.

2.2.5. Numerical analysis of sediment transport

Two numerical simulations are performed for both flow regimes included in Table 2.2.6, modelling the river-flow hydrodynamics and the suspended sediment transport for each one. The hydraulic boundary conditions of the model are (1) imposed constant flow rate at the outlet of Flix reservoir in subcritical regime given by the data in Table 2.2.6, and (2) outlet boundary condition in critical regime imposed at the sea. Moreover, water at the inlet has a suspended sediment concentration given by the data in Table 2.2.6. These numerical simulations are aimed at analyzing whether or not the Ebro River can transport those sediment concentrations down to the Ebro Delta.

The sediment used is characterized by a relative density of 2.65, a friction angle of 30 degrees, a median diameter of 0.0001 mm –clay–, a suspended sediment dispersion of 0.001 m^2/s, and a Schmidt number of 1.1.

The first simulation considered the mean water flow regime, starting from an initially dry river (i.e., water depth is 0), into which water was introduced through the inlet at the Flix reservoir. The flow at the inlet was 710 m^3/s and the concentration of sediments was 0.9 g/l. The flow propagated through the river until a steady-state regime was reached.

Figure 2.2.7 depicts the suspended sediment concentration at three different times. After 2 hours –Figure 2.2.7(b)– the flow had advanced 11 km and reached Ascó. The concentration of suspended sediments was 0.9 g/l along the whole stretch of Ebro River. After 12 hours, the flow was close to Xerta –Figure 2.2.7(b)–, and the concentration of suspended sediments was still 0.9 g/l along the whole stretch. The sediment deposition at this time step was zero (not shown), which means the flow can transport the given sediment concentration along the river.

The steady-state regime is shown in Figure 2.2.7(c). The concentration of suspended sediments is constant at 0.9 g/l, and the sediment deposition is zero. Under these simulated conditions, The flow can transport that sediment concentration from Flix reservoir to the Delta without deposition.

(c)

Figure 2.2.7: Suspended sediment concentration for the mean water regime given in Table I. Flow water is 710 m^3/s and suspended sediment concentration at the inlet is 0.9 g/l. We depict the contour plots of the concentration of suspended sediment after 2 hours in Figure (2), after 12 hours in (b), and under the steady-state regime in (c).

The annual flood conditions –Table 2.2.6– were also simulated, following the same procedure as in the previous case. Now, the flow at the inlet was 1760 m^3/s and the sediments concentration was 7.2 g/l. The flow propagated through the river until a stationary state was reached after several time-steps. Figure 2.2.8 depicts the suspended sediment concertation at three different times.

After 2 hours –Figure 2.2.8(b)– the flow had advanced further than during the mean flow regime. The concentration of suspended sediments was 7.2 g/l along the whole stretch of Ebro River, and the deposition was zero (not shown). After 12 hours, the flow was close to Tortosa –Figure 2.2.8(b)–, and the concentration of suspended sediments was still 7.2 g/l along the whole stretch. Finally, Figure 2.2.8(c) shows the steady-state regime. The concentration of suspended sediments was constant at 7.2 g/l, and sediments did not deposit along the river, except in some areas of the Delta (not shown). The river can transport the given sediment concentration to the Delta during the annual flood with the given concentration.

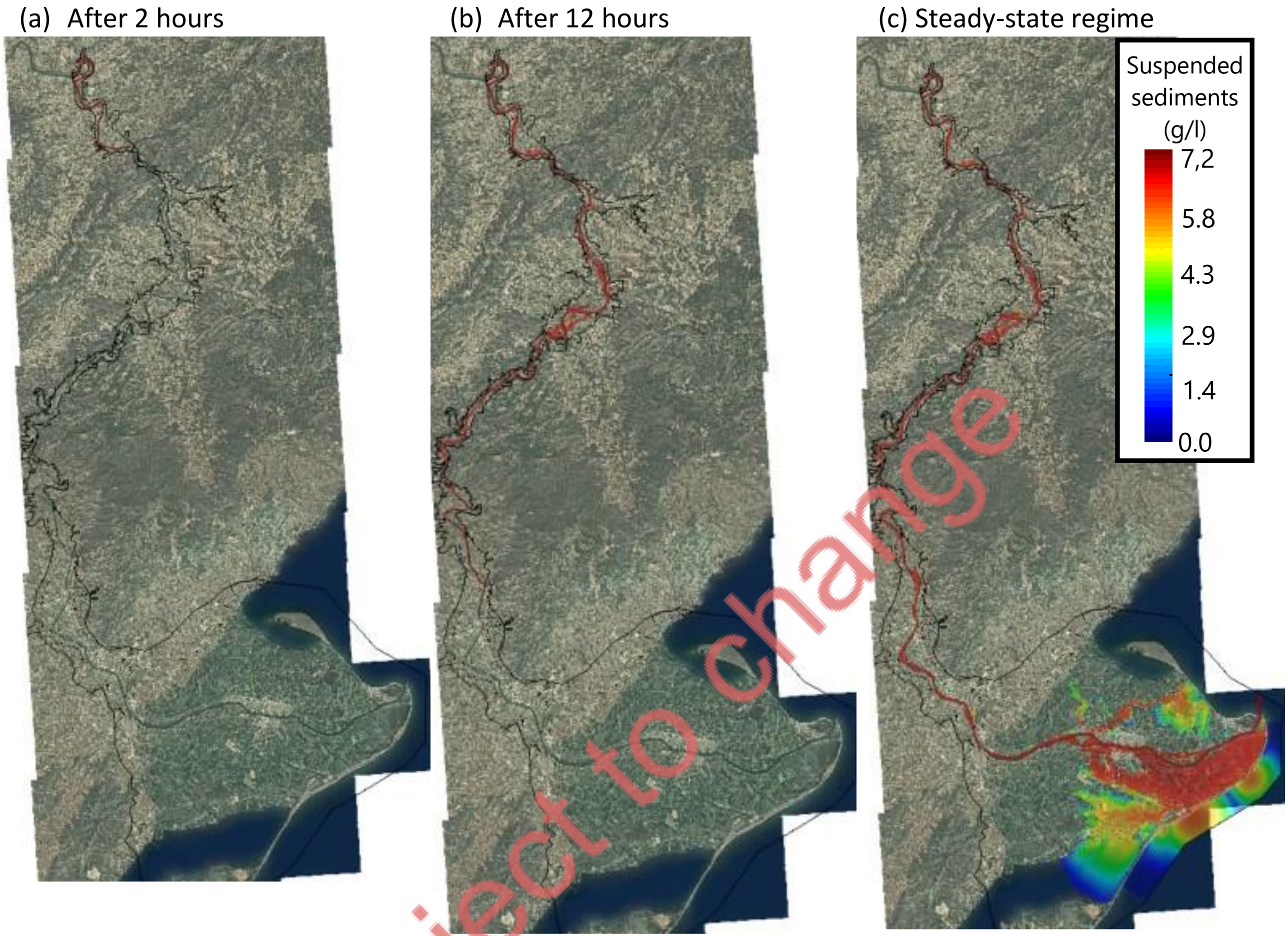

Figure 2.2.8: Suspended sediment concentration for the mean water regime given in Table I. Flow water is 1760 m^3/s and suspended sediment concentration at the inlet is 7.2 g/l. We depict the contour plots of the concentration of suspended sediment after 2 hours in Figure (2), after 12 hours in (b), and under the steady-state regime in (c).

2.2.6. Simulation of realistic scenarios of sediment transport under current water management strategy

The scenarios of sediment transport analyzed in section 2.2.5 are not realistic, because they assume constant discharge over a sufficiently long period of time to achieve steady state. In practice, flows vary according to the natural water availability and management strategy.

To evaluate sediment transport under current water management strategy, flow and turbidity data were compiled from the available measuring stations in the lower Ebro River. Flow data were compared with turbidity data in the sites where data are available for both variables, which are the stations of Ascó and Tortosa. The availability of turbidity data is very low. The series show numerous gaps and the years without failure are exceptional. The Ascó series includes data since 1996, but Tortosa only began measuring in 2011. Therefore, the periods of overlap of flow and turbidity data are intermittent and do not allow continuous analysis. For these reasons, the available data is analyzed globally, regardless of the date to which they correspond.

Figure 2.2.9 presents the relationship between flow (in m^3/s) and turbidity (in NTU units) at the two analyzed stations. The graphs on the left present the relationships in natural values and those on the right on a logarithmic scale. A linear fit line has been added in both cases. It can be seen that there is a certain tendency to increase turbidity when the flow rate is increased, but there is a great dispersion in the data and the trends are not clear. The R^2 coefficients of the correlations are very low, indicating that a linear relationship between the NTU and Q variables cannot be established. The station where the relationship is most evident is Tortosa on a logarithmic scale, although the law between variables is not linear, but seems to correspond to a logistic function. The Ascó station shows a similar trend, although the greater abundance of data produces a much greater dispersion.

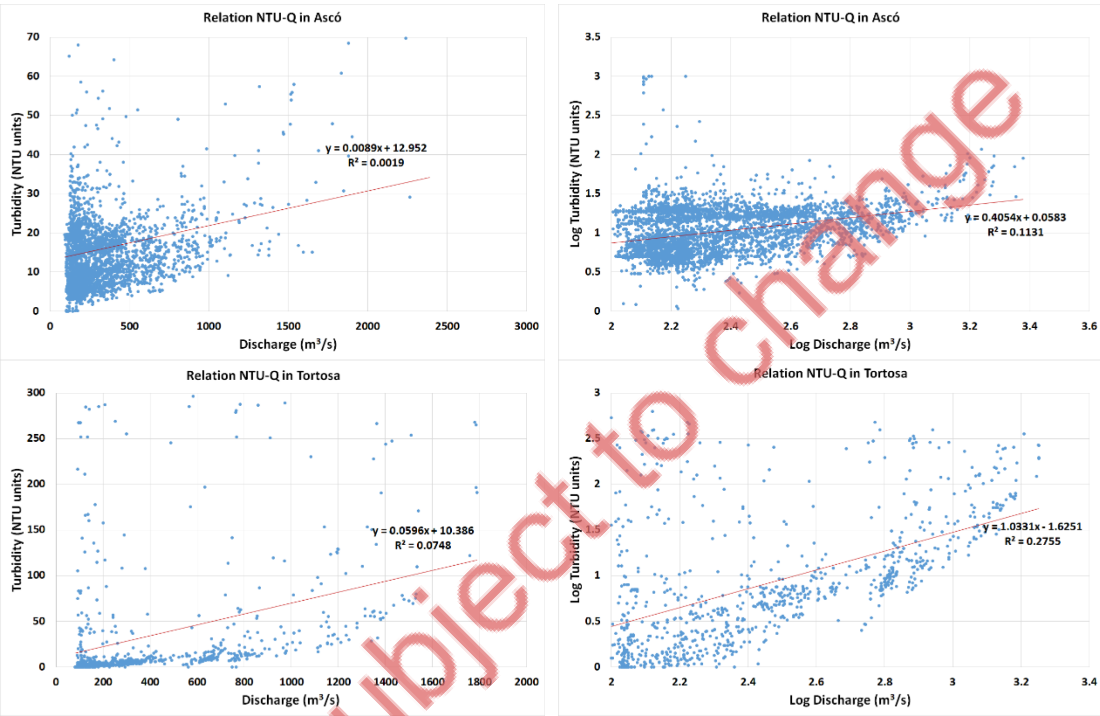

Figure 2.2.9: Relationship between flow and turbidity for the stations of Ascó (top) and Tortosa (bottom). The graphs on the left are in natural scale and those on the right are in a logarithmic scale.

The data compiled will be used to perform simulations of realistic scenarios of sediment transport under current management strategies. These data are conditioned by the fact that there is no sediment source for transport, although the influence of this factor can be explored with the help of numerical simulations.

2.3. Coastal and Marine environments of the Ebro delta simulations

The Ebro Delta coast is highly vulnerable against high-energetic events as well as to the rising MWL, specially in the Trabucador barrier beach that links the mainland with the southern arrow. The necessity to maintain this environment due to its value has led UPC to focus efforts in the implementation of ESS to reduce the suffered impacts.

To test the viability of such approaches,the COAWST and XBeach models are used to simulate the best hydrodynamic conditions and the most accurate response of the coast to these extreme events. Following the literature, together with the expertise and conclusions extracted from the field, the implementation of dunes is selected in the area as the most optimal ESS.

2.3.1.High-resolution coupled coastal models

To reach the proposed objectives, the framework synthesized in Figure 2.3.1 is developed. The final goal is to use this methodology in operational mode to create an EWS able to alert of possible hazards during storm events. First, meteorological and oceanographic forcings from CMEMS forecast products are gathered and processed to feed COAWST, which is a combination of SWAN + ROMS models. The obtained results serve as inputs for the XBeach model that is capable of reproducing the effect of flooding and erosion in the study area with high-resolution. The nesting is done through the passing of the COAWST-modelled wave spectra at several points along the open boundaries of the Xbeach domain. Routines are prepared to ease the transition from pre-operational to operational phases when required. Some tests have been made to check the viability of the operational approach, in which XBeach directly takes data daily from CMEMS and computes the flooded area for a three-day forecast period. Once the validation and calibration of the COAWST model for the Ebro Delta as well as the nesting with XBeach are completed, COAWST will be included in the operational chain to fill the presented framework.

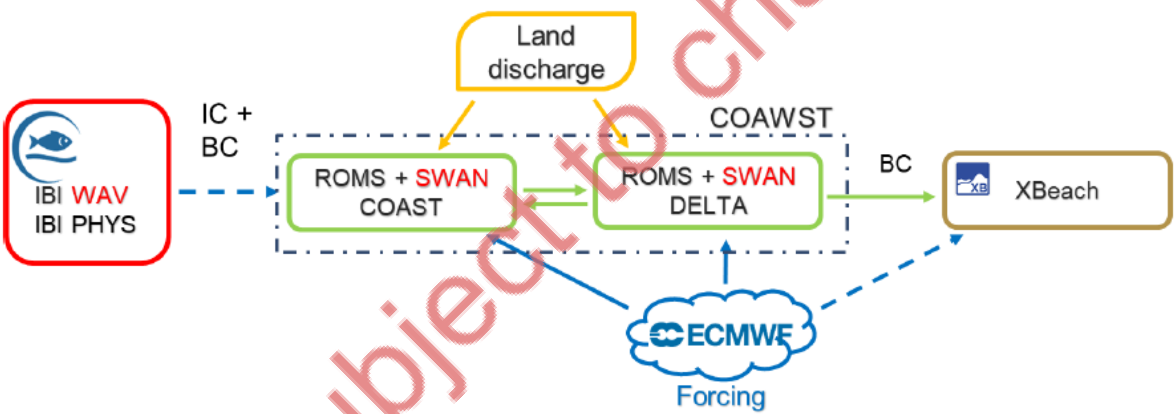

Figure 2.3.1: Framework strategy.

To evaluate the efficiency of the dune implementation in the Trabucador barrier beach, only XBeach has been used due to computational constrains, since both the calibration and validation of the model need a huge number of runs. Meanwhile, parallel validations of COAWST are being performed. When both models have been assessed individually, they will be combined to work together to provide an improvement of the results presented separately.

The computational grid of the COAWST model covers the Ebro Shelf with a horizontal resolution of 350m, which finally produces a 160x150 cells mesh at the area where XBeach is run. The vertical discretization has 8 sigma levels, which resolve both surface and bottom boundary layers over the continental shelf. The XBeach grid is focused on the Trabucador barrier beach reaching a resolution of 5x10m, with higher resolution in the cross-shore direction (Figure 2.3.2). As it is, the model is able to simulate 1 day in approximately 5 hours, although this configuration, used for the ESS viability test, will be changed to a coarser resolution mesh when running in operational mode, reducing the simulation time to adapt to operationality needs.

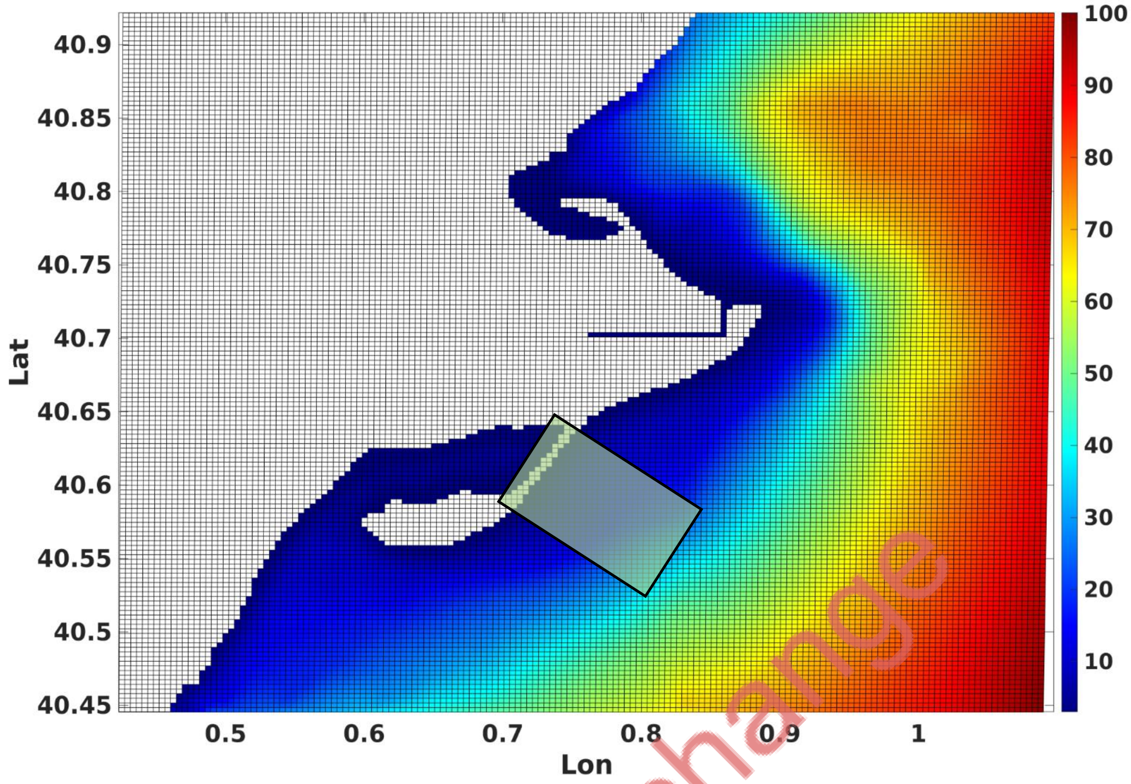

Figure 2.1.2: COAWST and XBeach grids location. The green rectangle represent the area of the XBeach mesh inside the COAWST mesh.

2.3.2.Parameterization of hydro-morpho-eco interactions to simulate ESS.

The Ebro Delta pilot site, specially the Trabucador barrier, frequently suffers breaching events during storms. The barrier connects the mainland with salt pans, and its breaching leads to productivity and economic losses due to the inability of the trucks to reach the pans. Besides, mostly during summer, the beach is used for recreational use. These factors ensure a dependency of the local economy on the correct preservation of the barrier. An improvement of the stability of the barrier during extreme events is thought to be reached through the incorporation of embrionary dunes.

The first necessity was to built the most realistic grid with the available data. The barrier's topobathymetry has been changing for years due to the sedimentary transport caused by wind, currents and waves. In order to use the most accurate mesh corresponding to the selected time scenarios, UPC used the best available sources. The bathymetry was generated with a digitization of the Navionics nautical chart using GIS sofware, combined with the existing topographies created by merging DTMs provided by the ICGC (Institut Cartogràfic i Geològic de Catalunya) and LiDAR data from 2021 done by Costas de Tarragona. The final grid, Figure 2.3.3, was done by coalescing both the bathymetry and the topography, checking for any incompatibilies and comparing the result with orthophotos to verify its correct fittin with reality.

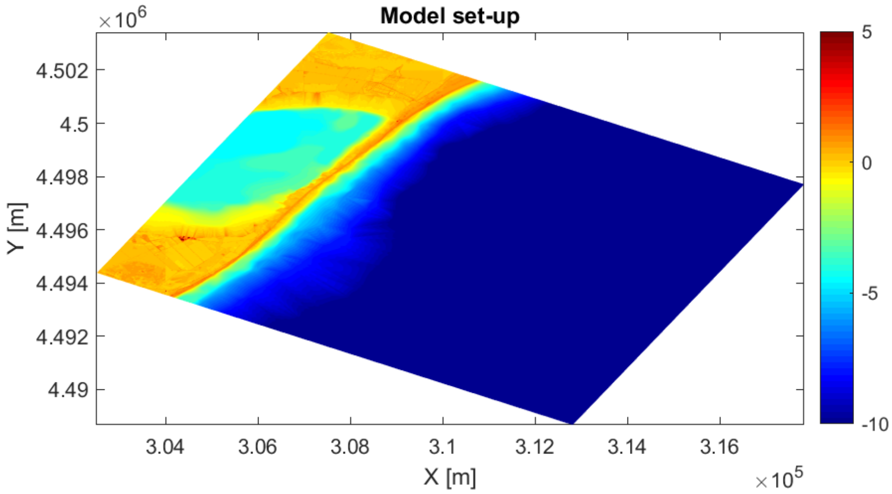

Figure 2.2.3: XBeach mesh.

In addition, during the beginning of 2023, the UPC was involved in a real test in which embrionary dunes were created on the Trabucador beach. These dunes were characterised on a DTM which was used to create a new grid to simulate events with the ESS strategy (Figure 2.3.4). During the time when the dunes were generated, storm Isaak hit the Trabucador beach (specifically on the first half of February 2023). The expertise of the UPC team, that saw the effects of the storm on the barrier and the level of mitigation provided by the dunes, jointly with drone flights allowed to see the resistance of the barrier to breaching. The gathered information helped to correctly characterise the event and validate both the XBeach model and the ESS mitigation strategy. In this case, the forcing wave data were taken from the "Puertos del Estado" observational network, but in the future they will be provided by the CMEMS + COAWST framework presented before to see that the strategy provides similar results.

Figure 2.3.4: Left: Alternate embrionary dunes placed on the Trabucador barrier beach. Right: DTM obtained previously to the Isaak storm event with the dunes placement.

2.3.3.Target operational period for testing the EWS nested into CMEMS products

Testing was done using two storms for calibration and validation. Since the LiDAR data used to generate the first topobathymetry was close in time to the Filomena storm, this event was the first one selected for the XBeach simulations. The storm, one of the most important meteo-oceanic events in Catalonia in the past years, hit the study area from 7th January to 12th January 2021, causing significant wave heights of up to 5 m of in some areas, being. The second storm, selected as a validation scenario and to test the linking between COAWST and XBeach, was Gloria. This was the most intense storm recorded in the last decades in Catalonia, from 18th January to 24th January 2020. Ortophotos show that this event completely breached the Trabucador barrierm so it is a good indicator of the maximum type of storm this beach is going to face.

Regarding the COAWST inputs, the open boundaries of the Ebro Delta Shelf ROMS domain were forced by a Mediterranean-scale circulation model (Med MFC) with a horizontal grid resolution of 1/24˚ (ca. 4-5 km) and 141 unevenly spaced vertical levels (Escudier et al., 2021). The Med MFC physical multiyear product (MEDSEA_MULTIYEAR_PHY_006_004) is generated by a numerical system composed of a hydrodynamic model, supplied by the Nucleus for European Modelling of the Ocean (NEMO) and a variational data assimilation scheme (OceanVAR) for temperature and salinity vertical profiles and satellite Sea Level Anomaly along track data. The SWAN open boundary conditions were provided by the MEDSEA_ANALYSISFORECAST_WAV_006_017 wave product of the Mediterranean Sea Forecasting system, composed by hourly wave parameters at 1/24˚ horizontal resolution covering the Mediterranean Sea and extending up to 18.125W into the Atlantic Ocean. The Med-WAV system is based on the WAM Cycle 6, and resolves the prognostic part of the wave spectrum with 24 directional and 32 logarithmically distributed frequency bins, correcting the solution with an optimal interpolation data assimilation scheme of all available along track satellite significant wave height observations. Atmospheric forcing (hourly heat and freshwater fluxes, and wind stress) was obtained from the European Centre for Medium-Range Weather Forecasts (ECMWF; www.ecmwf.int) and, alternatively, hourly winds from AEMET (Spanish Meteorological Agency) were also used. The Ebro River discharge was included in the model as a daily freshwater source with flow rates provided by the Confederación Hidrográfica del Ebro (CHE, Ebro River Basin Regulator). With these forcings, COAWST was used to simulate the Gloria storm from 18/01/2020 14:00h to 24/01/2020 22:00h. Figure 2.3.5 shows the comparison between the surface currents measured by the Ebro HF Radar (Puertos del Estado) and the ROMS model output for the Gloria storm simulation. Figure 2.3.6 shows the bottom currents obtained in the Marquesa (north of the Ebro Delta) and Trabucador (area of study) beaches during the peak of the storm.

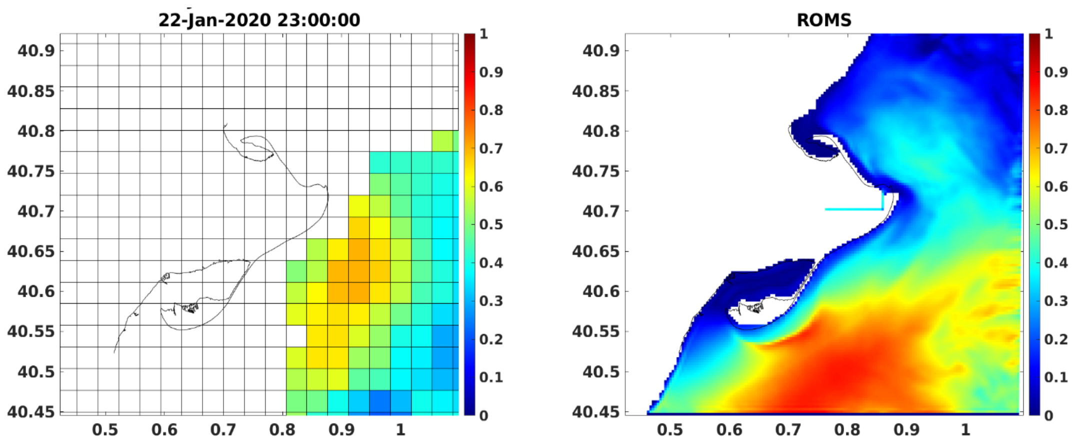

Figure 2.4.5: Comparison of the numerical results and HF-Radar from Puertos del Estado in terms of surface currents.

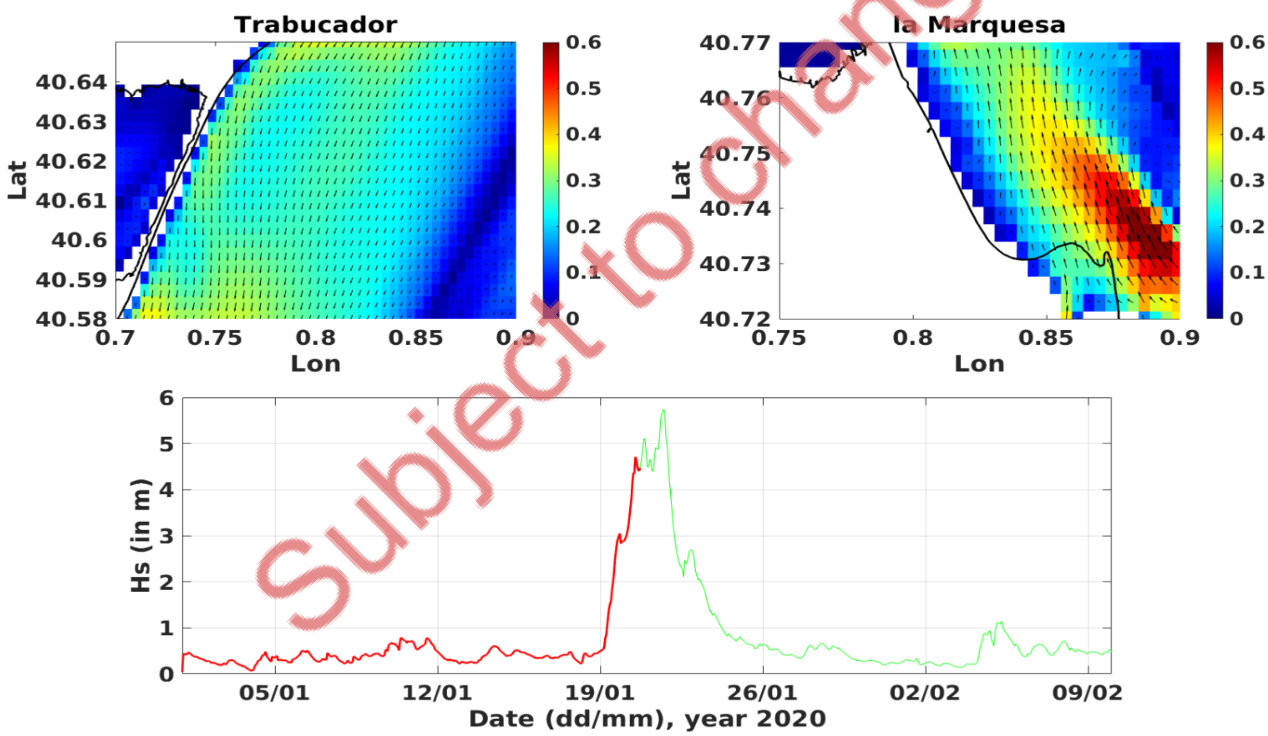

Figure 2.5.6: Bottom currents obtained during the peak of Gloria storm

Previous to the validation of Xbeach using Gloria , the Filomena storm was used to calibrate and validate the model because the topobathymetries available for the Filomena period was of better quality. Table 2.3.7 summarizes the model parameters that best reproduce the behaviour of the beach under storm conditions as compared with ortophotos, after performing nearly 65 runs. Generally, it was seen that morfac (morphological acceleration) was a parameter that helped the model to run faster rather than introducing significant changes in the model output (when ranging within reasonable values), whereas fallvelred, cmax, facua and gammax were the parameters that affected most in terms of erosion, which leads to breaching problems.

It has been observed that barrier breaching during a storm event leads to the formation of small sand islands, instead of only breaking the barrier continuity. To reproduce this, UPC has tried a novel strategy to validate the erosion outputs instead of using the Brier Skill Score (BSS), which is the most usual approach. In this case, the Goodness of Fit computing the similarity between polygons from two different sources was the selected methodology. As it can be seen in Figure 2.3.8, the comparison of the polygons obtained from the real scenario (taken from orthophotos at the end of the event) and the polygons produced by Xbeach for the same event yielded a similarity larger than 50%, plus the additional fact that the observed polygons fully match and the number of breaches coincide. It is also important to understand that this methodology is very strict, and results of more than 50% similarity rely on a very accurate reproduction of the observed behaviour.

Using the same optimal parameters obtained from the calibration and validation using Filomena storm, simulations for the Gloria and Isaak events were done, and the response of the beach was also checked by comparing ortophotos with the outputs of the model. Good correlations between modelling and reality were observed, confirming the capability of XBeach to reproduce the behaviour of the Trabucador barrier under storm events.

Table 2.3.7: XBeach calibration parameters. The box colour represents parameters that do not affect the results (white), parameters that slighty affect the results (light green), and parameters that strongly affect the results (dark green).

Parameter	Impact on the model	Storm Filomena
morfac	Speed-up model	10
	Bed Slope related parameters	
wetslp	Increasing it reduced off-shore bar formation during initial runs	1.2
dryslp	Increasing it reduced off-shore bar formation during initial runs	0.8
dilatancy	Reduce critical Shields number due to dilatancy (reduced and off-shore bar formation)	1
bdslpeffdir	Modify the direction of the sediment transport based on the bed slope (no Significant impact)	talmon
	Sediment Transport related parameters	
fallvelred	Switch to reduce fall velocity for high concentrations	1
cmax	Maximum allowed sediment concentration	1
facua	Reduced erosion over-estimation cross-shore transport and increased on-shore but during calibration process increasing it more than 0.2 produced over accretion and bars	0.15
	Wave Dissipation related parameters	
gammax	Reduced erosion-overestimation greatly	1.5

	Others	
wci	Initially enabled produced good results at barrier but every time model blow-out during calm period post storm with high degree of accretion in bay side (several meters)	0
lws	Long wave Stirring – no Significant impact	0
gwflow	Ground water flow - no Significant impact	1

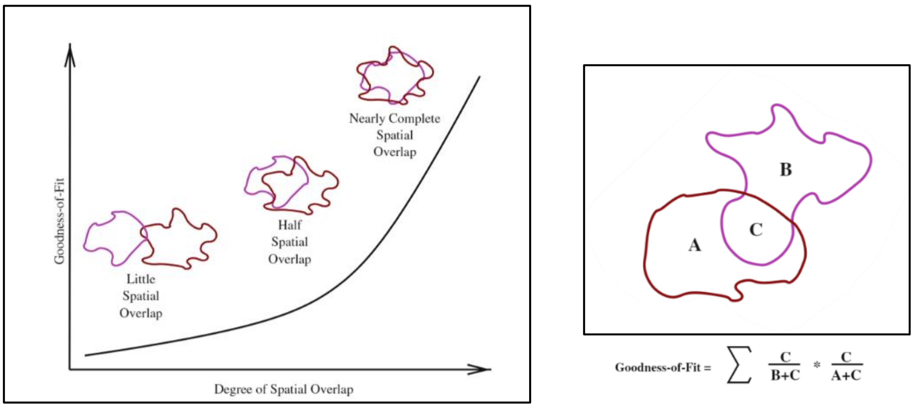

Model run	Goodness of fit
XB_45	0.3
XB_46	0.38
XB_53	0.36
XB_55	**0.52**
XB_64	0.44

Figure 2.3.8: XBeach validation. Top explains the concept of Goodness of Fit. Middle presents the results for the best runs from the calibration. Table at bottom shows the results from the index for each run.

2.3.4.Hazard reduction from ESS as a function of restoration scale.

Considering that the model reproduces the barrier beach for the studied scenarios, it was possible to generate like scenarios in which the introduction or removal of dunes was tested. As stated in Section 2.3.2, during the passing of the Isaak storm a series of alternate embrionary dunes were built along the barrier beach to test their effectiveness in reducing the breaching and flooding of the area. Since XBeach reproduced correctly the behaviour of the beach with these dunes, the same exercise was repeated but using a new mesh without the dunes. Figure 2.3.9 shows how the absence of the dunes clearly favours the breaching problem and leads to some breaking of the barrier during the storm, while their presence preserves the continuity of the beach, validating thus the ESS strategy used at this site.

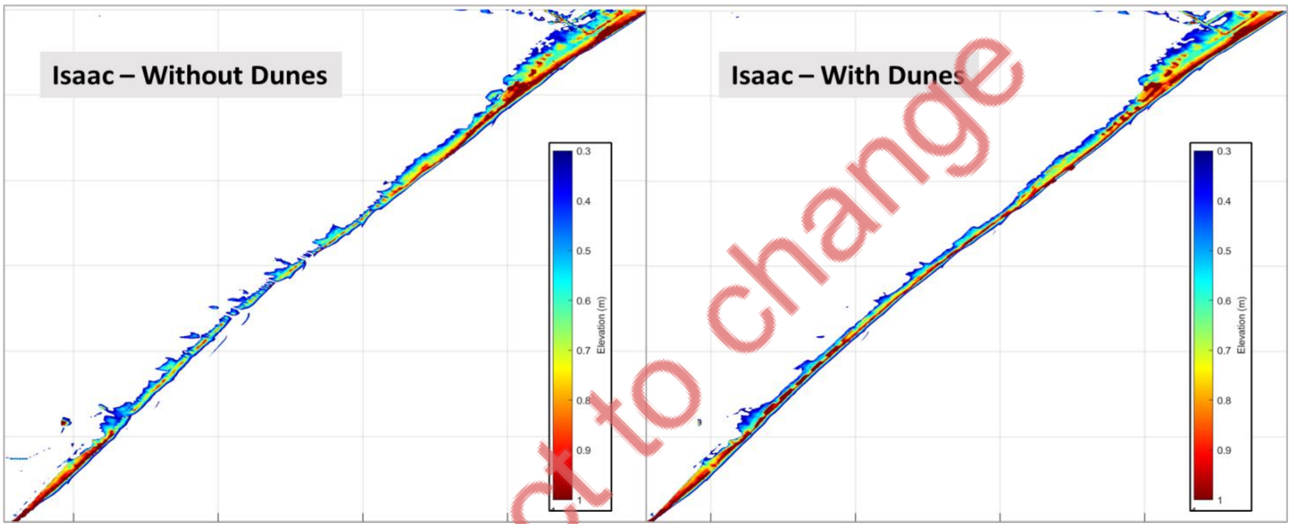

Figure 2.3.9: XBeach results for the Isaak storm with the dunes (right) and what could have happened if the dunes had not been placed (left).

To better understand the role of the dunes in the hazard reduction, the same test was done under the Filomena and Gloria storms. In this case, the beach faced the events without any protection measure and the new grid included the same dune configuration as for the Isaak storm. Figure 2.3.10 shows how for the Filomena storm the dunes reduced significantly the breaching processes and only small breaks are registered, mantaining the continuity of the barrier and allowing the pass of the trucks if necessary with few sand recoveries. By contrast, the Gloria storm produces a similar destruction for both cases and no big mitigations are observed at first sight. This event, as already described previously, was the strongest storm registered in Catalonia for the past decades and is highly infrequent. This test allows to see that there is a limit above which the dune strategy does not work as expected, enhancing the necessity to look for the tipping points in the future.

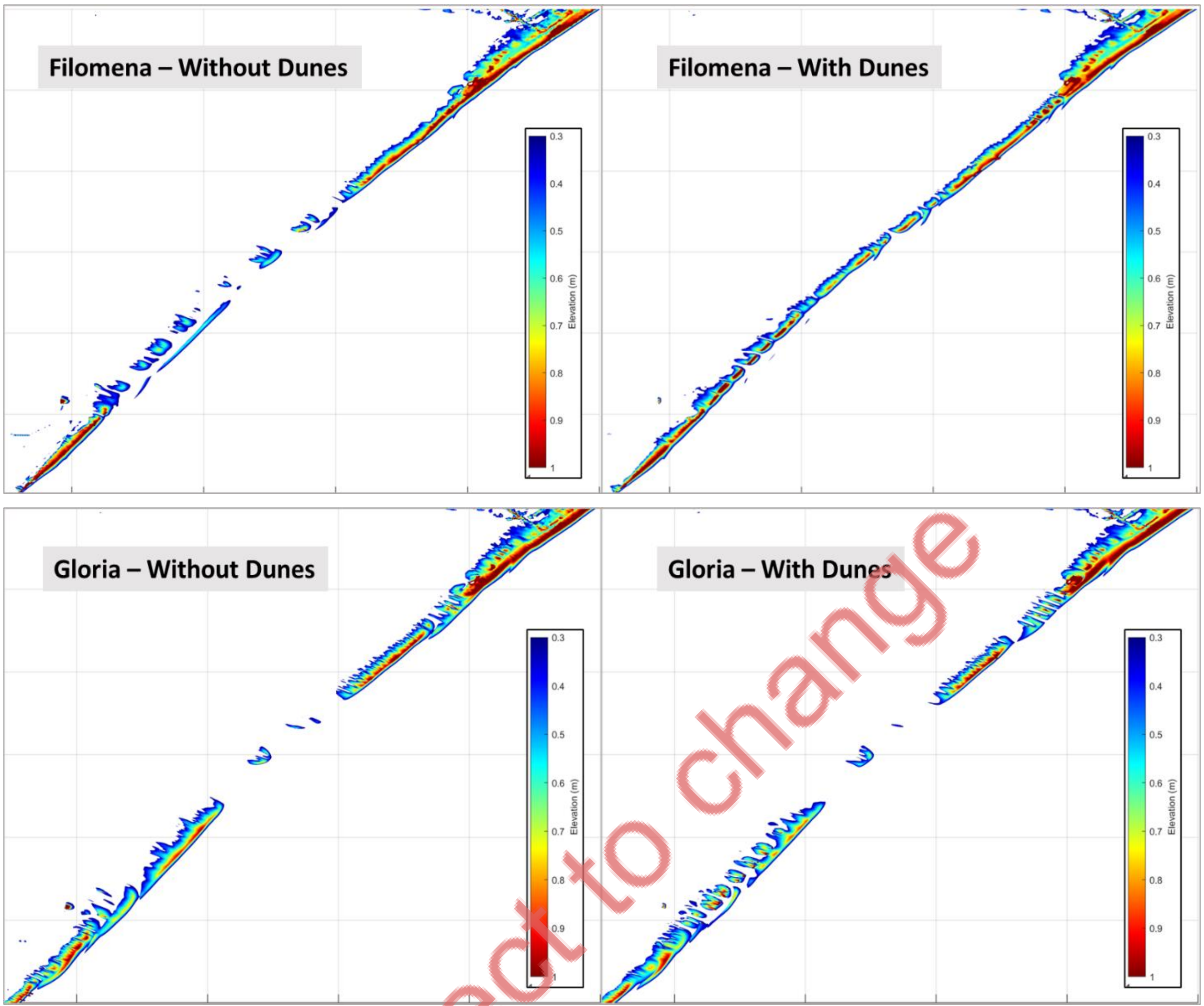

Figure 2.3.10: XBeach results for the Filomena and Gloria storms and what could be happened if the duned were placed.

Although the response of the beach under the storms with and without the dunes can be seen visually in Figures 2.3.9 and Figure 2.3.10, some metrics have been developed in order to quantify the reduction of the breaching. First, in order to check the magnitude, percentage of volume breached was computed as the total volume submerged at the end of the simulation from +0.3m (avoiding the storm surge effects) with respect to the total volume of the beach before the storm. Figure 2.3.11 shows that for all cases, there is an important mitigation of the volume breached, even for the Gloria storm, although this was not apparent from the figures. This enhances the usefulness of dunes to protect the beach from these problems. Even so, this metric does not account for the possibility in which many small barrier breaches have more volume than a single big breach and, in this case, it could be seen that the strategy works but the continuity of the barrier is on risk. For the trucks, it is better to have small breaches that are easier to restore than a larger one. In order to solve this problem, the percentage of breached area was also computed, to see if a truck would be able to progress along the barrier. Figure 2.3.11 also shows that, except for the Gloria storm, the area breached is highly reduced for Filomena and Isaak, thus strengthening the selection of the ESS. More metrics are under development to improve the interpretation of the results.

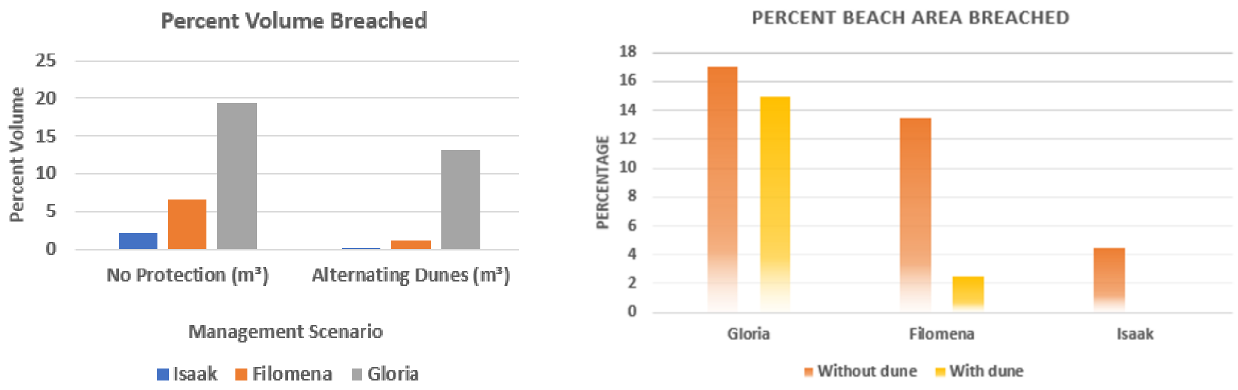

Figure 2.3.11: Metrics for breaching effects. Left: Percentage of volume breached for each storm scenario with and without dunes. Right: Percentage of area breached for each storm scenario with and without dunes.

2.4. Conclusions

XBeach is able to correctly simulate the evolution of the Trabucador barrier beach under storm scenarios with good accuracy after an exhaustive calibration. A novel validation of the erosion outputs has been used according to the needs and limitation of the available data, achieving high similarity between reality and model results. The incorporation of the COAWST model into the modelling chain will improve the performance of the whole framework since the capacity of this model to reproduce the waves and current dynamics of the Ebro Delta shelf has been also proved.

Based on both field tests and numerical modelling, it seems that dune seeding works effectivey as a hazard mitigator strategy in terms of breaching. A large reduction in both the volume and the area of breaching have been found for all the simulated scenarios when dunes are introduced as compared to the same scenarios without dunes.

The Gloria storm has helped to understand that there is a threshold above which the dunes do not work as expected, and that the tipping points for the strategy have to be found. Improvements on this problematic jointly with the study of new metrics to better represent the performance of the ESS will be tested in the future.

Operationality is starting to be implemented and working for the direct nesting between CMEMS and XBeach and it is planned that COAWST enters as a link between them to increase the accuracy of the results.

3. Multi-hazard forecasting (including a multidisciplinary calibration) and application limits Wadden Sea Pilot (DEL, FSK)

3.1. Introduction

The Wadden Sea is one of the most valuable areas of shoreline in the world. The Dutch and German areas have been listed as World Heritage Sites since 2009 (Common Wadden Sea Secretariat, 2008). It is a very dynamic tidal region where water column heights change depending on season, tide, and the weather conditions. Its tidal inlets are high-energy zones that are continually shifting in response to environmental influences.

The Ems-Dollard estuary of the Wadden Sea is the main focus of the Dutch partners, while the German partners are working on the Wadden Sea section along the coast of Niedersachsen with spatial focus on the Ems and Weser estuaries, as well as the tidal basins behind Borkum, Juist and Norderney barrier islands

3.2. High-resolution coupled coastal models

For the quantification of ecosystem services, the partners involved have further developed and applied different high-resolution model systems for different focus areas.

With the thematic focus of modelling morphodynamics of the Ems estuary, Deltares have advanced and applied a Delft3D configuration of the Ems estuary.

Therefore, a new morphological model was developed within the Delft3D flexible mesh software. This model builds on earlier morphological models developed in Delft3D4 by Deltares in 2016-2017 and the Delft3D FM hydrodynamic model developed by Schrijvershof et al. (2023). The shift towards the flexible mesh software is motivated by (1) its ability to flexibly expand or locally refine the numerical model domain, in order to flexibly implement ecosystem services and (2) the more advanced methodologies to model the morphodynamic impact of vegetation. The hydrodynamic model includes reduced tidal boundary conditions (see Schrijvershof et al., 2023) and wind-driven flow nested in the Dutch operational system, with a major point of attention during calibration being the alongshore water flux as this drives sediment supply (see details hereafter). Waves are computed with SWAN, using a wave climate schematization fitting the tidal input reduction. Sea level rise and changes in storm conditions will be derived from larger-scale CMEMS models.

Sediment transport is computed for both sand and mud using the sand-mud interaction model developed by van Ledden (2004). The primary interest is on modelling fine sediments, which largely determine the morphodynamics of the shallow subtidal and the intertidal areas. Sand transport is computed to better quantify mud availability and resuspension, but morphological changes resulting from sand transport are ignored; only morphological changes resulting from mud transport are accounted for. This allows the model to morphologically respond to changes in vegetation or sea level rise without suffering from morphodynamic aspects which are often poorly resolved on decadal timescales (such as deepening / shallowing or migration of tidal channels). The model is calibrated by quantifying sediment fluxes through the Wadden Sea / North Sea and Ems estuary, and large-scale morphological changes (reproduction of sediment sinks).

The focus of NLWKN is on modelling saltmarsh impacts on morphological evolution in the Oster-EMS (OEMS) using a Delft3D configuration for the eastern part of the Ems-Dollard estuary. The key aspect is to investigate the contribution of saltmarshes to sediment trapping, and hence to morphological evolution. Present and future scenarios are adopted to get a comprehensive understanding of forcing effects, and to identify the function of saltmarsh as the selected ESS for the potential of erosion reduction.

As a preliminary study, the sensitivity of sediment transport and morphological evolution to sea level rise (SLR) was investigated using an established model setup (Delft3D) by Dissanayake and Wurpts (2013). The model setup consists of 3 domains to downscale forcing from German Bight- to coastal- and tidal basin-scale. Five SLR rates were hypothesized: No SLR, 2, 5, 10, 15 mm/year. These SLRs were implemented in the models considering a 100-year mean sea level rise. It should be noted that SLR is the only variable among simulations, to get the first insights of SLR effects.

Sediment transport and morphological changes were simulated at the tidal-basin scale domain by forcing with water levels, currents and waves. Both water level and current were extracted by simulating the model chain of 3 domains, in which the German Bight domain was first simulated with the astronomical tide and increased mean sea level corresponding to the SLR scenarios. Wave propagation (Delft3D-SWAN) was simulated from the coastal domain to the tidal basin by forcing with the measured wave conditions at around 20 m water depth and increased mean sea level. Bed sediment composition consists of three sediment fractions representing mud, fine and coarse sediments, which vary spatially.

The main drawback applying the existing model setup is that the tidal basin domain consists of only the area behind the barrier islands in the Wadden sea. Therefore, the communication with respect to sediment transport is missing between the Wadden Sea and the North Sea. Hence, a new model setup is inevitable to cope with this issue, with a new basin-scale model encompassing the backbarrier basin and ebb-tidal delta, and extending up to about 20 m depth offshore. At the moment, this setup is calibrated and validated against measured water levels and wave data.

Hereon investigates the impact of seagrass on coupled hydro-, wave- and sediment dynamics of the Wadden Sea using the SCHISM and Xbeach model systems. In order to quantify the ecosystem services of seagrass restoration in the entire Wadden Sea region, Hereon´s SCHISM (Zhang et al., 2016) configuration for the German Bight (Stanev et al., 2019) was further upgraded incorporating the multi-physics coupling, involving waves, sediments, and the vegetation module. The wave component is contributed by the state-of-the-art 3D generation wind wave model WWM III (Roland et al., 2012), which solves the wave action balance action equation on an unstructured triangular mesh, corresponding to the core model, and involves shallow water wave breaking.

For the simulation of sediment dynamics, the 3D sediment model SED3D is coupled, which is an unstructured grid portation of the community Sediment Transport Model (Warner et al., 2008). The sediment model resolves the processes of erosion, deposition, bed load transport and suspended load transport. It was configured analogously to Stanev et al. (2019), using eight sediment classes with median grain sizes (D_{50}) of 0.06 mm, 0.07 mm, 0.1 mm, 0.125 mm, 0.24 mm, 0.5 mm, 1.0 mm, and 2.0 mm.
To represent the NbS/ESS for hazard reduction, vegetation effects are represented using SCHISM´s Vegetations module, which can simulate the first order vegetation effects approximating the plants as rigid cylinders. The vegetation model of SCHISM has been demonstrated to generally replicate vegetation effects at lab and field scales in good correlation with observation data (Zhang et al., 2020).

The German Bight model is hydrodynamically forced by the regional CMEMS product at the open boundaries (yellow line Fig 3.2.1); the resolution of the unstructured grid model is downscaled from 1.5 km at the open boundaries to 200-300 m in the Wadden Sea areas. The spectral wave forcing for the German Bight model is generated in-house applying a WaveWatch3 -based configuration for the North Western European shelf. Hourly atmospheric forcing is derived from the operational model of the German Weather Service (DWD).

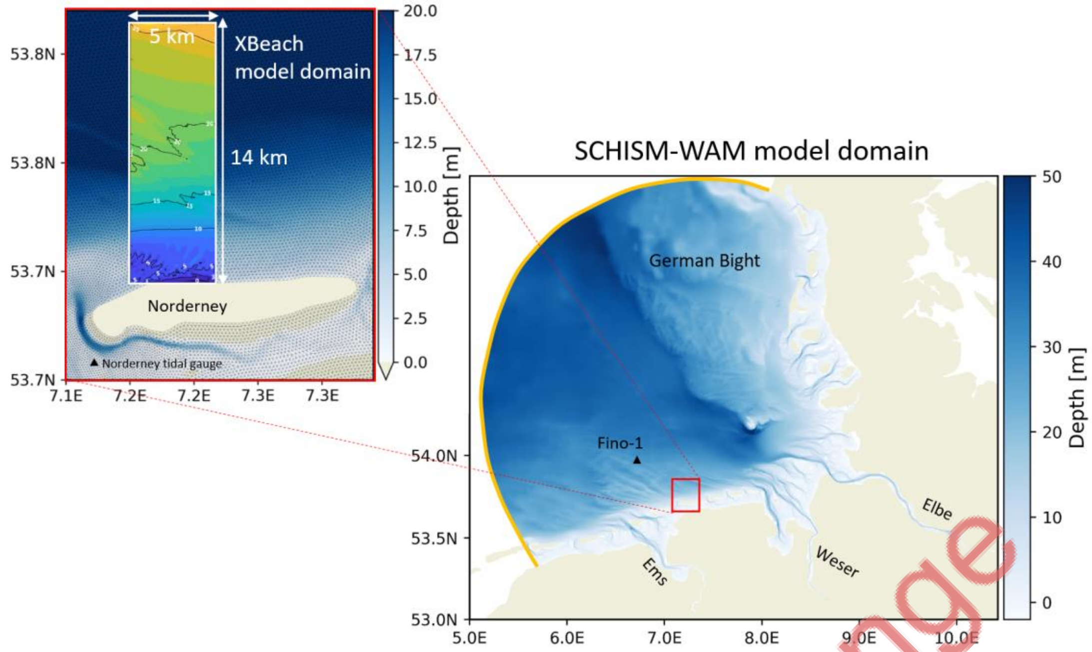

Figure 3.2.1: Domain and bathymetry of the SCHISM-WAM model (right) and the magnified box showing the study site Norderney (left, red box). The white box indicates the domain and bathymetry of the XBeach model. The open boundary of the SCHISM-WAM model is illustrated with an orange curve.

The model was applied to selected high-intensity storm events of the past, with the year 2017 and the storm Herwart being the main reference case for present-day storm conditions.

The model was successfully validated against tide gauge stations and wave buoys along the regional coast, and is generally able to simulate sea level during the calm and stormy phases (Fig. 3.2.2). As the next steps, sea level rise and changes in storm conditions will be derived from larger-scale regionalised RCP8.5 sea level data.

The research focus is on the potential risk reduction for coastal flooding and erosion as enhanced ESS for extended coastal vegetation in different scenarios. Therefore, the SCHISM setup is used morphostatically, and the impact of seagrass on hydrodynamic variables and sediment concentration has been evaluated.

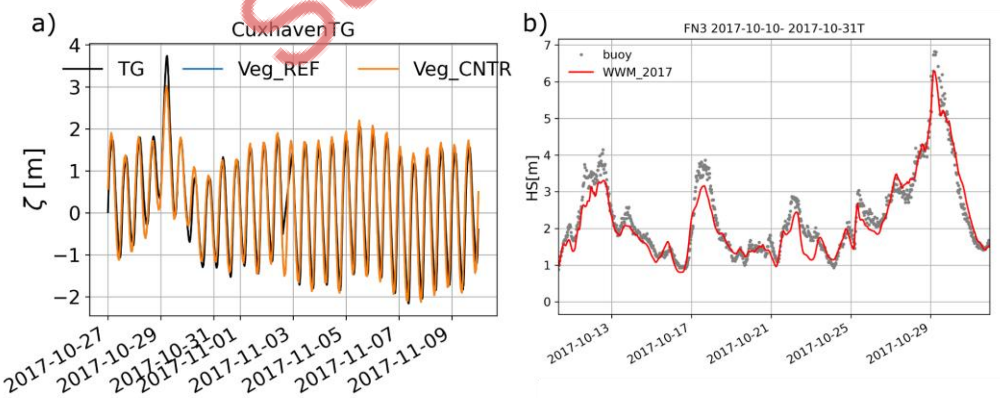

Figure 3.2.2: Exemplary validation of Sea level at North Sea tide gauge station Cuxhaven (a) and significant wave height at wave buoy FINO-3. The shown periods contain the storm Herwart on October 29th.

For direct erosion protection assessments due to enhanced coastal vegetation, an integrated framework is developed that contains two levels of simulation packages. The first level is the regional scale coupled hydro-dynamic model that simulates the processes of a specific storm and provides boundary forces to apply the morphodynamic model XBeach at the next level, simulating nearshore morphological evolution. The framework is applied at the open coast of Norderney (Fig. 3.2.1) in the German Bight of the North Sea. A series of what-if scenarios is designed for different features of seagrass meadow (see Fig. 3.2.3). The results demonstrate that optimizing the location and size of seagrass meadows is important to increase the efficiency of onshore sediment erosion mitigation.

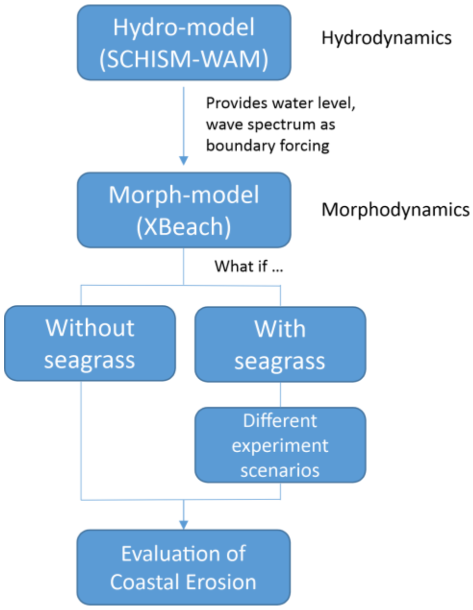

Fig 3.2.3: Flowchart showing the process applied when evaluating the impact seagrass has on coastal erosion.

3.3. Parameterization of hydro-morpho-eco interactions to simulate ESS

Deltares will quantify the five Ecosystem Services as follows. The reduction of erosion risk will be assessed with the morphodynamic model through a scenario-based approach (simulations with and without climate change and with/without relevant Nature-Based Solutions). The reduction of flood hazard is computed by running flood hazard models for various bed topographies computed with the morphodynamic model. Changes in coastal water quality regulation and food provisioning/fish stocks will be based on habitat suitability maps computed from the various morphodynamic simulations. Finally, blue carbon benefits will be quantified by estimating carbon storage resulting from sedimentation rates (again computed with the morphodynamic model).

For NLWKN, the selected ESSs are sediment, seagrass and saltmarsh by enhancing the understanding of the biogeomorphological couplings between seagrass biotopes and physico-chemical forcings aiming to improve the understanding of their mutual interaction in order to establish management principles for large scale biotopes. The model predictions are transferred to biotopes based on the selected parameters using the established classification EUNIS (Baptist et al., 2019). In this respect, all three partners (Deltares, HEREON and NLWKN) work together to develop a common list of biotopes. In addition, work is done to establish principles that link maintaining ecosystem quality to managing sediment balances in the estuary, since those relations should be quantified based on numerical model results.

Beyond the extra coupled physical modules, Hereon has advanced their modeling system accounting for the effect of coastal vegetation. The vegetation model of SCHISM (Zhang et al., 2020) physically involves the extra 3D drag introduced by the plants, as well as the generation of turbulence. The impact of seagrass is accounted for within both the hydrodynamic core and the wave model WWM III. The ESS provided by seagrass in the context of coastal flooding and erosion protection is evaluated.

The parameters of seagrass (i.e. the restoration experiment design) are given in terms of spatial fields for (1) the canopy height, (2) the stem diameter, (3) the plant drag coefficient, and (4) the stem density. The drag coefficient was selected as 1 from the range within literature. The parameters canopy height, stem diameter, and stem density were estimated from present day observation data using the average of the two present seagrass species *Zostera marina* and *Zostera noltii*. These observations translate into the reference scenario (REF) of the scenario-based approaches for the risk assessment.

The Xbeach code, forced by the coupled SCHISM-WWM model, applied the model domain (Fig. 3.2.1) of high-resolution bathymetry measured by NLWKN. Similarly to the SCHISM model, in the Xbeach model vegetation is represented as a rigid cylinder. The seagrass meadow size, shape and location of the seagrass domain is further controlled by two introduced parameters: hs and hr (Fig. 3.3.1). The first one initializes the depth where the seagrass meadow starts and the second measures the range of the depth covered by the seagrass meadow. Moreover, seagrass is characterized by stem height ah, diameter bv, and density Nv.

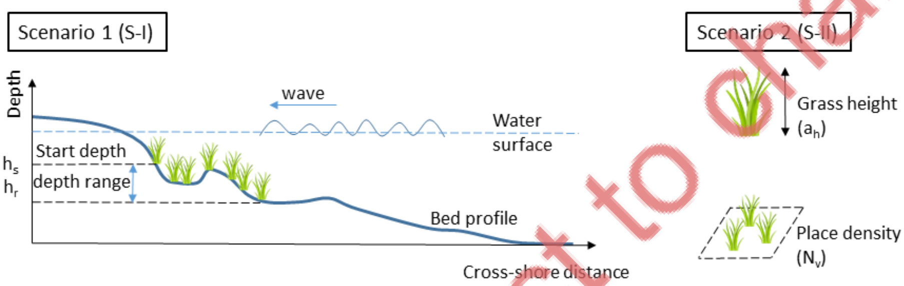

Figure 3.3.1: Experimental design of the scenario for different combinations of seagrass parameterizations.

For the assessments of the ESS of biodiversity, we follow the joint habitat mapping approach agreed upon by the Wadden Sea partners.

3.4. Target operational period for testing the EWS nested into CMEMS products

Experiments were conducted within the year 2017, focusing on the month of October as it contains one of the most severe storms (Herwart) to hit the Wadden Sea area. Experiments with SCHISM were conducted during calm and storm periods and (Herwart). Storm events of different severity will be further considered, together with additional scenarios for future climate projections.

A set of ESS restoration experiments were conducted for this period in addition to the vegetation observation based reference scenario (REF). Those further restoration scenarios were constructed by variation of the stem density and seagrass location (Fig. 3.4.1) and an increase of the stem density to the maximum observed value of about 7600 shoots per m². In addition to a control run without seagrass (Blank), other simulations involved restoration in the eintere for seagrass potentially habitable depth range (Vegmax), as well as on the shallowest (VegLE) and deepest (VegHE) 10% of the Vegmax area, to see the effect of restoring the low energy area vs restoring the high energy area.

Exploring seagrass as a nature-based storm buffer to mitigate beach erosion, the erosion assessment with Xbeach focuses on a short period during the Herwart storm event. Different series of what-if scenarios were conducted for testing the EWS. In total, 110 experiments were performed, including a reference case without seagrass, 4 default runs with square seagrass domain being placed at different cross-shore locations, 42 simulations with different depth range and start depth combinations, 33 simulations for different planting densities, and 30 simulations for different stem heights (Table 1).

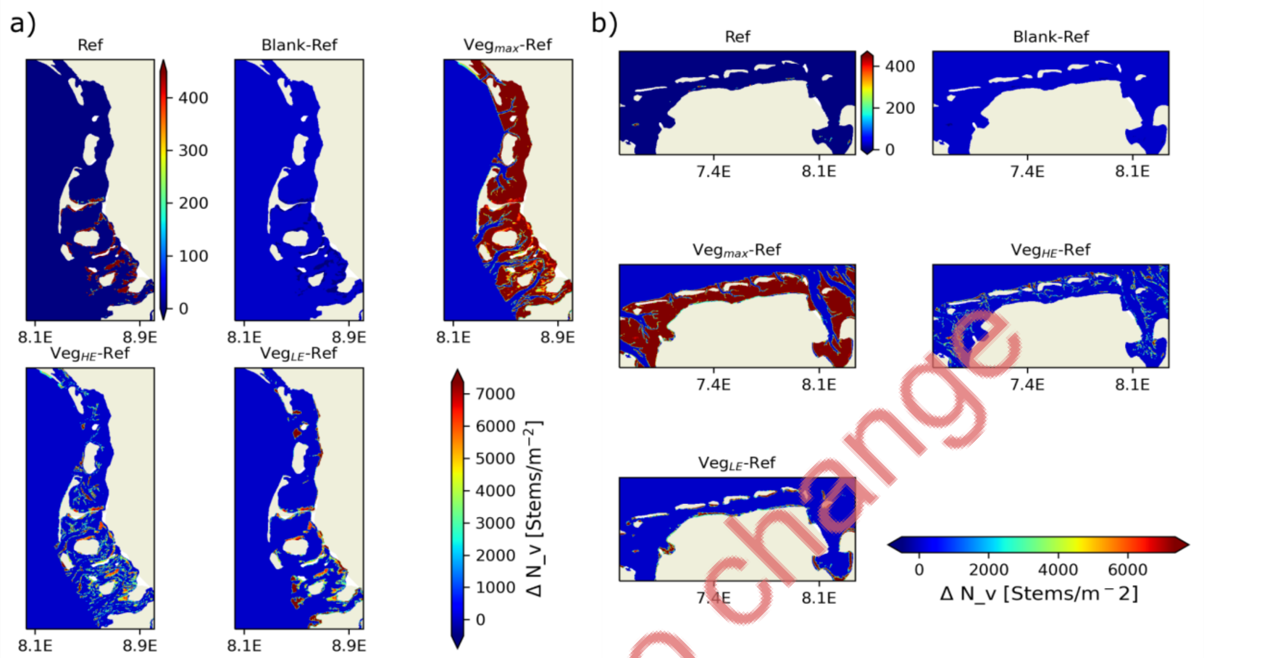

Figure 3.4.1: Restoration design via Seagrass coverage and shoot density in the different seagrass scenarios (a) in the NFWS and (b) in the EFWS. In (a)/(b) top left: Shoot density in reference run, followed by differences minus reference run.

Table 1. Overview of all what-if model simulations.

What-if	Run	Abbr.	No. Exp.	Description
no seagrass	Reference scenario	Ref.	1	----
with seagrass	Default scenario	Default	4	Seagrass characteristics: a_h=50 cm; b_v=1 cm; N_v=1000/m^2; Rectangular seagrass meadow places at different across-shore locations from the coast;
with seagrass	Scenario I	S-I	42	Seagrass characteristics are the same as Default runs, but with the meadow size and location depends on h_r and h_s.
with seagrass	Scenario II	S-IIa	33	b_v=1 cm; N_v=1000/m^2, but a_h= varies from 0 to 50 cm; Three h_r-h_s combinations are selected such that meadow size and location represents different typical meadow distributions; determined after S-I.
		S-IIb	30	as S-IIa, but for N_v varies from 0 to 1000;

3.5. Hazard reduction from ESS as a function of restoration scale

The key aspect within the approach followed with the morphodynamic model of the Ems estuary is not so much to focus on the direct impact of vegetation on hazard reduction, but on its impact via morphological changes (with the main reduction realized by these morphological changes). At this point, the Deltares partners are still in the process of improving the morphological model. The model does not yet include vegetation and is also not yet applied for hazard reduction.

Similar to the approach of Deltares, the main focus of NLWKN is to understand the contribution of saltmarsh in erosion risk reduction, by evaluating the saltmarsh effect on morphological changes. So far, the work is based on developing a model setup and its calibration and validation. Ongoing work is focused on the schematization on boundary forcing for morphological simulations. Therefore, seagrass is not yet implemented in the model domain, and so neither does the corresponding scenario testing to analyse the erosion risk reduction.

Hereon has assessed large-scale erosion risk reduction implicitly with SCHISM, examining kinematic attenuation and sediment mobilization reduction in response to seagrass vegetation. Different restoration scales and focal areas (high- or low-energy zone) were considered in the selected experiments. The scenarios were statistically analyzed based on differences in the monthly average and 95th percentile for various hydrodynamic variables relative to the reference run for the month of October 2017, when Storm Herwart occurred.
These differences show the hydrodynamic engineering capacities of seagrass on average and under more dynamic conditions.

The results show that the effect of seagrass on sea level is quite limited and varies locally, reaching only a few mm to cm with respect to average conditions (Fig. 3.5.1a). For the 95th percentile (fig. 3.5.1b), the presence of seagrass generally reduces the sea level elevation and, in the case of the maximum seagrass expansion scenario, also affects the ungreened tidal flat area, and shoreward the reduction can be as much as more than 15 cm (10-15%). However, as long as seagrass does not cover the majority of the mudflat area, the overall direct impact on sea level remains neglectable.

In contrast to sea level changes, seagrass has a very pronounced effect on the current velocity within the meadow (Fig. 3.5.2). The reductions within the meadows compared to the same areas in the scenario without seagrass are assumed to be potentially 10-30 cm/s (30% to nearly 80%). The widespread decrease in flow velocity is moderately offset by partially increased flow velocities in portions of a few seagrass-free intertidal channels.

This localized increase in current velocity occurs primarily in the maximum Vegetation scenario, and to a lesser extent in the VegHE scenario with seagrass at the edge of the channels. The differences in quantiles indicate a maximum reduction in flow velocity of 25 cm/s or more (up to 0.8 m/s). The presence of seagrass results in similar overall relative changes for the quantile compared to the changes in monthly average velocity (up to 20% in the deeper zones and up to more than 80% in the shallowest zones).

Seagrass restoration appears to be a similarly effective measure for reducing significant wave height. The simulated significant wave heights (HS) at the barrier island level correspond to approximately 1 to 1.5 m compared to the monthly average, and the 95th percentile of significant wave heights is about 1.5 to 2 m. Wave heights continue to decrease as they enter the back tidal flats in response to the shallow bathymetry, which favors wave refraction and friction, causing the Hs value to drop below 0.5 m and approaching 0 m. The presence of seagrass contributes to wave attenuation, which additionally increases HS reduction by a few cm up to more than 20 cm and on average up to more than 40 cm locally with respect to the quantiles (Fig. 3.5.3).

The seagrass restoration scenarios indicate a further reduction of a few cm in the shallow areas, and reductions of over 40 cm on average and over 60 cm with respect to the 95th percentile for the locations where seagrass would occur in deeper areas, where still relatively high waves occur. Generally, where seagrass is located, HS is reduced by over 20% in the deeper reaches and more than 50% in regions shallower than 1 m, approaching almost complete attenuation for the shallowmost regions that are still vegetated.

Naturally, the attenuation of currents and waves in the Wadden Sea results in lower stresses that can drive coastal erosion via the mobilization of bottom sediments. This is finally reflected by decreased monthly average bottom concentrations on the order of a few centi to maximum deci g/l, when introducing, respectively increasing the amount of seagrass. This denotes a reduction locally by over 30% compared to the REF scenario. During strong current conditions sediment mobilization seen from the 95th quantiles is reduced by up to more than half a g/l (Fig 3.5.4b).

Overall, the results from the experiments with the SCHISM setup show that seagrass can significantly influence hydro-morphodynamic conditions in favor of sediment accumulation and reduce erosion potential during extreme events. The effects are larger for a higher density of vegetation

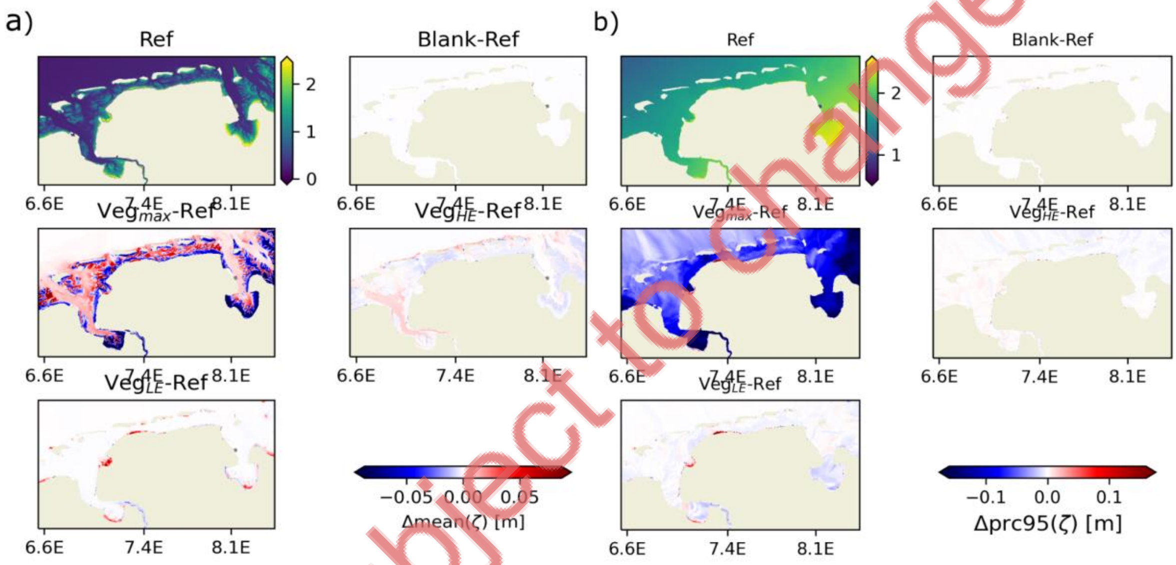

Figure 3.5.1: Differences in monthly average (a) and 95th percentile (b) sea surface height between seagrass scenarios and reference run .

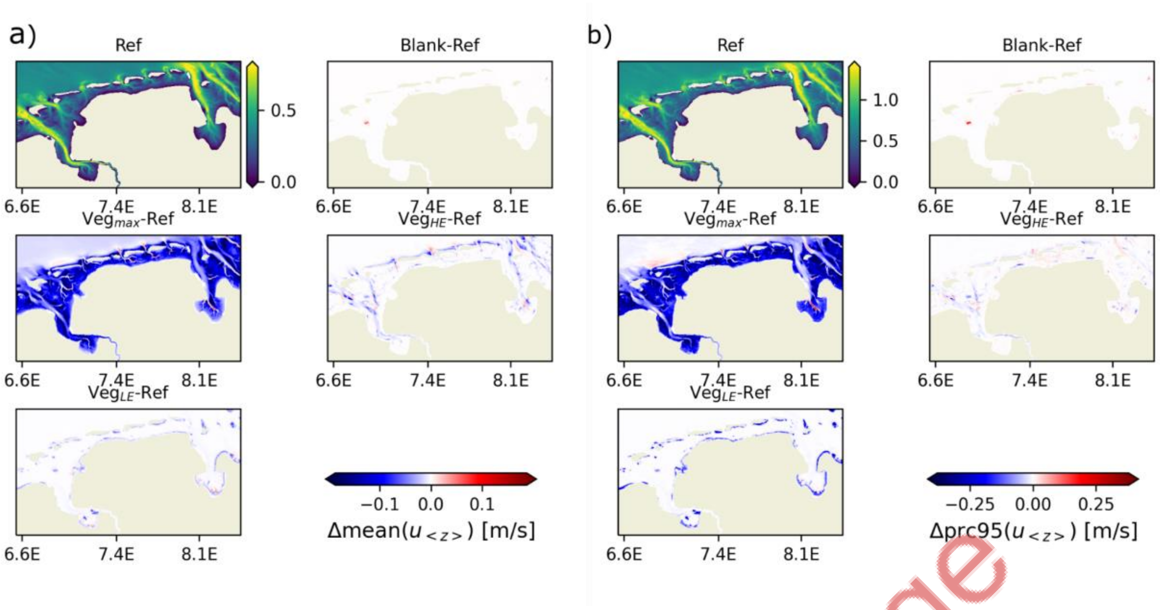

Figure 3.5.2: Differences in monthly average (a) and 95th percentile (b) of depth averaged velocity between seagrass scenarios and reference run.

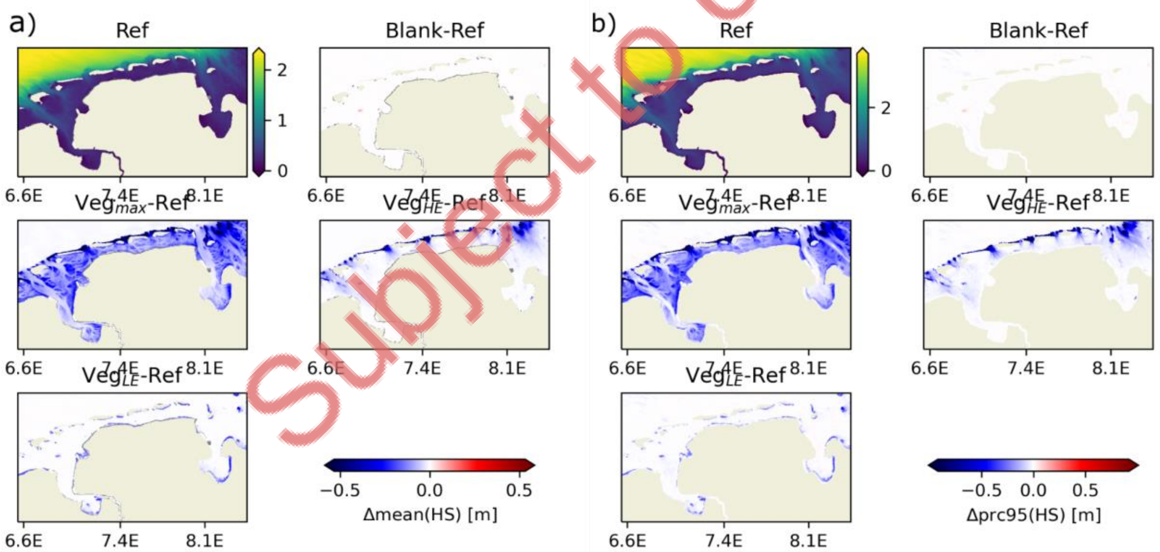

Figure 3.5.3: Differences in monthly average (a) and 95th percentile (b) of significant wave height between seagrass scenarios and reference run

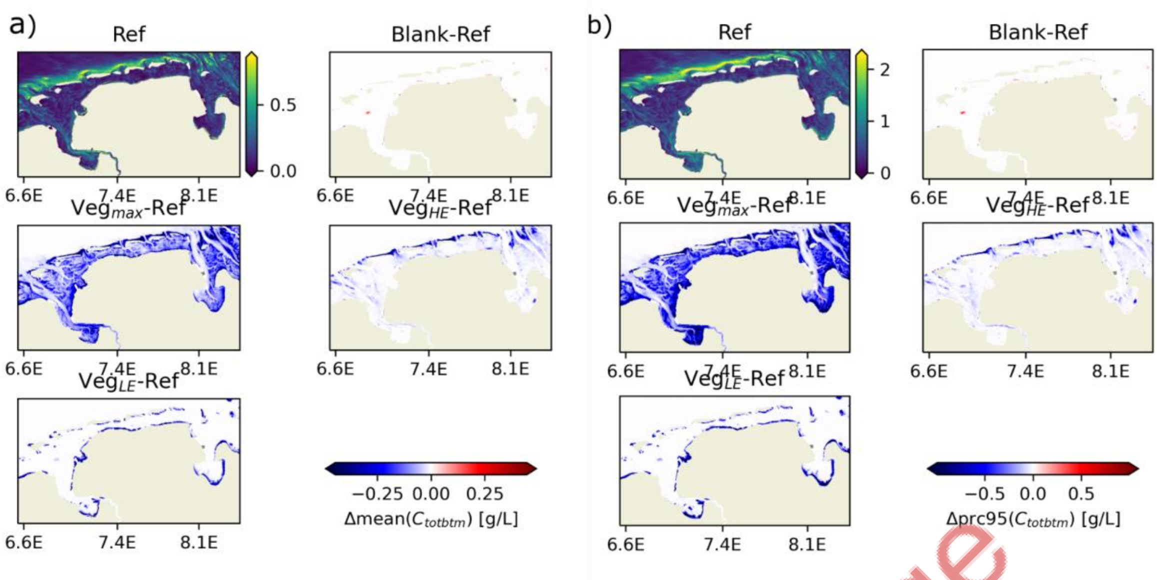

Figure 3.5.4: Differences in monthly average (a) and 95th percentile (b) of bottom layer suspended sediment concentration between seagrass scenarios and reference run .

The seagrass ESS of coastal erosion protection is directly assessed through quantifying the Norderney nearshore morphological evolution during a specific storm event.

As shown in Fig. 3.5.5, the seagrass meadow is able to effectively reduce wave height and roller energy, particularly when located in the wave-breaking region. Specifically, when the seagrass meadow is placed in this area, wave height is reduced from 1.5 m to less than 0.5 m and roller energy drops to approximately zero within the seagrass domain. This suggests that seagrass is able to preserve the beach behind the meadow by reducing the roller energy, which is strongest at a water depth of approximately 3 m.

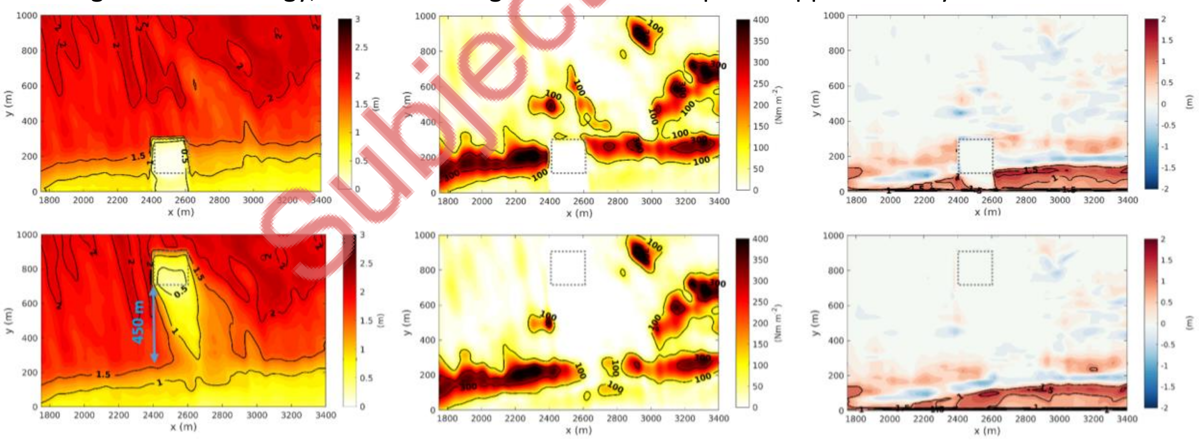

Figure 3.5.5: Sensitivity of (left column) the time mean wave height, (middle column) roller energy on Day 3 (storm day), and (right column) bathymetric differences before and after the storm for the locations of seagrass placement. Positive values in bathymetric changes denote erosion. The gray dashed square indicates the area of the seagrass meadow.

In general, a wider range of depths requires a larger area of seagrass (Fig. 3.5.6a). However, since the slope of the shoreface varies in the alongshore direction, the area and distribution of seagrass change when the plantings start at different depths and have different sizes (Fig. 3.5.6b and c). The seagrass area reaches an extreme when the combination of the two parameters intersects the white dashed line shown in Fig. 3.5.6a. The largest seagrass area was obtained when seagrass was planted with hs=1.6 m and hr=1.4 m.

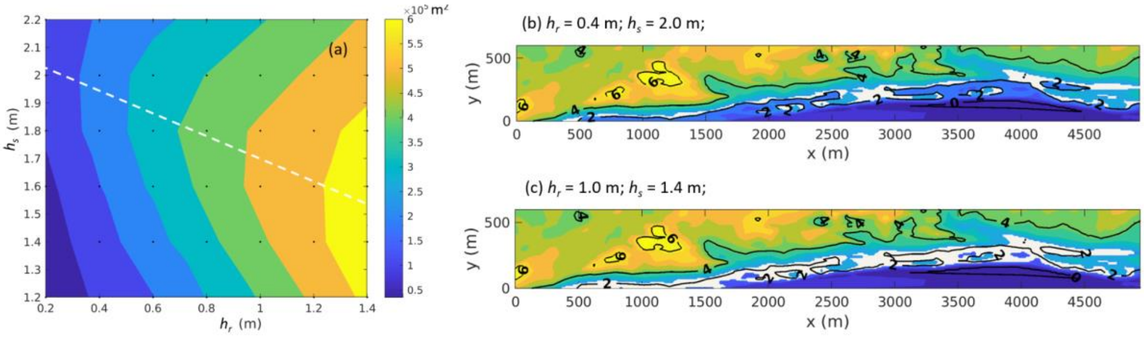

Figure 3.5.6: i. (a) Seagrass meadow area for experiments as a function of hr and hs. The black dots indicate experiments with different hr and hs combinations. Panel (b) illustrates the seagrass distribution (in white colour) for the 'deep start-narrow range' scenario (i.e.,hr = 0.6 m and hs = 2.0 m); (c) is the same as (b) but for the 'shallow start-wide range' scenario (hr = 1.0 m and hs = 1.4 m).

The reduced volume of erosion was compared with the eroded volume from the reference run, with the relative value E shown in Fig. 3.5.7. Even for the minimum seagrass planting scenario (i.e., hr=0.2 m and hs=1.2 m), the amount of erosion was found to be reduced by approximately 40%. For the same hr, when the seagrass meadow starts from deeper depths, it yields a greater reduction of erosion. In the case of hs=2.2 m, the reduced erosion reaches approximately 60%. Comparatively, the reduction in sediment erosion was found to be more sensitive to the increasing depth range of the seagrass plantings, hr, rather than increasing the starting depth hs. However, the relation between the reduction in erosion and seagrass location/size is not monotonic. An opposite relation was found between the starting depth of the seagrass plantings and the reduction in seabed erosion when the depth range increased. The white dashed curve in Fig. 3.5.7.a illustrates the combinations of hr and hs when the reduced erosion reaches the extrema.

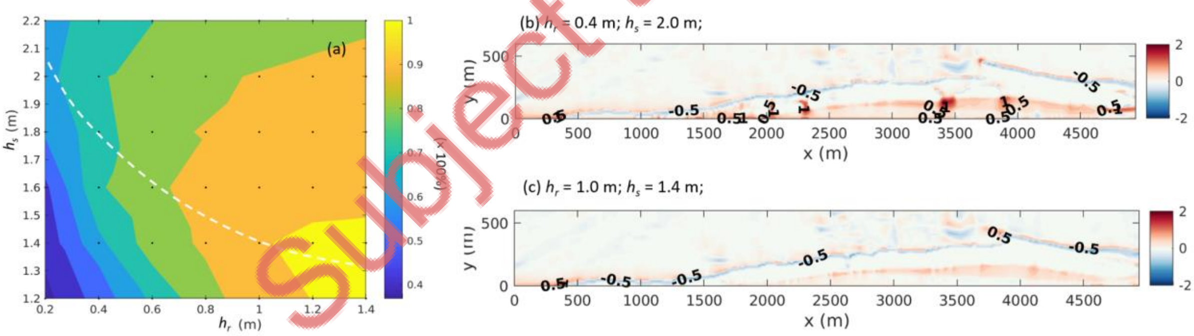

Figure 3.5.7: (a). The reduction of erosion with respect to the erosion (E) for experiments as a function of hr and hs. (b) and (c) are the results corresponding to experiments Fig. 3.5.6(b) and Fig.3.5.6(c).

A ratio, R, between relative erosion reduction E (Fig. 3.5.7a) and normalized seagrass area A (Fig. 3.5.6a) indicates the efficiency of erosion reduction for different seagrass area outcomes that result from the corresponding hr and hs combinations. The maximum efficiency rate of R equal to 6.5 is obtained when hr = 0.2 m and hs = 1.2 m (Fig. 3.5.8). This combination reduces erosion by approximately 40% while utilizing only approximately 6% of the maximum seagrass area. The steepest increase in R occurs along the direction of the normal, as represented by the grey dashed line. Along this line, the `optimal' combination is found at point `i', where hr=0.85 m and hs=1.35 m, which yields the maximum E of approximately 0.9 and is furthest from the maximum seagrass area. At this point, R is approximately 2. The grey line further crosses with the maximum seagrass area curve at `ii' (hr=1.25 m,  hs=1.6 m), which yields the `potential' combination, where R ~ 1.

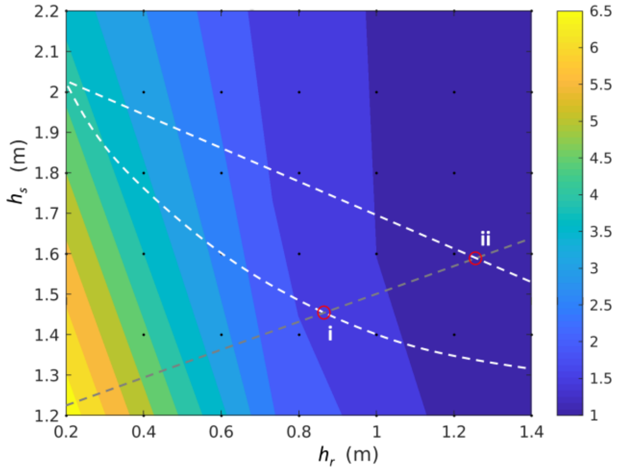

Figure 3.5.8: The ratio R between the relative erosion reduction E and the normalized seagrass area A for different combinations of hr and hs. The grey dashed line denotes the normal direction in which R decreases with increasing hr and hs. The white dashed line from Fig.3.5.6 i-a and the white dashed curve from Fig.3.5.6 ii-a are also repeated in this plot.

3.6. Conclusions

Preliminary results of NLWKN indicate that the existing sediment transport trend is enhanced by SLR, and the area close to the mainland of the basin is subjected to sedimentation. Both these observations appear to increase as the rate of SLR increases.

The results from Hereon indicate a negligible direct contribution of seagrass towards flood risk reduction, but a significant reduction of currents and waves, and also of the resulting mobilization of sediments. Thereby and via the general alteration of hydrodynamic conditions towards sediment accumulation it could indirectly contribute to flood risk reduction at long time scales supporting the vertical height growth in the Wadden Sea with respect to SLR. Wave and current attenuation under storm conditions appeared slightly increased compared to that under calm weather conditions, but this attenuation was reduced in relative terms.

The seagrass meadow is able to effectively reduce wave height and roller energy, particularly when located in the shore-breaking region. Specifically, when the seagrass meadow is placed in this area, wave height is reduced from 1.5 m to less than 0.5 m, and roller energy drops to approximately zero within the seagrass domain. As the seagrass meadow is placed further away from the coast, the erosion of the shoreface gradually decreases.

The layout of seagrass meadows has a significant impact on the efficiency they have of mitigating onshore sediment erosion. As the starting position of the planting moves towards shallow water and the depth range of the planting increases, the area covered by the seagrass meadow continues to expand. This leads to a greater reduction in coastal erosion as a function of seagrass planting. However, the study discovered that for a specific depth range, the most significant reduction in erosion is not achieved by starting at the depth that results in the largest meadow size. In terms of reducing erosion per unit area of seagrass, the most efficient combination of depth ranges and start locations is that the size of the meadow is minimized. However, the small size of these seagrass meadows may not provide adequate protection against damage caused by storms. The results overall suggest seagrass expansion to be a useful addition to engineered coastal protection measures and lore the risk of coastal erosion.

4. Multi-hazard forecasting (including a multidisciplinary calibration) and application limits Venice Lagoon Pilot (CMCC, COR)

4.1. Introduction

The Venice Lagoon, located in the Northern Adriatic Sea, is the largest transitional environment in the Mediterranean Sea. Its total surface is ca. 549 km^2 but, excluding islands and tidal marshes, ca. 432 km^2 are free waters. The lagoon is divided into three main hydrological basins (southern, central, and northern basins) by the Lido and Pellestrina watersheds, the edges of which depend on tidal excursions and winds. Three inlets, situated at the eastern boundary of the lagoon, ensure a water exchange between the Northern Adriatic Sea and the lagoon. These inlets are called, from north to south, Lido, Malamocco, and Chioggia. They are 500 to 1000 m wide and up to 15 m deep (Umgiesser et al., 2004).

The lagoon is a very polymorphous environment, exhibiting a mean depth of ca. 1.0-1.2 m, but with depth ranges between 10 and 20 m in the main canals and in the lagoon inlets with the exception of the Malamocco inlet, which is the deepest site of the Northern Adriatic Sea (ca. 50 m). The tidal sea-water exchange through the three inlets is approximately 1.46×10^9 m^3 in each tidal cycle (12 hr), which is more than half of the entire water loading, although the water renewal in the inner areas may take ca. 10-20 days. The mean annual freshwater input from 24 tributaries is ca. 35.5 m^3 s^{-1}, but under particularly adverse conditions, freshwater discharges can increase up to 344 and 273 m^3 s^{-1} on an hourly and daily basis, respectively (Zuliani et al. 2005). In the past, other authors had measured outflows of up to 600 m^3 s^{-1} (Cavazzoni 1973). The lagoon exhibits an annual mean water level difference of ± 31 cm (Pirazzoli 1974) but, under particular tidal events and/or meteorological conditions, the water fluctuations can be remarkably higher: from -80 cm to +160 cm (up to +196 cm in 1966) on the mean tide level.

Two major wind regimes are present, the Bora from north–east and the Scirocco from south–east. These wind regimes superimpose a strong circulation on top of the tidal pumping action inside the lagoon, important for mixing and transport. They also create wind waves locally that are then responsible for the resuspension of sediments in the shallow parts of the lagoon (Umgiesser et al.,2004). These wind regimes impact erosion of the different hydrological basins in different manners, where due to the geographical distribution of salt marshes and islands in the central-southern lagoon the Bora wind is free to generate fetch unlimited wave fields, thus adversely influencing the erosive trends in these basins (Carniello et al., 2009).

Apart from the tidal and wind-induced water level changes, the city of Venice has had problems with the global sea level rise. This rise, together with the well documented phenomenon of subsidence (Carbognin et al., 1995), is threatening the treasures of art contained in the old city. Moreover, human intervention like the dredging or creation of artificial channels, the creation of the railway bridge or the building of the industrial Port Marghera inside the lagoon have altered the natural equilibrium and evolution of the Venice Lagoon seen as a dynamical system, leading to the progressive degradation of the lagoon.

Due to the complicated morphology and bottom topography of the lagoon, the hydrodynamics of the lagoon can be understood only by massive use of mathematical modeling.

Increased frequency/ intensity of coastal risks and sea level rise related to climate change require fit-for-purpose and improved nearshore protection (Hanley et al., 2020; Ondiviela et al., 2020; Lobeto et al., 2021). In this context, the application of Nature Based Solutions (NBS) has gained great attention, mainly due to its ability to address social, environmental and climate concerns (Nesshöver et al., 2017; Kumar et al., 2020; Stankovic et al., 2021; Gómez Martín et al., 2021, Pillai et al., 2022). Since the 70s, the national and local Italian governments started to systematically address the safeguarding of Venice and its lagoon (Munaretto

& Huitema, 2012). Since the 90s, a variety of mitigation and adaptation interventions have been implemented, including Sistema Mo.S.E., Piano di Azione per il Clima del Commune di Venezia, Piano Europe, Piano Morfologico and a variety of LIFE projects. These interventions aim to improve the morphological, ecological and hydrological functioning of the lagoon by focusing on, for instance, saltmarsh restoration and seagrass transplantation.

In the Venice lagoon, the saltmarsh extension has reduced over 76% in the last two centuries, decreasing from 180 km^2 to 43 km^2 in the present day (Carniello et al., 2009). Saltmarsh disappearance is governed by a variety of physical and biological processes that drive their evolution in both the vertical and horizontal directions (Tommasini et al., 2019). Saltmarsh restoration in the Venice lagoon is carried out under the Piano Morfologico based on historical analysis of the morphological changes and hydraulic optimisation, and aims to protect from flooding and erosion, re-establish the hydro-geo-morphological equilibrium of the lagoon and abate pollution, while promoting the socio-economic development of the Venice area (Munaretto & Huitema, 2012).

Over the past 25 years various lagoon authorities have carried out seagrass transplantations both for the purpose of technical experiments and environmental restoration (Tagliapietra et al., 2018). In recent decades, a global decline in seagrass meadows has been observed due to numerous environmental activities (Waycott et al., 2009; Donatelli et al., 2019; McKenzie et al., 2020). Furthermore, the European Union (EU) supports ecological quality levels in coastal regions and has established principles for the use of seagrasses as indicators of the health of the ecosystem.

Many studies have reported that seagrasses enable “wave damping” (Koch and Gust, 1999; Méndez and Losada, 2004; Paul and Amos, 2011), and modify local hydrodynamics (Fonseca and Fisher, 1986; Zhang and Nepf, 2019). Water waves which propagate through submerged vegetation lose energy by performing work on the plant which directly results in smaller wave heights (Dalrymple et al., 1984).

In the Venice Lagoon, five marine and freshwater angiosperms are present, three of which are common species and exhibit abundant biomasses: *Cymodocea nodosa, Zostera marina, Zostera noltii*, where *Z. marina* shows the highest coverage. The other two species, *Ruppia cirrhosa* (Petagna) *Grande* and *Ruppia maritima Linnaeus* are rare and rarely studied. Angiosperm meadows play an important role in the ecology of the Venice Lagoon, in that they provide habitats for many species (den Hartog 1977, Fonseca 1990), favour the stabilization of sediments, enhance their deposition, and prevent their resuspension (Sfriso et al. 2004, 2005).

4.2. High-resolution coupled coastal models

4.2.1. Wave Model

The wave core of the modelling system is based on WaveWatch3 (hereafter, WW3; Tolman et al, 2019), a community wave modeling framework that includes the latest scientific advancements in the field of wind-wave modeling and dynamics. This model solves the random phase spectral action density balance equation for wavenumber-direction spectra. The implicit assumption of this equation is that properties of medium (water depth and current) as well as the wave field itself vary on time and space scales that are much larger than the variation scales of a single wave. The model includes options for shallow-water (surf zone) applications, as well as wetting and drying of grid points. Propagation of a wave spectrum can be solved using regular (rectilinear or curvilinear) and unstructured (triangular) grids, individually or combined into multi-grid mosaics.

Source terms for physical processes include parameterizations for wave growth due to the actions of wind, exact and parameterized forms accounting for nonlinear resonant wave-wave interactions, scattering due to wave-bottom interactions, triad interactions, and dissipation due to whitecapping, bottom friction, surf-breaking, and interactions with mud and ice. The model includes several alleviation methods for the Garden Sprinkler Effect and computes other transformation processes such as the effects of surface currents to wind and wave fields, and sub-grid blocking due to unresolved islands. Wave energy spectra are discretized using a constant directional increment (covering all directions), and a spatially varying wavenumber grid. First-, second- and third-order accurate numerical schemes are available to describe wave propagation. Source terms are integrated in time using a dynamically adjusted time stepping algorithm, which concentrates computational efforts in conditions with rapid spectral changes. The model is used worldwide by several institutions to simulate waves of several systems in many regions of the world, from global to coastal scale.

The wave modelling approach is based on downscaling CMEMS Marine products released at the regional scale of the Mediterranean Sea. The current Med_Waves-CMEMS (Korres et al., 2021) implementation is based on WAM Cycle 4.6.2 with an horizontal resolution of 1/24° (~4.6km). The model solutions are corrected by an optimal interpolation data assimilation scheme of along-track significant satellite wave height observations. The scalar fields from Med-Waves-CMEMS (significant wave surface height, peak wave period and mean direction) are treated at the boundary nodes of the nested system through the Yamaguchi (1984) approximation, to rebuild local wave spectra. The model is initialized using the fetch limited approach: the local JONSWAP spectrum is calculated using the local wind speed and direction, using the spatial grid size as fetch.

Meridional and zonal wind components at 10-m height (U10M and V10M) of well-consolidated atmospheric products from ECMWF (6.5 km resolution and 3h frequency) are adopted as forcing. The atmospheric fields are corrected by land-contaminated points following Kara et al. (2007) and horizontally interpolated at each ocean grid node by means of linear interpolation.

The wave model has been implemented following WAM Cycle4 model physics (Günther et al. 1992). The propagation scheme used is a third order scheme (Ultimate Quickest) with the Garden Sprinkler Effect alleviation method of spatial averaging. Wind input and dissipation are based on Ardhuin et al. (2010), in which the wind input parameterization is adapted from Janssen's quasi-linear theory of wind-wave generation (Janssen, 1991, Chalikov and Belevich, 1993), following adjustments performed by Bidlot et al. 2005 and Bidlot 2008. Nonlinear wave-wave interaction have been modelled using the Discrete Interaction Approximation (DIA) (Hasselmann et al. 1986, Hasselmann et al. 1985). The model system includes shallow water physics for coastal processes as nonlinear triad interactions, modelled using the LTA-model of Eldeberky (1996). Depth-induced breaking has been implemented using the approach of Battjes and Janssen (1978). Ripple-induced bottom friction has been parameterized according to SHOWEX formulations from Ardhuin et al. (2003). The wave spectra for the Venice implementation have been discretized in 24 directions (covering the full circle) and 32 frequencies, from 0.05 Hz to 0.96 Hz.

4.2.2. Circulation model

The circulation modelling system is based on the SHYFEM model, which is a 3-D finite element hydrodynamic model (Umgiesser et al., 2004) solving the Navier–Stokes equations by applying hydrostatic and Boussinesq approximations. The unstructured grid is Arakawa B with triangular meshes (Bellafiore and Umgiesser, 2010; Ferrarin et al., 2013), which provides an accurate description of irregular coastal boundaries. The scalars are computed at grid nodes, whereas velocity vectors are calculated at the center of each element. Vertically a z layer discretization is applied and most variables are computed in the center of each layer, whereas stress terms and vertical velocities are solved at the layer interfaces (Bellafiore and Umgiesser, 2010). The peculiarity of unstructured meshes is the ability of representing several scales in a seamless fashion, reaching higher resolution where necessary.

The model uses a semi-implicit algorithm for integration over time, which has the advantage of being unconditionally stable with respect to gravity waves, bottom friction and Coriolis terms, and allows transport variables to be solved explicitly. The Coriolis term and pressure gradient in the momentum equation, and the divergence terms in the continuity equation are treated semi-implicitly. Bottom friction and vertical eddy viscosity are treated fully implicitly for stability reasons, while the remaining terms (advective and horizontal diffusion terms in the momentum equation) are treated explicitly.

The model has been already applied to simulate hydrodynamics of several systems in many regions of the world, proving its quality and accuracy. Exploiting the variable mesh approach, the model has been successfully applied to several scales, from the open sea (e.g., Mediterranean Sea, Black Sea, Gulf of Mexico) to the coastal seas and estuaries (e.g., coastal areas of Adriatic Ionian and Western Mediterranean Seas in Italy, Kotor Bay in Montenegro, Danube Delta in Romania) to open-sea islands (e.g., Malta) to the fjords (e.g., Roskilde, Denmark, Oslo) to the lagoons (e.g., Venice, Menor in Spain, Nador in Morocco, Dalyan in Turkey, Curonian in Lithuania, Tam Giang in Vietnam) to the ports (e.g., Apulian ports in Italy) to the rivers (e.g., Po river in Italy, Savannah river in Georgia, US) to the lakes (e.g., Geneva in Switzerland, Garda in Italy).

The modelling approach is based on the downscaling of CMEMS Marine products released at the regional scale of the Mediterranean Sea. The current Med-CMEMS implementation is based on NEMO (Nucleus for European Modelling of the Ocean; Madec, 2008) finite-difference code with a horizontal resolution of 1/24 of a degree (4–5 km approximately) and 141 unevenly spaced vertical levels. The results are corrected with a data assimilation system based on the 3D-VAR scheme developed by Dobricic and Pinardi (2008). The modelling system is three-dimensionally downscaled from Med-CMEMS both in terms of initialization and open boundaries. The scalar fields from Med-CMEMS (sea level, temperature, and salinity) are treated at the boundary nodes of the nested system through a clamped boundary condition. The velocity fields are imposed as nudged boundary condition from the parent model in the barycentre of the triangular elements using a relaxation time of 3600 s.

Three basic surface boundary conditions are used:

a) For temperature, the air-sea heat flux is parameterized by bulk formulas described in Pettenuzzo et al. (2010).
b) For momentum, surface stress is computed with the wind drag coefficient according to Hellermann and Rosenstein (1983).
c) For the vertical velocity and the salinity, the salt flux boundary condition is adopted and the water flux advected through the air-sea interface is given by precipitation minus evaporation.

For the atmospheric fields, well-consolidated products from ECMWF (10 km resolution and 1h frequency) are adopted as forcing. The atmospheric fields are corrected by land-contaminated points following Kara et al. (2007) and horizontally interpolated at each ocean grid node by means of Cressman's interpolation technique (Cressman, 1959).

The atmospheric variables used for the parametrization are 2 m air temperature (T2M), 2 m dew point temperature (D2M), total cloud cover (TCC), mean sea level atmospheric pressure (MSL), and meridional and zonal 10 m wind components (U10M and V10M) and total precipitation (TP).

About the main numerical settings, we use a TVD (total variation diminishing) scheme for both the horizontal and vertical advection in the transport and diffusion equation for scalars, with constant diffusivity.

Horizontal advection of momentum is discretized by an upwind scheme and horizontal eddy viscosity is computed by the Smagorinsky's formulation.

For the computation of the vertical viscosities and diffusivities, a k–ε turbulence scheme is used, adapted from the GOTM (General Ocean Turbulence Model) model described in Burchard et al. (1999).

The bottom drag coefficient is computed using a logarithmic formulation via bottom roughness length, set homogeneous over the whole system to a value of 0.01 m (Ferrarin et al. 2017).

4.2.3. Bathymetry and grid generation

In REST-COAST a specific and hyper-resolution configuration for the Venice lagoon has been developed. The system covers the entire lagoon and a portion of open-sea shallow water of the Northwestern Adriatic Sea (Figure 4.2.1). The horizontal resolution ranges from 1 km at open-sea to 50 m in the coastal waters to 10-30 m in the lagoon. Figure 4.2.1 shows the grid and bathymetry. A single rounded open boundary is created connecting the Po River delta and Lido di Jesolo (see Figure 4.2.1). The horizontal grid has been created adopting advanced and customized tools (mainly python-based) of meshing based on GMSH[1] and BLENDER[2] software.

The bathymetry of the gulf was derived from the EMODnet[3] product at a resolution of 1/8 x 1/8 arcminutes (approx. 230 x 230 meter), resolution for open sea and coastal waters and integrated with higher-resolution bathymetry (resolutions of order of half meter) for lagoon, inlets, and near-inlet coastal areas (Provveditorato for the Public Works of Veneto, Trentino Alto Adige and Friuli Venezia Giulia, n.d.).

WW3 and SHYFEM share the same unstructured meshes.

4.2.4. Inclusion of vegetation in the wave model

To account for vegetation-induced dissipation, we modify the SHOWEX bottom friction equation by incorporating the wave damping due to vegetation (Sds,veg; Dalrymple et al., 1984; Mendez and Losada, 2004) as indicated below;

$$S_{ds,veg} = -\sqrt{\frac{2}{\pi}}\; g^2 \widetilde{C_D}\, b_v\, N_v \left(\frac{\tilde{k}}{\tilde{\sigma}}\right)^3 \frac{\sinh^3 \tilde{k}\alpha h \;+\; 3 \sinh \tilde{k}\alpha h}{3k \cosh^3 \tilde{k} h} \sqrt{E_{tot}}\; E(\sigma,\theta)$$

where $\widetilde{C_D}$ is the bulk drag coefficient that may depend on the wave height, bv is the plant stem diameter, Nv is the number of plants per square meter, αh is the vegetation height, h is the water depth, $\tilde{k}$ is the mean wave number, $\tilde{\sigma}$ is the mean frequency, E_{tot} is the total wave energy, and E(σ, θ) is the wave variance spectrum.

[1] http://gmsh.info/

[2] https://www.blender.org/

[3] https://www.emodnet-bathymetry.eu/

Afterwards, the total bottom friction (*St*) is redefined by adding SHOWEX bottom friction (*Sbot*), with the *Sds,veg*.

$$S_t = S_{bot} + Maskveg \times S_{ds,veg}$$

where *Maskveg* is the mask file which specifies the location of the vegetation.

4.2.5. Inclusion of vegetation in the circulation model

In SHYFEM, seagrass was implemented in the governing equations following an approach similar to the one described in Beudin et al. (2017), and Zhang et al. (2019). The seagrass form drag was written as:

$$F_{veg,x} = \frac{1}{2} C_{Dv} D_v N_v \left| \vec{u} \right| u$$

$$F_{veg,y} = \frac{1}{2} C_{Dv} D_v N_v \left| \vec{u} \right| v$$

where C_{Dv} is a plant drag coefficient, with values that can vary from close to zero to 3 (Nepf and Vivoni, 2000; Tanino and Nepf, 2008), D_v is the stem diameter, N_v is the vegetation density (number of stems per m^2), u and v are the zonal and meridional components of the velocity, respectively, and $\vec{u}$ is the velocity vector.

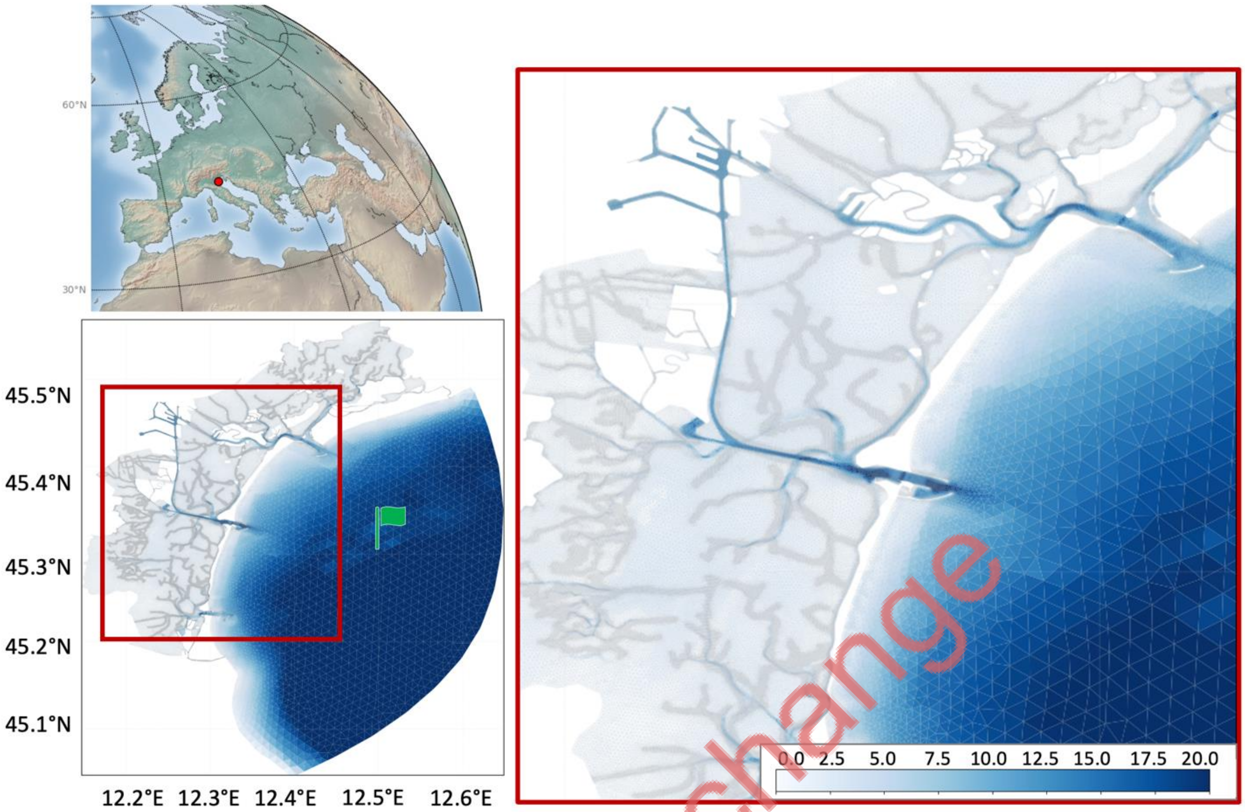

Figure 4.2.1: Numerical grid and bathymetry [m] for REST-COAST Venice pilot (left panel), and magnification (right panel). Green flag shows the CNR "Acqua alta" platform location.

4.3. Parameterization of hydro-morpho-eco interactions to simulate ESS.

The Venice pilot of REST-COAST project implements two morpho-ecological structures in the numerical models:

- Wetlands;
- Seagrasses.

In our numerical implementation, wetlands are considered as small islets. A wave approaching the coast (in general) and thus an islet, is affected by several processes such as shoaling, refraction, dissipation of wave energy by depth-induced breaking and reflection at the coast. The spatial distribution of the wetlands has been defined according to the shapefiles obtained from the the open source Atlante della laguna (https://www.atlantedellalaguna.it) and commissioned by the Venice Water Authorities.

In the REST-COAST Venice wave model implementation, we considered a mono-species distribution of the most common angiosperm for the Venice lagoon, *Zoostera marina.* The related vegetation parameters (Table 4.3.1) have been set following Mazzella et al. (1998).

Figure 4.3.2 shows the spatial map of both the structures in the lagoon, and highlights that the Northern lagoon is the poorest in vegetation and wetlands presence, on the contrary, Southern lagoon has a large presence of vegetation and several wetlands.

Table 4.3.1: Seagrass parametrization included in the wave model, from Mazzella et al. (1998)

Wave Model parameters				
Seagrass Type	**Seagrass distribution**	**Stem diameter of plant (Bv in m)**	**No. of plants per square meter (Nv)**	**Length of seagrass (Lv in m)**
Zostera marina	**According to open source Atlante della laguna**	0.0032	270	0.213

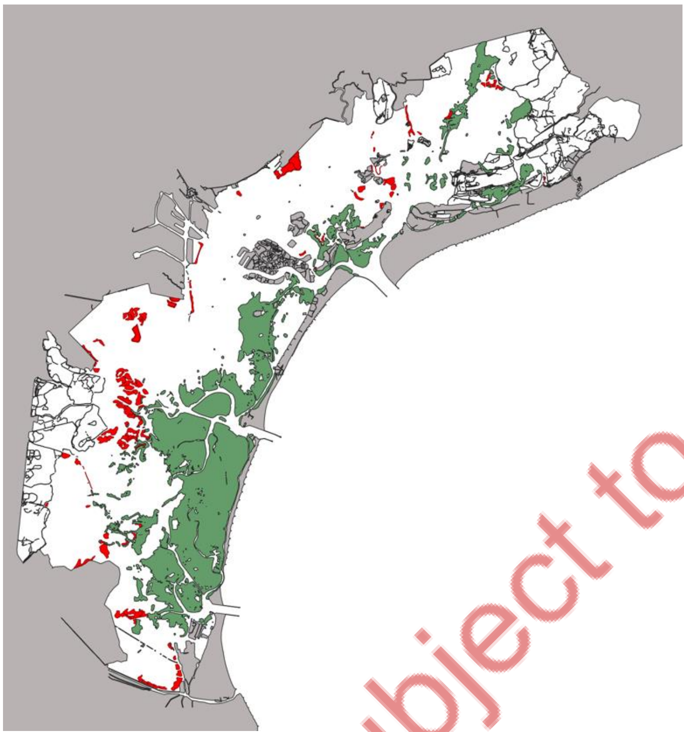

Figure 4.3.2: Morpho-ecological structures adopted for the Venice lagoon: in red wetlands, while in green seagrass are highlighted

4.4. Target operational period for testing the EWS nested into CMEMS products

Calibration and validation of the wave model was carried out according to the availability of data from the CNR ”Acqua alta” platform (http://www.ismar.cnr.it/infrastrutture/piattaforma-acqua-alta). Installed in March 1970 about 8 miles off the coast of Venice, on a water depth about 16 m (GPS 45° 19' N, 012° 30' E), the Acqua Alta Oceanographic Platform is one of the main research infrastructures managed by the National Research Council. It consists of a laboratory module, as well as sophisticated distribution systems for management and data transfer in real time from numerous measuring stations and sensors such as: sea level, sea state, sea currents, salinity, temperature, oxygen and nutrients.

The WW3 model for the REST-COAST Venice pilot has simulated 3 years (2020-2022), and Figure 4.4.1 shows the averaged Significant Wave Height (SWH) for the lagoon. Northern lagoon represents the calmest area of the domain, with an average SWH approximately of 4 cm maximum. Central and Southern lagoons showed higher SWH on average, reaching 10 cm maximum close to the Malamocco channel. In all the three mouths, the wave height is higher than 10 cm on average, because of the swell approaching the lagoon from the Adriatic Sea; however, due to shallow depths, waves are promptly dissipated.

Due to the lack of observational data, the model accuracy could be assessed only for 10 months, from March to December 2022. Figure 4.4.2 compares the time series of hourly values from model (in black) and observation (in red), at the “Acqua Alta platform” location. The WW3 implementation can reproduce wave statistics with high confidence, well describing the wave pattern. On average, the model has a slight general tendency to underestimate the measurements, both during calm and rough conditions. Table 4.4.3 shows the validation statistics for the available time. The qualitative underestimation highlighted by the time series is quantified by a negative bias of ~12 cm. A high correlation is shown, with a Pearson correlation of 0.93 and a RMSE of approximatey 20 cm.

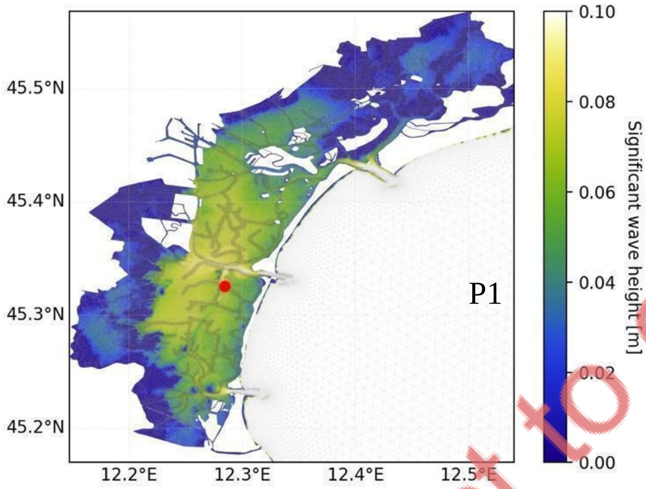

Figure 4.4.1: Three-years averaged significant wave height for the Venice lagoon. Red dot (P1) indicates the location selected for the time series comparison.

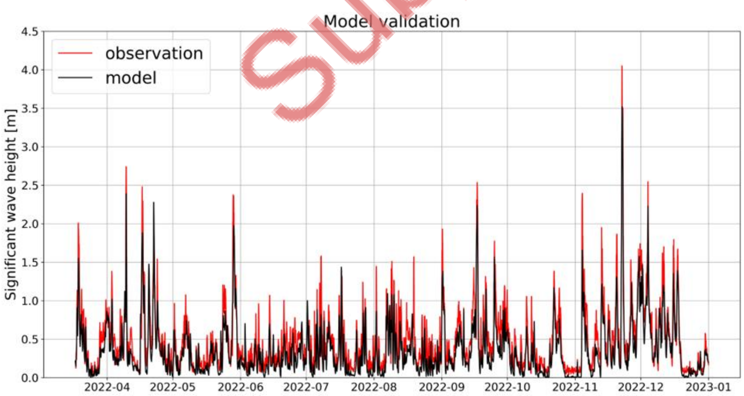

Figure 4.4.2: Timeseries plot of significant wave height (m) from model, in black, and CNR ”Acqua alta platform”, in red.

Table 4.4.3: Skill scores for the wave model

Statistics	Score
Bias [m]	-0.124
RMSE [m]	0.198
Pearson correlation	0.93

4.5. Hazard reduction from ESS as a function of restoration scale.

In this section the ESS provided by the inclusion of wetlands and seagrass in the modelling framework was investigated. The ESS has been quantified comparing the simulation (named ESS-run) with a reference run showing the same configuration but with the exception of seagrass and wetlands. In particular, the seagrass has been completely removed from ESS-run, while wetland has been moved below the sea level at 0.2 m of depth. The skills assessment has been carried out for an extreme event that occurred in 2022. Both the runs were also compared over a one-year period at point P1 (Figure 4.4.2), with coordinates 45.35 °N, 12.27 °E. This position has been selected because it is located in one of the roughest areas of the lagoon, and it lays on the seagrass pattern.

As anticipated in the previous section, the average SWH in the Central lagoon is approximately 10 cm. This value has been confirmed by observing the SWH timeseries in Figure 4.5.1; however the hourly plot helped in the assessment of the extremes during the 2022. At P1, SWH rarely exceeded 0.6 m, while 0.5 m occurred in all the seasons, except for Summer. As a general rule, the SWH has fast fluctuations, with higher values reaching for a few hours and rapidly dropping. Only during Autumn and Winter did longer storms occurr.

The difference between the reference run and the ESS-run is reported by the red line in Figure 4.5.1. In few cases SWH is higher in ESS-run than the reference, this is probably related to the direction of the wave approaching the point which begin to shoal before breaking. In almost all the cases ESS-run has lower SWH than the reference, from approximately 1 to 9 cm maximum. The highest dissipation we observed was on 11th November with a reference wave of 62 cm and 53 cm in the ESS-run (~17%).

The SWH spatial map (Figure 4.5.2) of the storm event showed that the highest waves are located at the lagoon mouths because of the swell from the Adriatic Sea, and along the largest channels because of the deeper water. However, SWH rarely exceeds 0.6 m inside del lagoon, and the roughest area is represented by the Southern part.

The difference between the reference and the ESS-run is shown in Figure 4.5.1 and allows to quantify the dissipation of SWH due to seagrass and wetlands. The negative difference indicated lower waves in the ESS-run with respect to the reference, and the spatial pattern fits well the vegetation distribution. This is quite evident in the Southern and Central lagoons where most of the vegetation is located, and waves are higher. Reduced SWH can be found even at the Northernmost part where some wetlands and vegetation are present.

From the difference map we can distinguish 2 patterns, the first related to the vegetation dissipation, with smoothed large patches and reduction of SWH around 2-5 cm, the second one related to wetlands where the SWH reduction is localized, slightly extended down-wave, and exceeding 10 cm in some cases.

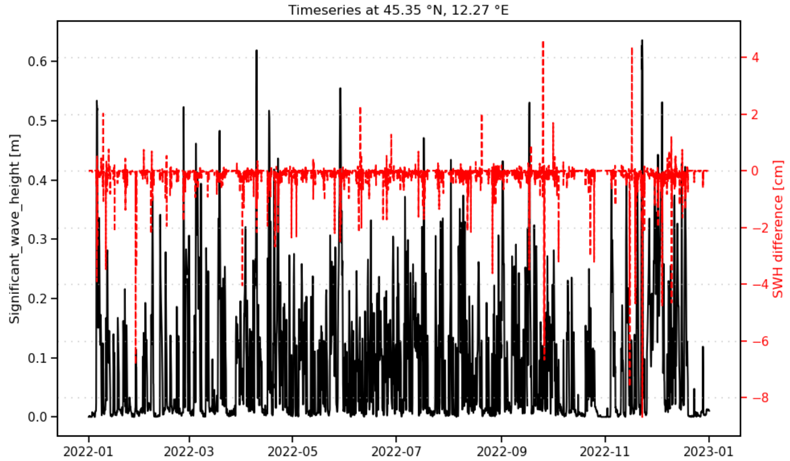

Figure 4.5.1: Significant wave height at P1 for the 2022 for the reference run (in black). Red line indicates the difference between reference run and simulation including ESS.

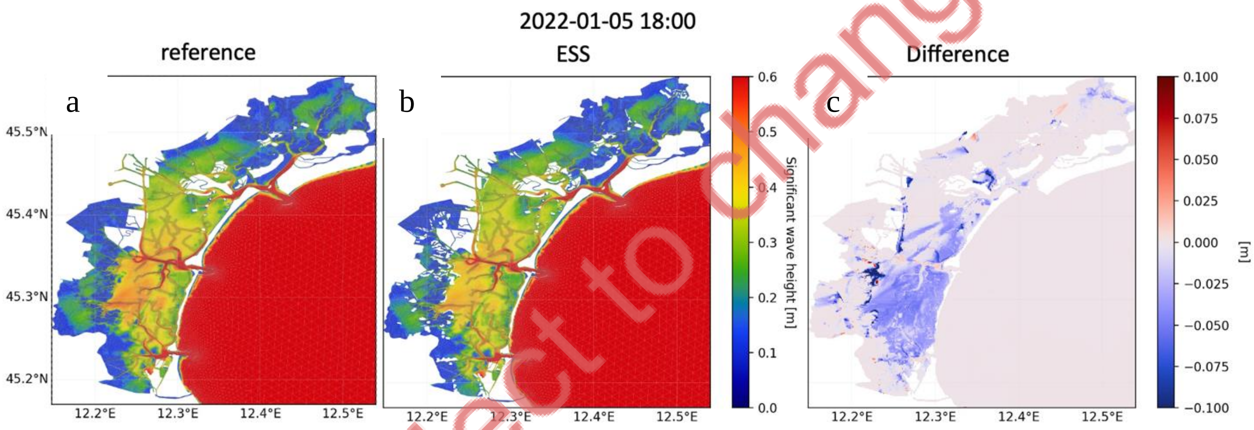

Figure 4.5.2: Significant wave height (m) during a storm at the Venice lagoon. Left panel shows the reference run (without wetlands and seagrass), middle panel shows the simulation including wetlands and seagrass, right panels show the difference between the simulations.

Hydrodynamics and ESS itself are shown here, considering one of the worst storms that hit the Venice lagoon, in November 2019.

In Figure 4.5.3 a snapshot of the event is presented. The hour was chosen to have the highest water level in the Southern lagoon, where most of the vegetation and wetlands are located. In detail, the Southern lagoon has a sea-level approx. 140-150 cm, which decreased down to 110-120 cm in the Northernmost part. Observing the difference map (Figure 4.5.3c) almost al the lagoon has a lower sea-level in the ESS-run compared to the reference, with a minimum of approx. -2.5 cm in the Northern part, and a maximum of -6 cm in the Southern one, up to a maximum decrease of -5%. An increase of the water level is evident in the ESS-run along the three lagoon mouths and nearby. We assumed that this pattern could be related to the reduced circulation inside the lagoon of the incoming water, due to the increased bottom stress.

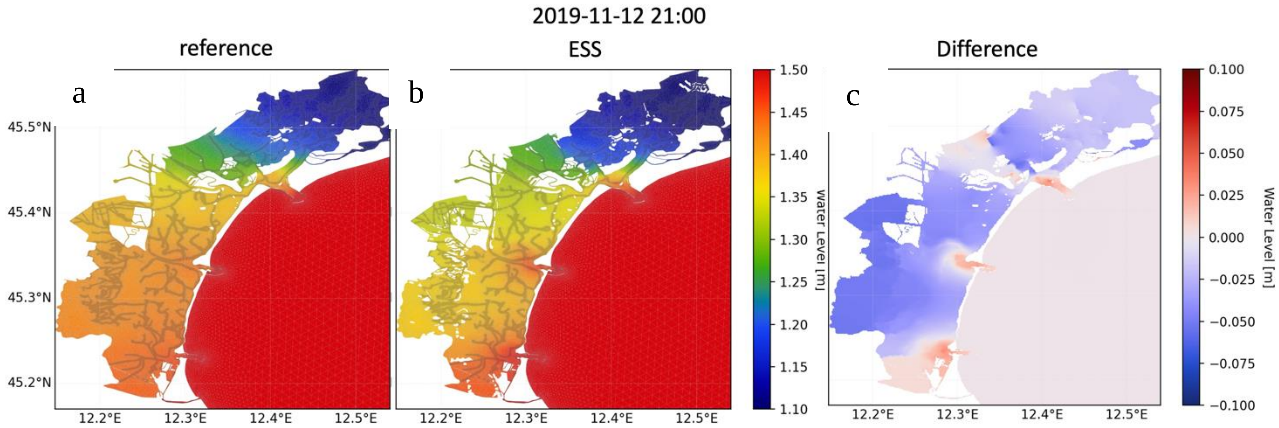

Figure 4.5.3: Water level (m) during a storm at the Venice lagoon. Left panel shows the reference run (without wetlands and seagrass), middle panel shows the simulation including wetlands and seagrass, right panels show the difference between the simulations.

In Figure 4.5.4 we report the time series of sea level for the reference and ESS-run configurations at point P1. For the entire period (and simulation), the ESS-run exhibited a smaller amplitude than the reference run, revealing that seagrass and wetland presence mitigate both high and low extremes. On average, the difference between the two runs has been quantified as approx. 2 cm, while the maximum difference was 9 cm.

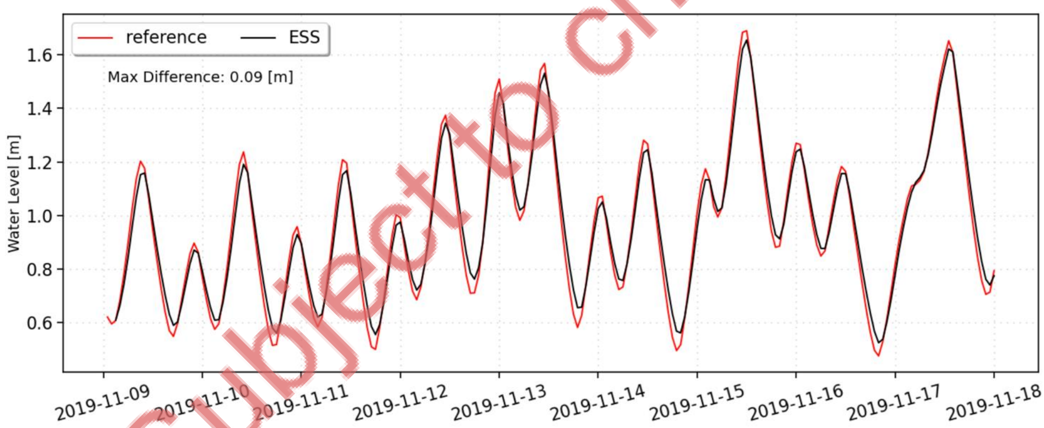

Figure 4.5.4: Water level (m) time series during the extreme event of November 2019 at P1 showed in Fig.4. Red line refers to the reference run (no seagrass, no wetlands), black line shows the ESS-run (inclusion of seagrass and wetlands).

The presence of wetlands and vegetation has a significant impact on the bottom stress, thus on erosion and deposition processes. For this reason, Figure 4.5.5 shows the spatial maps of bottom velocity for the reference and ESS-run simulations. All over the lagoon, excluding deeper channels, bottom velocity reached 20 cm/s maximum. The reduction of velocity in the ESS-run well reproduced the spatial distribution of the seagrass throughout the lagoon, although, due to the larger spatial vegetation covering is more evident in the Southern and Central lagoons.

The increase of bottom velocity, in some areas, related to the presence of wetlands and vegetated bottom is also appreciable. It is evident that wetlands reduce the section through which water flows, increasing the velocity, as shown at North of the Murano Island in the ESS-run. In addition to this, bottom velocity is also increased along the deeper unvegetated channels, more evident in the Southern lagoon, where water flows through lower resistance.

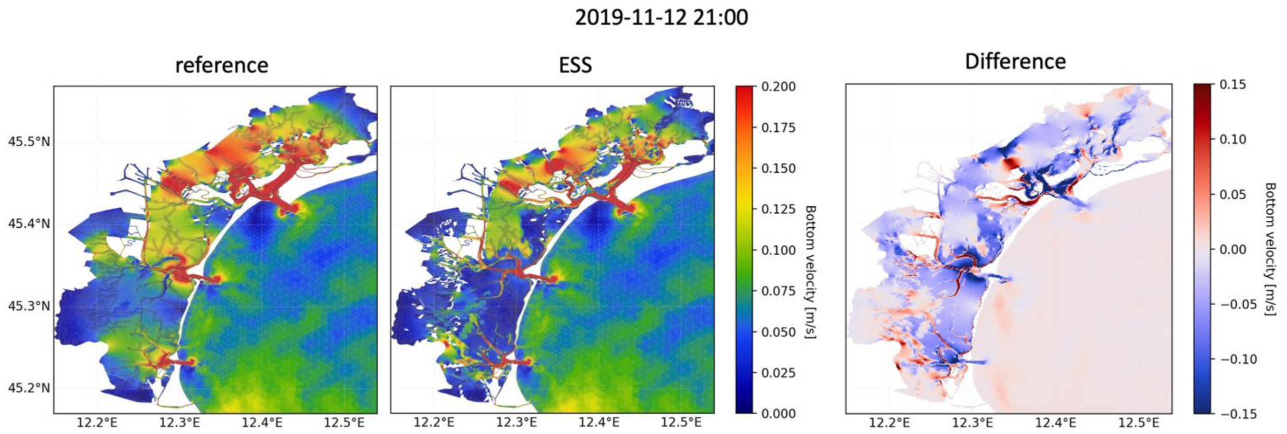

Figure 4.5.5: Water velocity at bottom (m/s) during a storm at the Venice lagoon. Left panel shows the reference run (without wetlands and seagrass), middle panel shows the simulation including wetlands and seagrass, right panels show the difference between the simulations.

4.6. Conclusions

In Task 2.1, CMCC developed an hydrodynamic-wave modelling system to simulate near past conditions at the Venice lagoon pilot for the assessment of ESS. Models have been validated using data from the CNR "Acqua alta platform", providing good accuracy and precision. Two configurations have been implemented: with wetlands and seagrasses, and without them. The comparison between the different configurations allowed to appreciate and quantify the ecosystem services due to the inclusion of wetlands and seagrass in the lagoon. Their role has been assessed both for hydrodynamics, through water level and water velocity at bottom, and waves through the significant wave height.

In detail, the comparisons carried out highlighted the following ESS:

- a reduction of wave height due to the presence of seagrass (on average -15%, in some cases above 30%) and, as expected, on a greater extent, wetlands;
- a reduction of water level (up to 5%) in the vegetated zones;
- a general reduction of water velocity at the bottom in the vegetated zones.

The work also identified a side-effect given by the inclusion of wetlands and vegetation in the lagoon which could be considered during planning of restoration activities. In particular, the increased bottom friction brought in some cases to the increasing water level along the main mouths during the flooding phase. Even currents at the bottom showed an increase along the unvegetated deeper channels and where the wetlands presence reduced the section through which water flows.

5. Multi-hazard forecasting (including a multidisciplinary calibration) and application limits Rhone Delta Pilot (TDV)

5.1. Introduction

The Rhone Delta Pilot, namely the "Former Saltworks", located in the south-eastern part of the Rhone delta (Figure 5.1.1), is an area of 6,527 ha which was acquired by the Conservatoire du Littoral (French "Coastal Protection Agency") between 2008 and 2012. For about 50 years, and until its sale in 2008 for industrial and economic reasons, this site was devoted to industrial salt production. The acquisition of this site by the Conservatoire du Littoral involved changes in management, compared to that implemented in an industrial salt production model. Water management by means of hydraulic pumps, as well as continuous maintenance of the dikes of the former salt production site in the context of sea level rise, was no longer economically sustainable without the financial benefits of salt production. In addition, with the existing dikes of the former salt production site, and without the use of hydraulic pumps to generate water flows, the Former Saltworks site would have been with no change in management a very confined site with long residence times. Due to the high evaporation rates in Mediterranean areas, this site would have been exposed to very high salinity and water absence for several months of the year, which would have been problematic for several plant species, birds and fish. In addition, the reconnections with the sea allow new biological connections on this site.

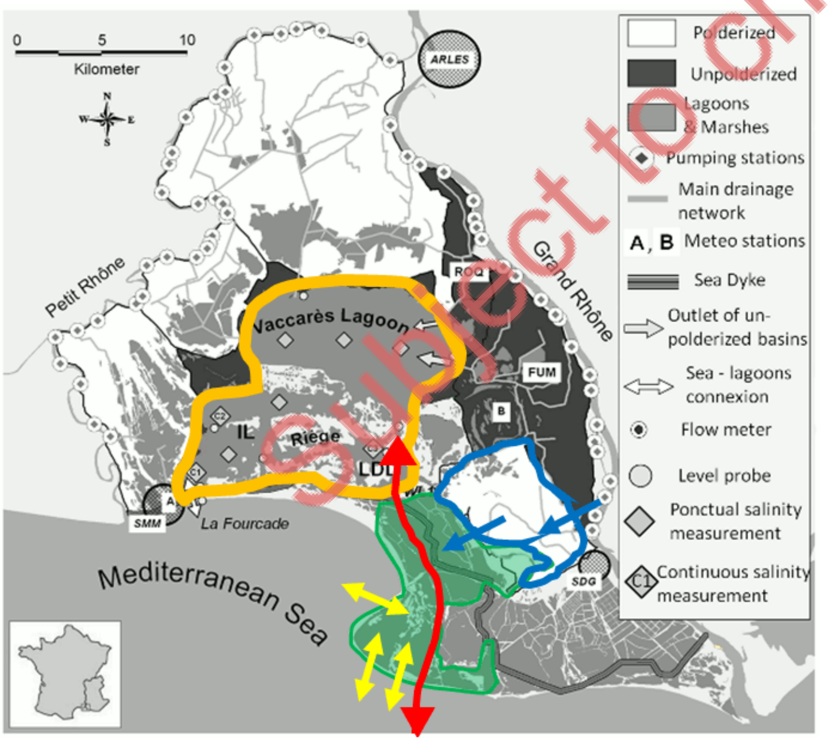

Figure 5.1.1: Location of the Fellow Pilot in the Rhone delta (in green). Also shown in blue is the agricultural catchment area reconnected to the Pilot Site, and in orange the central lagoons of the Rhone delta, which can be connected to the Pilot Site via a hydraulic structure. The new connections between the Pilot Site and the sea resulting from the choice to no longer maintain the historic dykes are indicated in simplified form by yellow arrows. The red arrow indicates the path of the main flows targeted by the restoration of the site.

It was therefore decided since 2010 to implement a realignment strategy on the site, by re-establishing gravity flows and no longer depending on pumping stations:

- The sea-dikes protection of the former salt production site are no longer maintained, and the protection effort is now focused on a maintained dike which is located about 7 km inland, resulting in a new 4600 ha "Climate change buffer area" between the former and the inland dikes.
- Several works have been carried out (opening of dikes, dredging works, etc.) to create connections between the various former salt production basins.
- Hydraulic works have reconnected the site to a nearby agricultural catchment, itself irrigated from the Rhone river, allowing new fresh water flows in the site.
- A new hydraulic structure was created to have the possibility to hydraulically connect the site to the central lagoons of the Rhone delta, namely the Vaccares Lagoon Hydrosystem, thus creating a reconnected whole of over 16,000 hectares.

Within REST-COAST, the following two types of restoration are implemented/pursued for this site:

- **passive restoration**, with the continued non-maintenance of the sea-dikes protection of the former salt production site.

- **active restoration**, which consists in accompanying the site managers in the implementation of a management of the remaining hydraulic works of the site which i) favours at the same time the biodiversity, the restoration of the habitats, the 5 ecosystem services considered in REST-COAST and the economic activities and ii) that adapts to the effects of the non-maintenance of the sea-dikes protection (e.g. continuous modification of hydro-saline exchanges with the sea with the non-maintenance of the former sea-dikes protection) and iii) that anticipates the effects of climate change.

The habitats targeted in REST-COAST for the Rhone Delta Fellow Pilot are: **Coastal lagoons** (N 1150); **Beach areas** (N 1140); **Mediterranean and thermo-Atlantic halophilous scrubs** (N 1420); **Salicornia and other annuals colonising mud and sand** (N 1310), and the associated plant species.

5.2. High-resolution coupled coastal models

In WP2, several models are developed for the Rhone Delta Fellow Pilot, in particular to study the consequences of restoration on ESS **"Water quality purification"** (through hydro-saline regulation), **"Reduction of coastal flooding risk"** and **"Reduction of coastal erosion risk"**. Furthermore, the results of these models will be used, in combination with data acquired in WP1 on GHG emission and sequestration, and historical data on fish populations, to study the consequences of the restoration on ESS **"Climate change regulation",** and **"Food (fish) provisioning".**

The models developed consist of three TELEMAC-2D hydro-saline models, one XBEACH morphodynamic model, and one model of the evolution of the coastline using SDAS.

5.2.1 Hydro-saline models

The three hydro-saline models used in REST-COAST for the Rhone Delta are implemented with the two-dimensional hydrodynamics code TELEMAC-2D.

Two models are specific to the Rhone Delta Fellow Pilot. Their objective is to show the influence of the restoration implemented on the hydro-saline dynamics of the site, with a particular focus on the ESS **"Water quality purification"** and **"Reduction of coastal flooding risk".** The first model simulates the hydro-saline dynamics of the site that would have occurred without the implementation of restoration. The second model simulates the hydro-saline dynamics of the site following restoration. These two models use the same mesh, but with different topo-bathymetric data. An example of the interpolated topo-bathymetry for the pre-restoration site is shown in Figure 5.2.1.

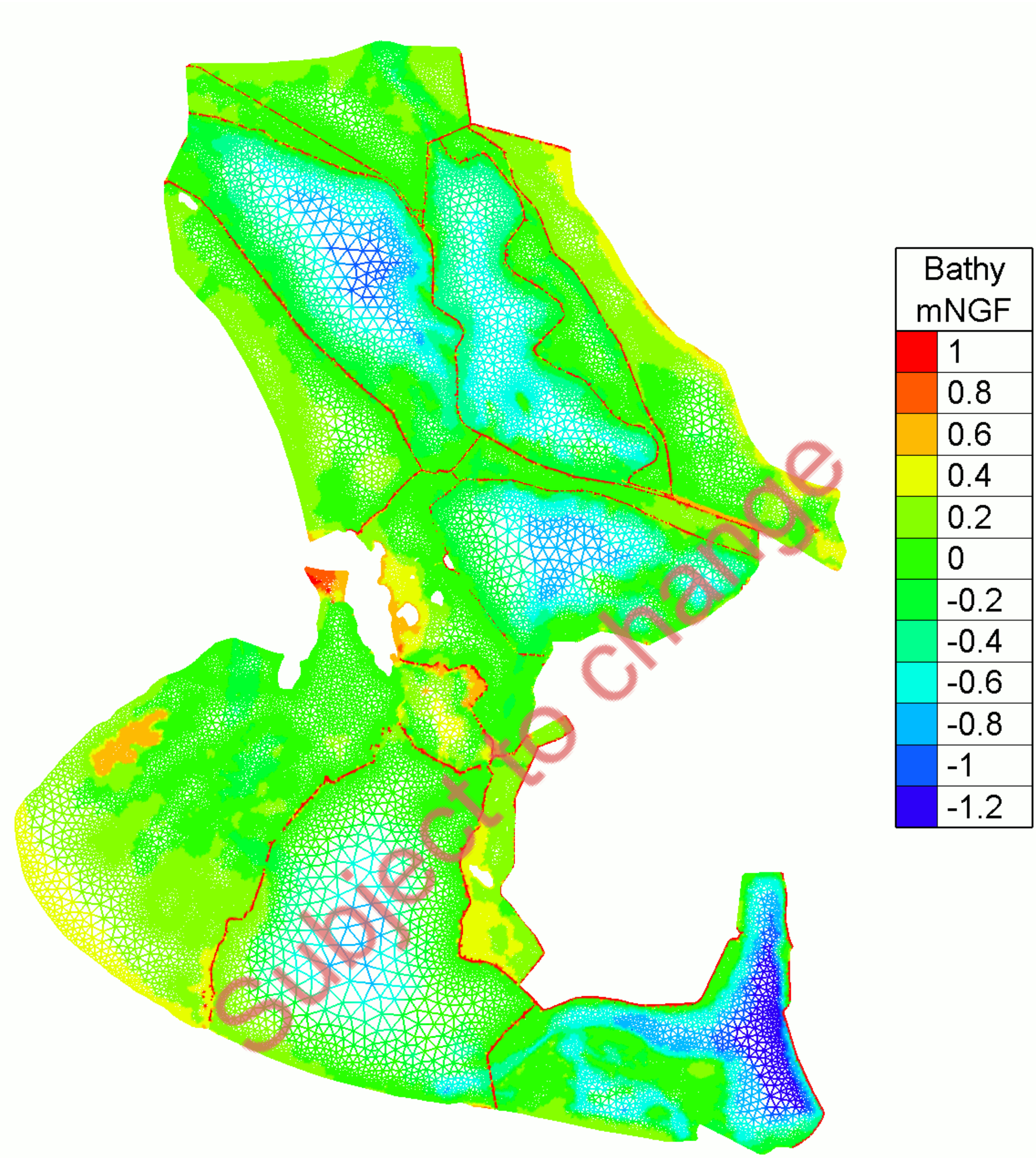

Figure 5.2.1: TELEMAC-2D mesh of the Rhone Delta Fellow Pilot, and interpolated topo-bathymetry for the configuration without restoration.

The third model (Figure 5.2.2) aims to study the influence of the restoration of the pilot site on the surrounding ecosystems, in the upscaling stage studied in REST-COAST. This model encompasses the Pilot site, and the system of lagoons located in the centre of the Rhône delta and the National Reserve of Camargue, in orange in Figure 5.1.1

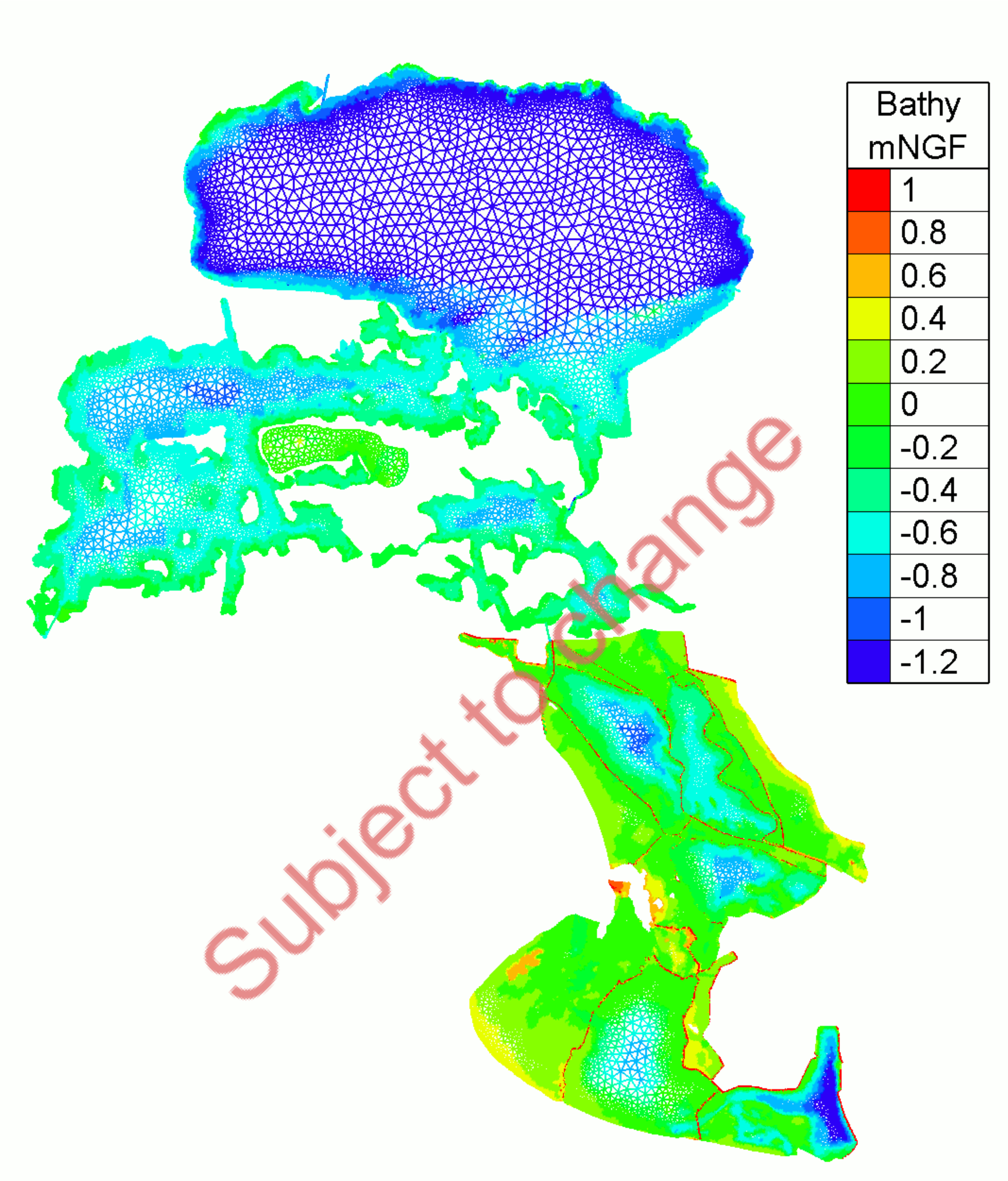

Figure 5.2.2: TELEMAC-2D mesh and interpolated topo-bathymetry of the Rhone Delta Fellow Pilot and the main lagoons of the central part of the Rhone Delta

For the three models, we use the hydrodynamic model TELEMAC-2D to simulate the hydrodynamics, water temperature and salinity dynamics. The choice of using a two-dimensional model is justified by the very shallow depths of the systems studied, the absence of water over a large part of the site for a good part of the year, and measurements of salinity and temperature carried out vertically at several points of the site, showing no notable difference in these two variables.

The TELEMAC-2D software solves the second-order partial differential equations for depth-averaged fluid flow derived from the full three-dimensional turbulent Navier-Stokes equations (Hervouet, 2007, 2000). This provides a system consisting in an equation for mass continuity and two force-momentum equations. The equations are averaged over the vertical by integrating from the bottom to the water surface by considering the assumption of the Shallow Water equations (hydrostatic pressure and vertical velocity negligible).

The averaged form of the continuity equation is:

$$\frac{\partial h}{\partial t} + \vec{u}.\vec{\nabla}(h) + h.div(\vec{u}) = S_h \qquad (5.1)$$

The averaged form of the momentum equations are:

$$\frac{\partial u}{\partial t} + \vec{u}.\vec{\nabla}(u) = -g\frac{\partial Z}{\partial x} + S_x + \frac{1}{h}div\left(h\nu_t\vec{\nabla}u\right) \qquad (5.2)$$

$$\frac{\partial v}{\partial t} + \vec{u}.\vec{\nabla}(v) = -g\frac{\partial Z}{\partial y} + S_y + \frac{1}{h}div\left(h\nu_t\vec{\nabla}v\right) \qquad (5.3)$$

with u and v the depth-averaged velocity components (m.s-1) in the x and y Cartesian directions, h the water depth (m), S_h the point injection or removal of fluid (m.s-1), ν_t the coefficient of turbulent momentum diffusion (m2.s-1), g the gravitational acceleration (m.s-2), t the time (s), Z the free surface elevation (m), S_x and S_y (m.s-2) the source terms of the momentum equation in u and v, respectively, including the Coriolis force, bottom friction, surface wind shear and source/sink of momentum in the domain.

Salinity and temperature are modeled as tracers, with equation 5.4:

$$\frac{\partial T}{\partial t} + \vec{u}.\vec{\nabla}(T) = S_T + \frac{1}{h}div\left(h\nu_T\vec{\nabla}T\right) \qquad (5.4)$$

where T is the tracer (in this study the salinity or temperature in psu and °C, respectively), ν_T the tracer diffusion coefficient (m2.s-1), and S_T the source or sink of tracer (psu.s-1 or °C.s-1). The influences of rain, evaporation and wind are taken into account in the model.

Equations 5.1 to 5.4 are solved using a finite element method on an unstructured mesh, made with more than 107,190 triangular elements of varying size and 55,081 nodes for the Rhone Delta Fellow Pilot (Figures 5.2.1), and 160,000 elements and 85,500 nodes for the model encompassing the lagoon in the central part of the Rhone delta. The advection of h (equation 1) is solved applying the conservative PSI (Positive Streamwise Invariant) scheme (Hervouet, 2007). The advections of u and v (equations 2 and 3) are solved applying a PSI distributive scheme with a locally implicit predictor-corrector and a full implicitation only in the dry zones (Hervouet et al., 2015). To solve the advections of T (salinity or temperature) we use the N distributive scheme with a locally implicit predictor-corrector and a full implicitation only in the dry zones (Hervouet et al., 2015). These numerical schemes, although time consuming, have the advantage of greatly limiting the numerical diffusion in the presence of dry zones, which can be temporarily covered by water.

For the temperature of water, the term S_T in equation 4 is the heat source $Q/\rho_w c_w h$, with Q the heat flux (W.m-2) between the atmosphere and the water, ρ_w is the water density, and c_w the specific heat of water. Q is computed by the following thermal radiative model (Ata, 2017):

$$Q = RS - RE - CV - CE + RA \tag{5.5}$$

with RS the sunray flux, RE the free surface radiation, CV the advection heat flux, CE the evaporation heat flux and RA the atmospheric radiation.

5.2.2 Morphological models

To study the morphodynamics of the site in relation to restoration, two types of modelling are used. The first, applied to the entire pilot site, is based on the use of the USGS DSAS tool. A study of the dynamics of shoreline change has been carried out from 1936 (date of the first usable data) to 2020 (Figure 5.2.3). Over this period, the results generally indicate a zone of accretion to the west of the site, and a zone of erosion to the south (Figure 5.2.3). Following this initial analysis with the available data, we will study the consequences of the passive restoration strategy implemented on the site by comparing, with DSAS, the dynamics of change before and after 2008, the date on which maintenance of the dikes in the south of the site stopped.

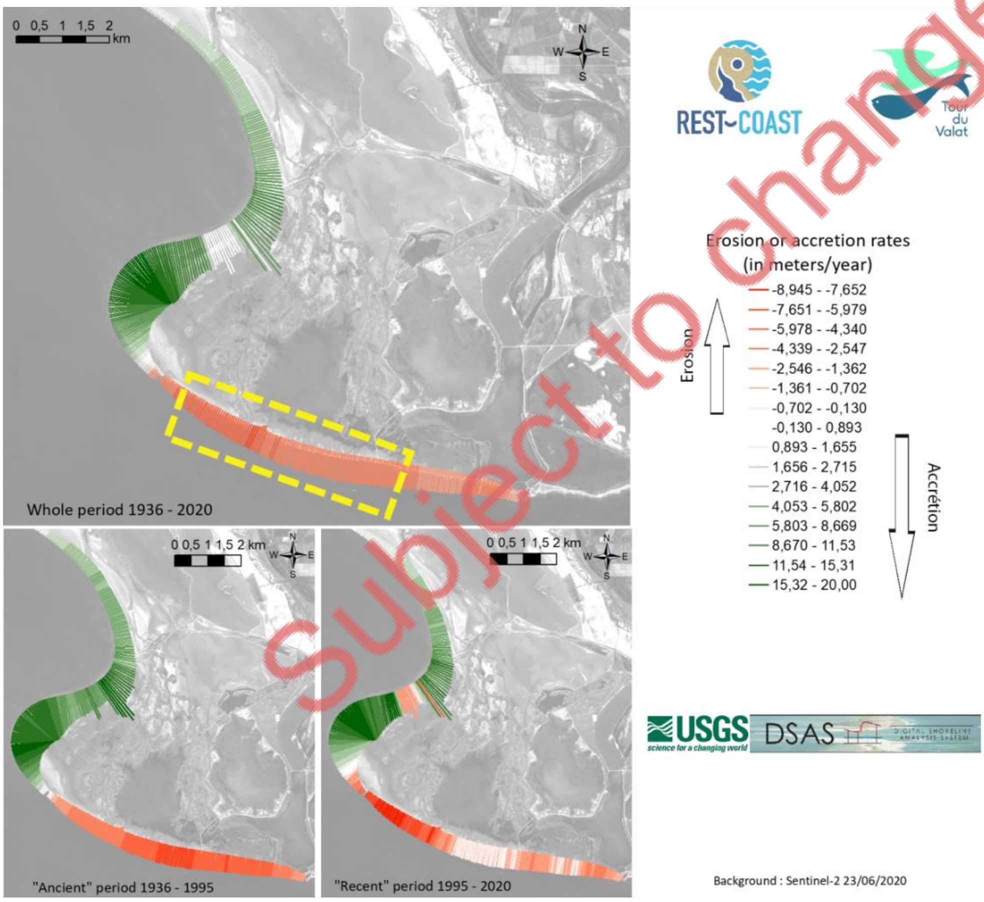

Figure 5.2.3: Results of DSAS: dynamics of the shoreline for several periods.

In addition to this analysis of the entire site, specific modelling using XBeach and TOMAWAC was carried out on one of the site's erosion zones, indicated by the yellow dotted lines in Figure 5.4, where a beach area was reconstituted to the north of the unmaintained dykes by overwash phenomena, and several new connections with the sea were formed during storms (Figure 5.2.4).

Figure 5.2.4: Aerial drone views highlighting the geomorphological dynamics observed in the southern part of the Rhone Delta Fellow Pilot with the non-maintenance of sea-dikes protection of the former salt production site. To the left: formation of new connections to the sea. To the right: creation of beaches areas. On both views the sea is on the left and the Fellow Pilot is on the right.

The TOMAWAC numerical model (Benoit et al., 1996) is made up of a triangular mesh (Figure 5.2.5). The cell sizes range from 500 m offshore to 20 m at the coast. The boundary conditions on the coast correspond to wave absorption conditions. On the other boundaries, Hs, T and directions were prescribed via ERA5 and the flow velocities were left free i.e. calculated by the model. The offshore domain extension corresponds to the location of the ERA5 model grid extraction point. The topo-bathymetry corresponds to a linear interpolation between different data sets (topo-bathymetric LiDAR with the Optech Titan DW600 of Nantes and Rennes French Universities, and bathymetry from the European Marine Observation Data Network, EMODnet).

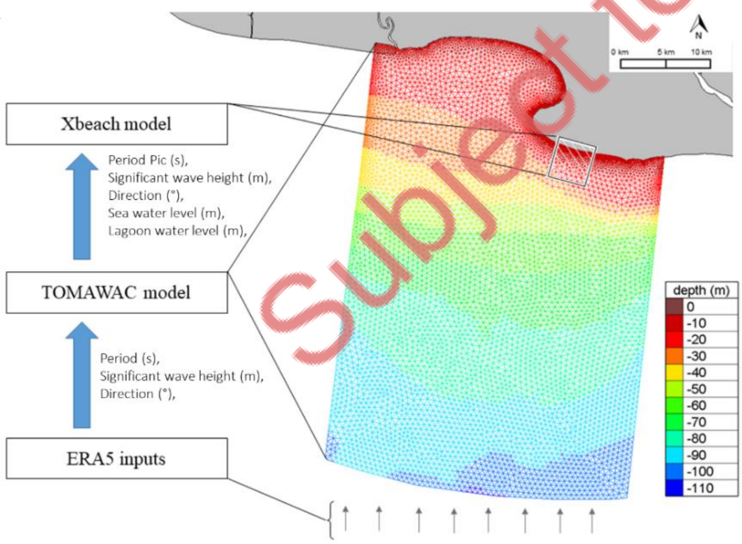

Figure 5.2.5: XBeach and TOMAWAV models used to investigate the qualitative geomorphological evolution of the southern part of the Former Saltworks during storm events.

The XBeach numerical model (Roelvink et al., 2010) is made up of a regular mesh comprising 280x201 cells of size 20m x 20m (Figures 5.2.5 and 5.2.6). The offshore domain extension corresponds to the location depth where the TOMAWAC model was validated. Short waves are generated from the JONSWAP spectrum using the peak wave period, Hs and direction from TOMAWAC model simulations at the boundaries of the Xbeach offshore domain (Figures 5.6). Temporarily varying water levels were applied in the lagoons and in the sea.

Water levels in the lagoon and in the sea correspond to the data recording every 5 min from two probes, one being located in the lagoon directly north to the non-maintained dike, and the other (sea level) being located at la Fourcade, see Figure 5.1.1 The topo-bathymetry corresponds to a linear interpolation of the same data sets as those used for the TOMAWAC model.

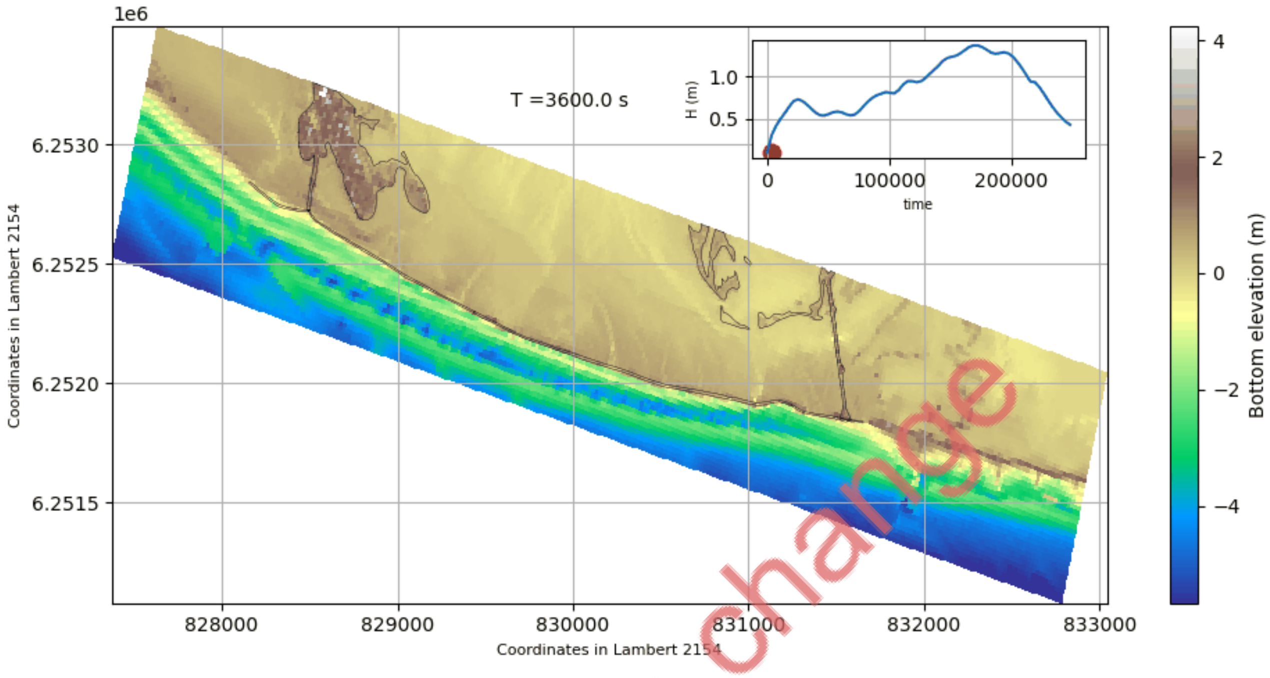

Figure 5.2.6: XBeach model used to investigate the qualitative geomorphological evolution of the southern part of the Former Saltworks during storm events. The location of the model is shown in Figure 5.2.5

5.3. Parameterization of hydro-morpho-eco interactions to simulate ESS.

During REST-COAST, the TOMAWAC and XBeach models did not require any specific developments, but rather classic calibration and validation stages by comparison with existing experimental data or data specifically acquired during REST-COAST.

On the contrary, the TELEMAC-2D models used to estimate the impact of restoration on ESS **"Water quality purification"** required significant development work. Thus, within REST-COAST, several code modifications had to be made to be able to simulate the hydro-saline dynamics of the Pilot Site, and quantify the benefits of the restoration on ESS **"Water quality purification"**, through hydro-saline regulation, and through improved water circulation in the site (decrease in residence time).

Due to the high evaporation on the Rhone delta, the overall shallowness of the pilot site, and the limited connection with the sea, a large part of the site is subject to periods of drying, with salt crystallisation/dissolution phenomena, as illustrated in Figure 5.3.1.

Figure 5.3.1: Illustration of the potential for prolonged drying out and crystallization of salts on the Rhone Delta Fellow Pilot.

Taking into account these phenomena of crystallisation/dissolution of the salts contained in the water is essential to correctly model the hydro-saline dynamics of this site, and thus study the consequences of the restoration of the site on **ESS "Water quality purification"**.

Furthermore, the predominance of evaporation on the evolution of water levels in these environments makes the methodologies based on concentration evolutions classically used to estimate the residence time of this type of environment not applicable.

Finally, the influence of salinity on evaporation is very often not taken into account in the models classically implemented on such sites.

In view of all these limitations of the current models, we have made the following changes to TELEMAC-2D within REST-COAST:

- <u>Modification n°1:</u> a simplified formalism has been implemented for taking into account crystallisation/dissolution of the salts
- <u>Modification n°2:</u> a new approach has been defined for simulating residence times in these hypersaline and choked wetlands
- <u>Modification n°3:</u> several terms have been added in the equations to take into account influence of salinity on evaporation rates.

To account for the possibility of precipitation and dissolution of salts, a source or sink term S_{salt} has been added to equation 5.4.

The rate of salt crystallization or dissolution S_{salt} is modelled with equation 5.6, as described by (Lionberger et al., 2004; Manganaro and Schwart, 1985):

$$S_{salt} = k_1 A_d \left(c_1 - c_1^* \right) \qquad (5.6)$$

Where k_1 is the average mass-transfer coefficient for salt dissolution (m.s^{-1}), A_d is the wetted area of the considered mesh element (m^2), c_1 is the concentration of salt in solution (kg.m^{-3}), c_1^* is the saturated concentration of salt in solution at the considered temperature (kg.m^{-3}). S_{salt} is expressed in kg.s^{-1}.

The hydro-saline dynamics of the site involve a large number of different salts. Indeed, when the seawater that has entered the site evaporates, it deposits its detrital particles and the ions it contains precipitate in the form of salts. The deposited materials constitute an evaporitic sequence. The order of precipitation of the salts is as follows: first ***CaCO3***, then ***CaSO4***, then ***NaCl***, then ***MgSO4*** and finally salts of ***Br*** and ***K.***

The phenomena of precipitation and dissolution of all these salts are complex. Their modelling is possible thanks to models such as PHREEQC (Parkhust and Appelo, 2013), but it requires the modelling of all the solid and aqueous phases of these salts, which, in the context of a coupling with a hydrodynamic model such as TELEMAC-2D solving the classical transport equations for each tracer, would lead to computation times that would be prohibitive for an application on a site of the size of the Rhone Delta Fellow Pilot. In the context of REST-COAST, a simplified approach has therefore been adopted, in which c_1 in the equation has been taken to the salinity (kg.m^{-3}). With this assumption, c_1^* in equation is the maximum salinity that can be reached in the system.

Acknowledging that ***NaCl*** is the major salt in the seawater entering the site, it was considered to be representative of the overall salt dynamics at the Pilot Site regarding the values of solubility, precipitation and dissolution rates, and the dependence of these quantities on temperature. This assumption allows only one tracer to be considered for salt dynamics, making it possible to use hydrodynamic modelling to the site with acceptable calculation times.

To estimate whether there is precipitation of the salts contained in the water column, or dissolution of the salts deposited on the bottom, we then decided to base ourselves on the solubility product of Sodium Chloride in water, equal to 358.5 g.L^{-1} at 20°C. As the solubility of sodium chloride varies little with temperature over the range of temperatures observed at the site (approximately 0 to 40°C), we also assumed that this solubility product was independent of temperature. In equation 5.6, c_1^* is then considered as independent of water temperature and is equal to 358.5 g.L^{-1}.

Increasing water salinity reduces evaporation since the dissolved salt ions lower the free energy of the water molecules, i.e., reduce the water activity, and hence reduce the saturation vapor pressure above the saline water at a given water temperature (Harbeck, 1955; Lee, 1927; Salhotra et al., 1985; Stumm & Morgan, 1981). The reduced latent heat flux of evaporation from saline water increases the surface water temperature, which promotes evaporation, yet, the effect of salinity overcomes the effect of temperature rise and the evaporation is eventually reduced (Salhotra et al., 1985).

Given the very high salinities that can be reached on the Pilot Site, leading to possible salt crystallization, the effect of salinity on evaporation must be taken into account. In our approach, it was decided to calculate in TELEMAC-2D this effect by adding the new equations 5.7 and 5.8 (Kokya and Kokya, 2008; Martínez-Alvarez et al., 2011):

$$e_s^* = \beta . e_s \tag{5.7}$$

$$\beta = 1 - 571.10^{-6} S \tag{5.8}$$

With β the water molar fraction, S the water salinity, e_s^* the the saturated vapour pressure for saltwater, and e_s the saturated vapour pressure above pure liquid water. The salinity-corrected e_s^* is then used in the various terms of equation 5.5.

Within REST-COAST, the benefits of the restoration on ESS "Water quality purification" is also estimated for the Rhone delta through improved induced water circulation in the site, which we study through the notion of residence time.

In lagoons, residence time is classicaly assessed through the mathematical expression given by (Takeoka, 1984a, 1984b), known as the remnant function. The remnant function $r(t)$ of the concentration is given as $r(t)=c(t)/c_0(t)$, where $c(t)$ is the concentration at time t of the passive tracer in the lagoon basin and $c_0=c(t=0)$ is its initial value. The **local residence time** $\tau(x,y)$can then be defined for every mesh node (coordinates x,y) as:

$$\tau(x,y)=\int_0^\infty r(x,y,t)dt \qquad (5.9)$$

2D or 3D hydrodynamic models are typically used to estimate local residence times: the tracer is released into the lagoon basin with an initial concentration corresponding to a given value and zero elsewhere, and its evolution is computed for each element of the grid domain, the computation being carried out till the ratio between c(t) and c_0 becames lower than 5% for all the elements of the mesh. The **global residence time** is defined as the highest value of all the local residence times. **However, a major assumption made during these simulations is that the water level in the lagoons does not vary, so c(t) can only decrease over time, as the water in the lagoon is replaced by 'outside' water**. This assumption is not applicable to choked sites subject to very high rates of evaporation, which may exceed the site's exchanges with the outside systems. In such sites, such as the Rhone Delta Fellow Pilot, the concentration $c(t)$ may increase over time due to evaporation.

Within REST-COAST, we had to adapt the formalism described above in order to calculate the residence time.

It was therefore decided to calculate for each node the local residence time $\tau_{Evap}(x,y)$ for these highly evaporative systems as follows:

$$\tau_{Evap}(x,y)=\int_0^\infty \frac{M(x,y,t)}{M_0(x,y,t_0)}dt \qquad (5.10)$$

With $M(x,y,t)$ the mass at time t of the passive tracer, and $M_0(x,y,t_0)$ its initial value.

To assess $\tau_{Evap}(x,y)$, we used TELEMAC-2D: a tracer is released into the Pilot Site with an initial concentration of 1kg/m^3 and zero elsewhere, and the evolution of its mass is calculated for each element. The global residence time has been defined as the time required for all the elements of the mesh to replace 95% of the mass of the conservative tracer originally released, with a volume of "new" water at least equal to the initial one. In other words, calculations are carried out until equations (5.11) and (5.12) have been verified for all the mesh elements of the site:

$$\begin{cases} \dfrac{M(x,y,t)}{M(x,y,t_0)}<0.05 \\ Vol(x,y,t)\geq Vol(x,y,t_0) \end{cases} \qquad (5.11) \text{ and } (5.12)$$

The global residence time is defined as the highest value of all the local residence times.

All the modifications required to calculate the residence time for these confined sites subject to heavy evaporation have been implemented in TELEMAC-2D for the purposes of REST-COAST.

5.4. Target operational period for testing the EWS nested into CMEMS products

For the Rhone delta, the EWS considered are linked to the risk of very high salinity levels on the site, closely related to the risk of prolonged drying out of the site, as well as to the risk of flooding.

In consultation with local stakeholders, the identified variables on which the EWS is based are:

- for the **risks of very high salinity levels and prolonged drying out of the site**:
    - for each location of the site, average, minimum or maximum **local salinity thresholds** during more than YYY days of for specific months
    - range of average **water levels** in different areas of the pilot for different months
    - drying of specific areas, i.e. **nil water depth** for more than XXX days.
    - **residence times** greater than ZZZ days in specific areas

- for the **risk of flooding**, the considered variables are:
    - **water depth** during flooding higher than XXX m and lasting more than YYY hrs at the foot of the inland dyke on which the protection effort is now focused
    - loss of xxx **ha of beach** south of the Fellow Pilot (wave damping)

Regarding the EWS linked to the risk of very high salinity levels and prolonged drying out of the site, the target operational period for testing the EWS must cover a sufficiently long period to have contrasting conditions of precipitation and evaporation, sea levels and flows at the outlets of the agricultural catchment areas connected to the site, over a period when all these data must exist and be usable (i.e. be of sufficient quality). Although flow data at the outlets of agricultural catchments only exist since 2015, when their connection to the Fellow Pilot was created, **the period chosen for testing the EWS is 2001-2022, for which several sub-periods will be studied.**

Regarding the EWS linked to the risk of flooding, the period chosen for testing the EWS is **1959-2022,** for which data of significant wave heights (Hs) and wave periods (T), are available from the ERA5 model at longitude 4.4° and latitude 42.9°, relevant for the Rhone Delta Fellow Pilot.

5.5. Hazard reduction from ESS as a function of restoration scale.

Where the dikes to the south of the site were not maintained, beaches appeared in some areas as a result of overwash, and in other areas new connections with the sea were formed (Figure 5.2.4). These restored natural coastal dynamics have consequences for the ESS considered in REST-COAST.

To study the hazards reduction from the ESS induced by the implemented restoration, the modelling tools developed to simulate the hydro-saline dynamics of the site before and after the restoration are being used. For each of the ”before/after” restoration configurations, the simulations' results are analyzed regarding the variables identified on which the EWS are based, as described in paragraph 5.4. This enables to quantify the impact of the restoration implemented on these hazards, through the considered **ESS “Water quality purification”**, **“Reduction of coastal flooding risk”** and **“Reduction of coastal erosion risk”**.

Furthermore, the results of these ”before/after” restoration simulations will be used, in combination with data acquired in WP1 on GHG emission and sequestration, and historical data on fish populations, to study the consequences of the restoration on ESS **“Climate change regulation”,** and **“Food (fish) provisioning”.**

The effect of restoration scale will also be studied: between the Rhone Delta Fellow Pilot (in green in Figure 5.1.1) and the central lagoons of the Rhone delta (in orange in Figure 5.1.1) there is a hydraulic structure that provides a possible connection between the two systems, but which is closed most of the time. The impact that the restoration of the Rhone Delta Fellow Pilot (new connections with the sea) could have on reducing the risk of very high salinity in these central lagoons, if this hydraulic connection was permanent, will be demonstrated using the REST-COAST modelling tools.

5.6. Conclusions

For the Rhone Delta Fellow Pilot, five models are used in the WP2 of REST-COAST. The DSAS tool did not necessitate any particular development or calibration. The XBeach model developed for the southern part of the Pilot Site did not require the development of new functions to study the consequences of restoration on the ESS considered, but it did require calibration and validation stages. The three hydro-saline models developed using TELEMAC-2D required the development of new functions, in particular to study the consequences of the restoration on ESS "Water quality purification".

In addition to making it possible to study the impact of restoration on ESS "Reduction of coastal erosion risk" and "Reduction of coastal flooding risk", the DSAS tool and XBeach model will make it possible to provide, in a prospective phase, possible scenarios for the evolution of the site's connections with the sea, which will be used in the hydro-saline modelling under TELEMAC-2D, enabling us to focus on the risk of flooding and the risk of excessive salinity over the whole site.

6. Multi-hazard forecasting (including a multidisciplinary calibration) and application limits Arcachon Bay Pilot (EGIS)

6.1. Introduction

Seagrass beds are present throughout all European coastlines and serve many critical ecological functionalities and ecosystem services amongst which: coastal inundation mitigation, erosion control and coastal stabilization, habitats for a high diversity of marine species and support of coastal fisheries, carbon capture and storage. As stated in the latest IPBES report (2019), these key habitats are declining rapidly worldwide including in Europe. Urgent large-scale actions must be undertaken for their preservation and restoration in order to enhance coastal resilience and tackle rapidly declining marine biodiversity. The EU Biodiversity Strategy for 2030 specifically mentions these habitats as crucial carbon-rich ecosystems to protect and the need to anticipate the climatic effects, which will trigger spatial shifts.

Following the REST COAST rationale, Egis contribution is proposed to be on the restoration of the functional coastal dynamics for large-scale Zostera recolonization at Arcachon Bay pilot site. Indeed, Zostera species show the most potential for rapid large-scale restoration given both their ecological traits and the current technology readiness of restoration methods. Specific Egis contribution to WP2 consists of preparing a risk assessment suite based on a hydro-morpho-eco coupled model with ESS parameterized as a function of restoration scale and climatic conditions.

6.1.1.Geographical and physical context for the simulation domain

Arcachon Bay is a semi-confined triangular-shaped lagoon, located in the southeast of the Bay of Biscay (the Aquitaine and Landes coast ; Figure 6.1). Offshore of the Bay, the narrowness of the shelf and the local topography lead to the generation of very weak barotropic tidal currents as well as weak tidal (Eulerian) residual currents (Lazure and Dumas, 2008). The mixed layer depth ranges typically from 10 to 20 m during spring, when thermal stratifications are more frequent than salinity stratification. Nonetheless, under particular conditions of winds (northwesterly), the Gironde river plume can reach that area (Puillat et al., 2006). Hence, water mass circulation in this area is governed mainly by winds and, secondarily, by density currents (Lazure and Jegou, 1998 ; Puillat et al., 2006 ; Lazure and Dumas, 2008).

The surface of Arcachon Bay is about 174 km2 at high tide, and about 65% of this surface emerges at low tide. The tidal cycle is semi-diurnal with a weak diurnal inequality; tidal amplitude ranges between 0.8 and 4.6 m for neap and spring tides, respectively, whilst the mean depth is 4.6 m. The Bay communicates with the sea through two main mouths, separated by the Arguin Bank. Many little streams run into the lagoon, but the two main rivers, the Eyre and the Porges Canal, contribute for more than 95% (73% and 24%, respectively) of the total annual freshwater inflows (Plus et al. 2009). The mean monthly flows range, respectively, from 8.4 to 38.6 m3 s-1 and from 1.8 to 12.9 m3 s-1 , for the Leyre and the Porges canal, with the maxima occurring in February and the minima in August.

The wind generates wind-waves as the second main hydrodynamic forcing in the Bay after tidal forcing (Parisot et al. 2008). The propagation of offshore waves within the Bay is limited due to the configuration and associated bathymetry at the entrance of the Arcachon Bay. Within the Bay, the main waves are generated by wind-induced processes. This process is nonetheless largely controlled by the tide which influences the water height and the length of the fetch.

Several types of sediments are present within the Bay. On the main entrance and in the channels, mainly medium sand (between 320 and 500 µm) and gravels are found. The secondary channels are mainly composed of sand and muddy sand (mix between 175 and 365 µm). The intertidal flats correspond to sandy mud ad muddy sands (Cayocca, 1996; Bouchet et al. 1997).

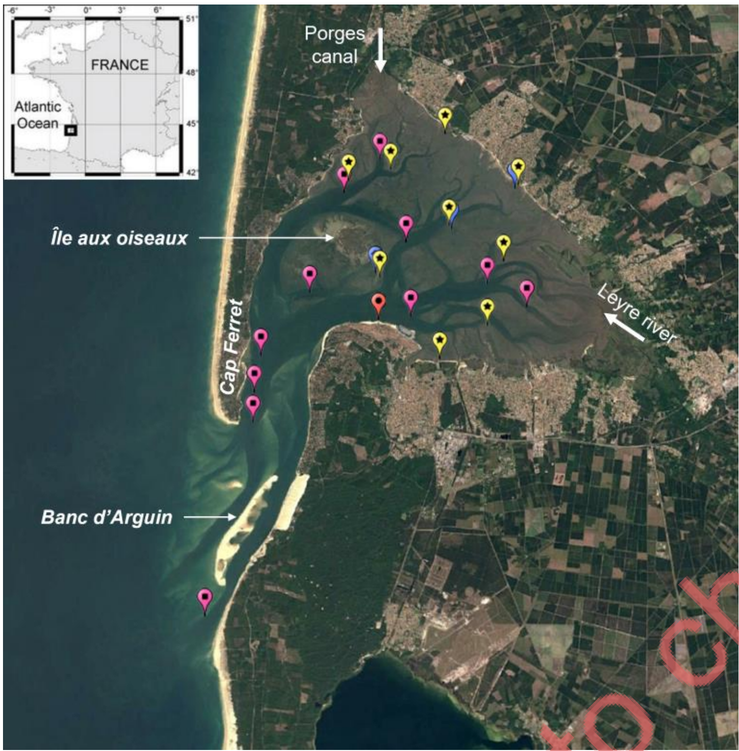

Figure 6.1.1: Overview of the Arcachon Bay area showing freshwater inputs and locations of the observations sampling stations used for validation. The map shows observation stations for hydrodynamics (yellow), waves parameters (blue) and sediment parameters (pink).

6.1.2. ESS provided by seagrass meadows

Ecosystem services (ESS) are widely used among scientists and policy makers to highlight the importance of the environment (including biodiversity) in sustaining human livelihoods (Convention on Biological Diversity, 2010, 1998; Costanza and Kubiszewski, 2012; Maes et al., 2016; La Notte et al., 2017). An important milestone of ecosystem service research was the Millenium Ecosystem Assessment (MA, 2005) which made prominent the idea that human well-being depends on ecosystems, and that such linkages can be tracked and framed through the notion of ecosystem services. The MA found that more than 60% of ecosystem services is being degraded or transformed endangering future human well-being. Ecosystem services research has since progressed at different levels—from theoretical conceptualization to practical applications (see Braat and de Groot, 2012; Egoh et al., 2012; Seppelt et al., 2011; Potschin et al., 2016 for a review).

The Zostera meadows located in the Arcachon Bay also provide ESS. Balle-Beganton et al. (2015) gives an overview of this ESS linked with anthropogenic forcings and activities, including: stabilization of soil in favorizing sediment deposition, improve water clarity, feed fishes and other species, improve biodiversity, stock carbon into sediment, etc.

In the Arcachon Bay, two species of Zostera meadows co-exist: Zostera noltii – mainly located in intertidal parts –, and Zostera marina – located in submerged areas on the edges of the channels –. However, a large regression of these seagrass species has been observed since the beginning of the 21st century, leading to an increase of fine sediment concentration inside the Bay and changing tidal dynamics as well (Cognat, 2019

; Figure 6.1.2). The reasons for this regression are not clear but main hypotheses link the regression to climatic events, water pollution and/or the set-up of feedback loops processes (Cognat, 2019). In the Arcachon Bay, the total surface of Zostera meadows has decreased by 38% and 85% for Z.noltii and Z.marina respectively between 1989 and 2012.

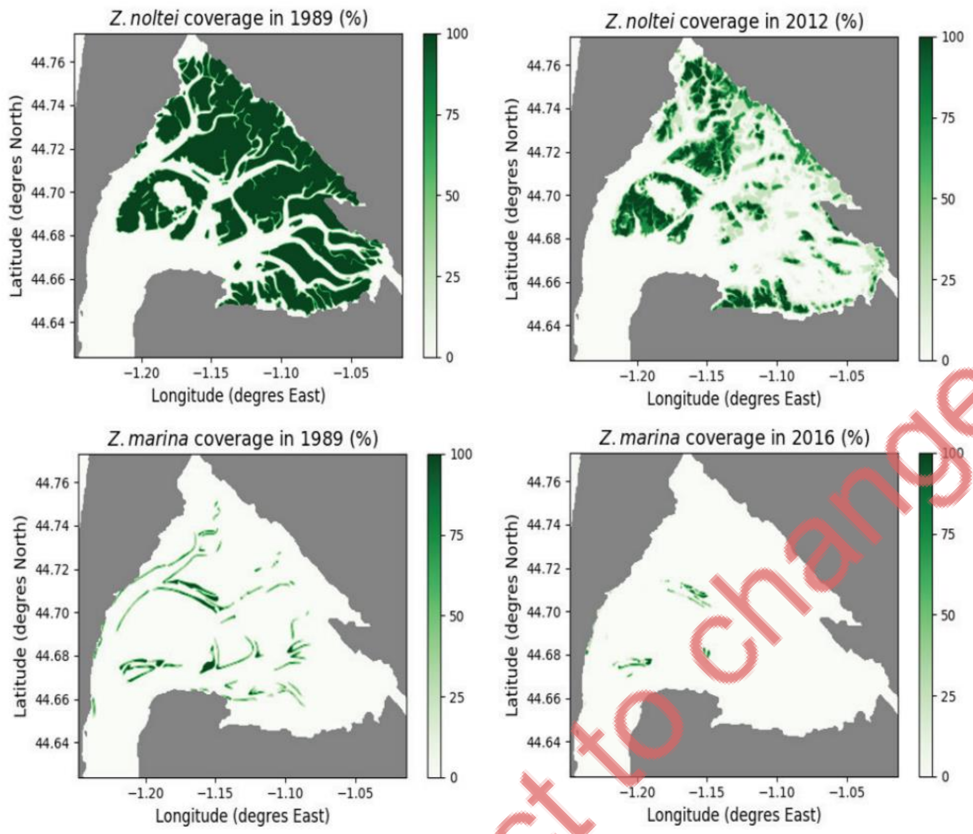

Figure 6.1.2: Map showing Zostera meadows decline (normalized area coverage) between 1989 (pre-regression state) and actual state : 2012 for noltii and 2016 for marina. From Cognat (2019).

6.1.3.Objective

Within the WP2 scope at the Arcachon Bay, the two main objectives are the assessment of (1) a potential reduction of coastal inundation risk and (2) coastal erosion risk due to the restoration actions. The species targeted by the restoration actions are the Zostera noltii seagrass meadows. The improvement of water quality, carbon sequestration and food production can then be considered as secondary objectives for the Arcachon Bay pilot.

Taking into account physical, social and economic contexts of the Arcachon Bay, the coastal erosion hazards refer to (1) the sedimentation of fine sediments within the Arcachon Bay – increasing the requirements for dredging activities within the harbors –, (2) the erosion of the intertidal areas, and sedimentation and migration of the channels – affecting the location of oyster natural reefs and thus the health of the biodiversity. The coastal flooding hazard refers to the coastal inundation extent in areas bordering the Arcachon Bay with impacts on population and infrastructures.

6.1.4.Methodology

In order to estimate those hazards, a coupled model is developed, describing wind-induced waves propagation, hydrodynamics and morphodynamics. Based on the Delft3D Flexible Mesh suite (DFM), the model also includes the effect of marine vegetation in dampening wave energy and current velocities, as well as reducing turbidity levels and sediment transport rates. The effects of seagrass meadows are now implemented in the coupled model and have a non-neutral impact on the assessment of coastal flooding and erosion hazards (M2.1). The wave propagation and hydrodynamics are simulated and the coupled model is validated (M2.2) using in situ observations. At this stage, further improvements are required for the validation of the morphodynamics.

This chapter therefore presents activities and modelling results as follows:

- Presentation of the modelling tools and how the vegetation is implemented in the coupled model in sections 1.2 and 1.3.1,
- Sensitivity analysis for the definition of vegetation parameters in section 1.3.2,
- Validation of the coupled hydro-sedimentary model in section 1.3.3,
- Description of operational period for testing the coupled morphodynamic model in section 1.4,
- Results concerning hazard assessment in section 1.5.

6.2. High-resolution coupled coastal models

6.2.1.Modelling platform presentation

Within this project, the DFM platform is chosen to address the different objectives in term of hazard assessment. Therefore, the coupled model is set-up to simulate wave generation and propagation, hydrodynamics, sediment transport and morphodynamics. Different modules are coupled (Figure 6.2.1) with the effect of the vegetation on hydrodynamics taken into account.

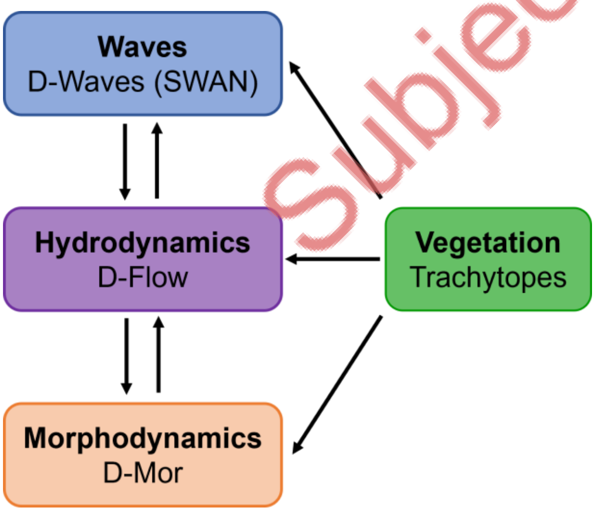

Figure 6.2.1: Diagram representing DFM coupled modules. Arrows are indicating interactions between modules. The vegetation module affects waves propagation, dampen currents and decrease sediment erosion.

The main module is the D-Flow module, computing hydrodynamics resulting from tidal, meteorological and continental inflows perturbations. It solves non-linear shallow water equations in two dimensions, following

Boussinesq assumptions on Navier-Stokes equations. D-Waves is based on a third-generation SWAN model, computing generation and propagation of waves, accounting for non-linear wave-wave interactions and wave dissipation. Sediment transport and bed updating (morphological changes), varying from erosion/sedimentation fluxes, is calculated by D-Mor module. Both bedload and suspended sediment transport are calculated, due to waves and currents. In addition, different types of sediments can be defined, following non-cohesive and cohesive sediment transport formulations. To take into account the complex sand-mud mixtures present within the Bay, the formulation of Van Ledden (2003) is followed, coupled with Van Rijn (1993) transport formula for sand.

In practice, two models are used: (1) a flooding hazard model (FH model) including wave propagation, hydrodynamics, and vegetation, and (2) a coastal erosion hazard model (CEH model) including hydrodynamics, morphodynamics and vegetation.

6.2.2. Model configuration

The model is implemented on a 2D curvilinear grid (6.2.2.), with a resolution ranging from about 300 m near the offshore boundaries to 100 m in the Arcachon Bay. The bathymetry is based on bathymetric surveys processed by Ifremer in 2016. The coupled model is forced by: meteorological data (coming from reanalysis model ERA5 by ECMWF), tidal harmonic components (deducted from tidal gauge timeseries located in Arcachon harbor), freshwater inputs from the Leyre river, and offshore waves from IOWAGA database (waves characteristics products coming from large-scale model; Ardhuin et al. 2014). The vegetation is initialized with the actual cover, measured in 2012 for Zostera noltii and in 2016 for Zostera marina.

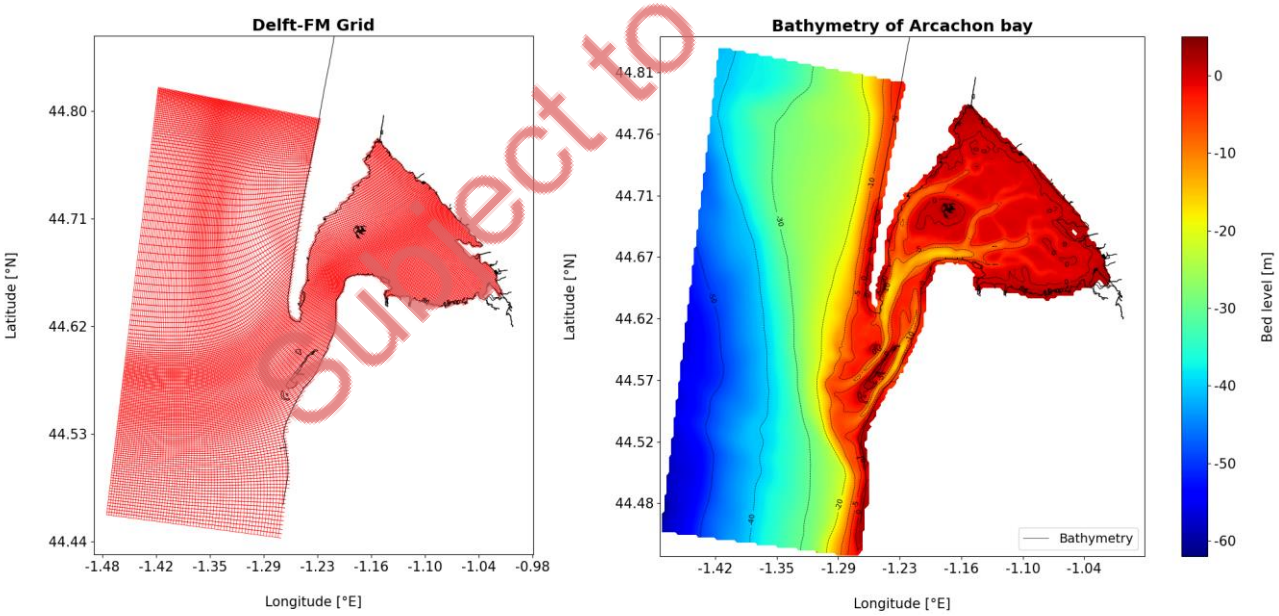

Figure 6.2.2: DFM curvilinear grid (left). Initial bathymetry applied in the model (m with respect to MSL ; right).

Depending on the modelling purpose, different time scales are considered. A first aim is to calibrate and validate the hydrodynamic model. To that end, in-situ observations available at different sampling stations located within the Arcachon Bay (Figure 6.1) are used. Those stations measured water levels (m ; 9 sampling stations), wave characteristics (Hs in m, Tp in s, Direction in °N, etc. ; 3 stations), and sediment characteristics and concentrations (11 stations) during the 2015-2016 period. Data collected in 2015 are used to calibrate both FH model and CEH model. Then, the FH model is validated against data collected in 2016. The CEH model is validated against sediment concentration data collected in 2016 and morphological changes occurring between 2016 and 2019 (from new bathymetric surveys made by SIBA, Syndicat Intercommunal du Bassin d'Arcachon).

6.3. Parameterization of hydro-morpho-eco interactions to simulate ESS.

6.3.1. Including vegetation module

The effect of seagrass meadows is implemented in the coupled model in order to have a non-neutral impact on the assessment of coastal flooding and erosion hazards (M2.1).

Following the formulations of Baptist (2005), the effect of the vegetation on flow resistance and bed roughness are separated. Actually, some formulations only consider the calculation of the flow resistance by means of the increase of the bed roughness (James et al. 2012). However, it leads to higher bed shear stress and larger sediment transport rates in case of morphological modelling. This is typically the opposite to what is expected. In the trachytopes formulations used in DFM, a $-\frac{\lambda u^2}{2}$ term is included in the momentum equation where λ represents the flow resistance of the vegetation, and u the flow velocity.

The vegetation is also dampening the energy of waves. It is expressed with the formulation of Mendez and Losada (2004) following the work of Dalrymple et al. (1984) on cylinders, which was implemented in SWAN by Suzuki et al. (2012):

$$S_{d,\ veg} = -\sqrt{\frac{2}{\pi}} g^2 \widetilde{C_D} b_v n_v \left(\frac{\tilde{k}}{\tilde{\sigma}}\right)^3 \frac{\sinh^3(\tilde{k} l_v) + 3\sinh(\tilde{k} l_v)}{3\tilde{k}\cosh^3(\tilde{k} h)} \sqrt{E_{tot}}\, E(\sigma,\theta)$$

Where $\widetilde{C_D}$ is a bulk drag coefficient, $\tilde{k}$ is the mean wave number, $\tilde{\sigma}$ is the mean wave frequency, h is the water depth, E_{tot} is the total wave energy, and E is the wave energy at frequency σ and direction θ. The vegetation is defined by b_v the width of individual plants, n_v the number of stems per unit area, and l_v the height of the vegetation. Beudin et al. (2017) schematically represents the effect of vegetation on hydrodynamics (Figure 6.3.1), highlighting vertical current profiles and turbulence schemes.

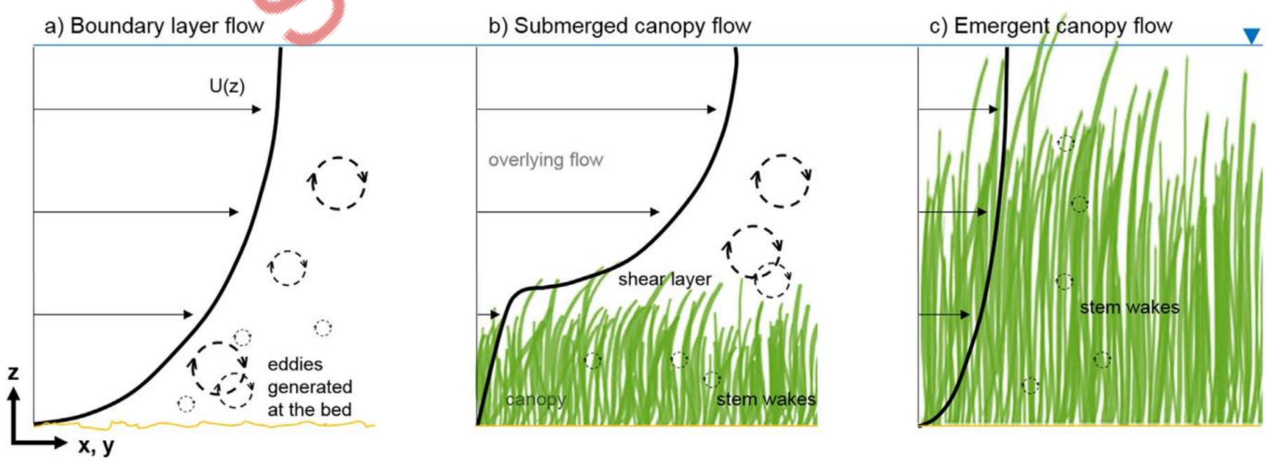

Figure 6.3.1: Sketch of different flow regimes showing the dominant source of turbulence (left: bed, center: the top of canopy, right: stem wakes). From Beudin et al. (2017).
In the simulations, the vegetation is spatially fixed and its parameters are not changing over time. A summer configuration is considered and a sensitivity analysis is conducted on vegetation parameters (see next section). Table lists the parameters used for representing the vegetation in the coupled model.

Table 6.3.1: Vegetation parameters used in coupled modelling. They correspond to summer configuration (Mütterlein et al. 2016).

Normalized cover(-)	Leaf length l_v (m)	Leaf width b_v (m)	Leaf density n_v (n.m^{-2})	Drag coefficient C_D (-)
< 0.25	0.13	1.1	20 000	0.7
$0.25 \leq . < 0.75$	0.14	1.1	40 000	0.7
≥ 0.75	0.20	1.1	80 000	0.7

6.3.2.Sensitivity analysis concerning vegetation parameters

In order to better understand the influence of vegetation on hydrodynamics components, different vegetation configurations are used. In particular, Mütterlein et al. (2016) suggested parameter values for coverage, leaf length, leaf width and leaf density used in the MARS3D model and representative of the Arcachon Bay. The latter model is developed by Ifremer and integrate vegetation as well (e.g. Kambiadou et al. 2014 ; Cognat, 2019). They suggested different configurations depending on the season, as it is known that those parameters have higher values in summer than in winter.

With the aim to assess the impact of vegetation on hydrodynamics components, Figure 3.3.2 shows the vertically averaged currents anomaly (m.s-1), averaged on an entire tidal cycle, between with and without vegetation and between summer and winter configurations. On the left panel of Figure 6.3.2, the current velocities are reduced all over the areas where vegetation is established. On intertidal areas, the reduction in current velocities is greater than 0.14 m.s-1. Along the decrease on the tidal flats, current velocities are greater in the channels. This should lead to larger erosion of the channels and higher sedimentation on the tidal flats with vegetation. On the right panel of Figure 3, a clear decrease of currents in vegetated areas can be observed when differentiating between summer and winter configurations, but it does not affect the whole Arcachon Bay.

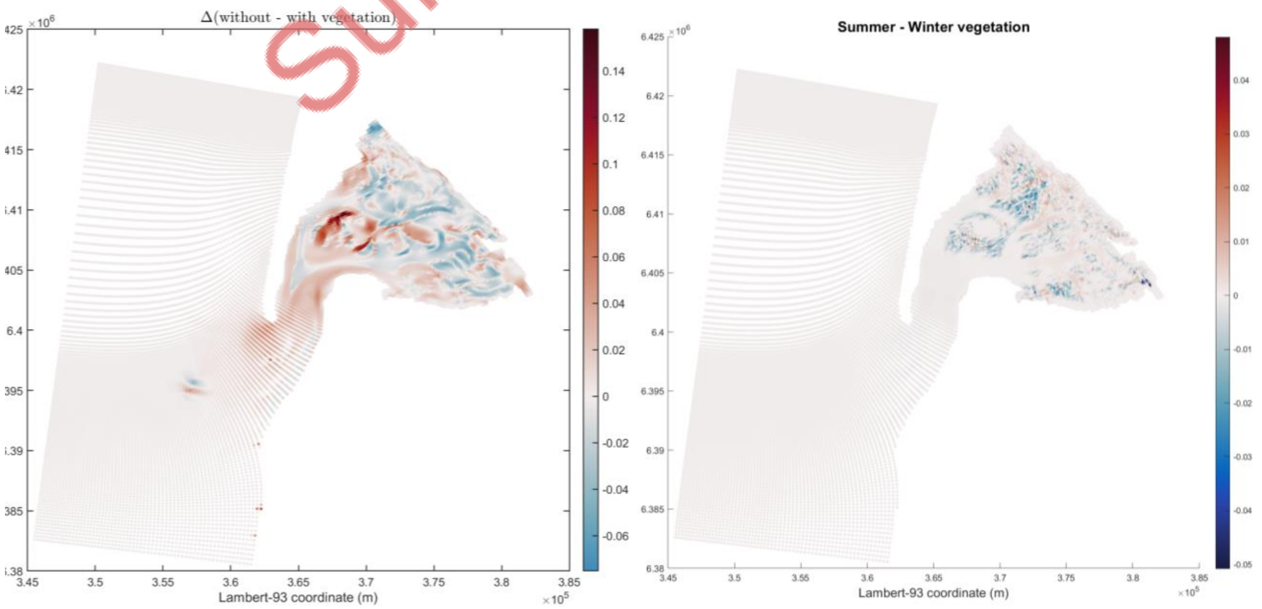

Figure 3.3.2: Vertically averaged currents anomaly (m/s) for the difference between with and without vegetation (left), and between summer and winter vegetation configurations (right).

On Figure 6.3.3, the different configurations are compared in terms of water levels, in several stations located within the Arcachon Bay. Tide propagation within the Bay is affected by the presence of vegetation. The asymmetry between ebb and flood is more pronounced, in particular on tidal flats areas. In the presence of vegetation, water levels are generally higher at high tide on those stations, with about 20 cm gap at high tide. However, no notable difference between the summer and winter configurations is observed.

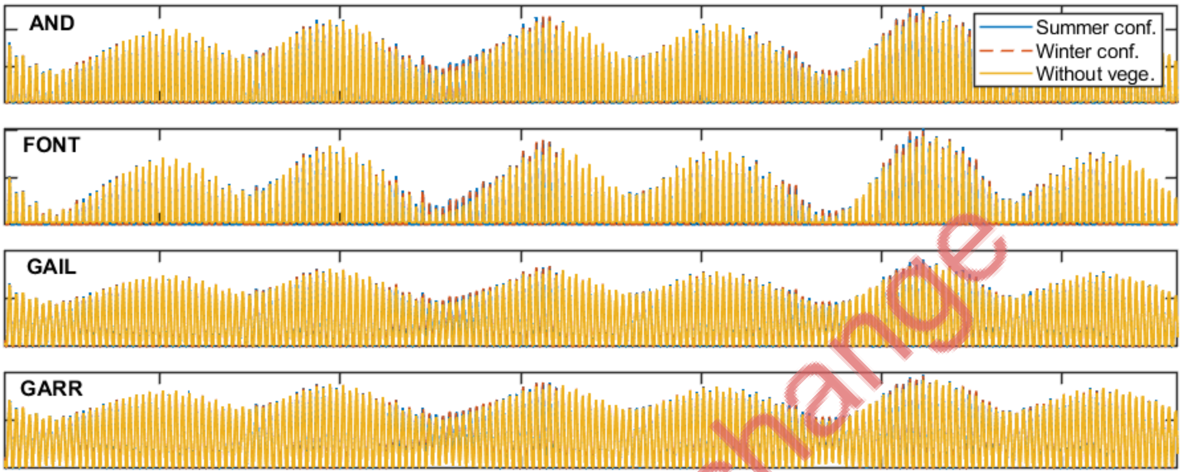

Figure 6.3.3: Water levels (m) during several tidal cycles for different vegetation configurations: without (yellow), winter (blue), summer (red).

To evaluate the effectiveness of restoration scenarios, the summer configuration is used for the next steps.

6.3.3. Validation of the coupled model using in-situ measurements

In-situ observations for water levels and wave characteristics were available for the period 2015-2016. Those data were collected and exploited by Cognat (2019) and Le Pevedic (PhD in progress). The hydrodynamic part is validated against water level observations (Figure 6.3.4). The model results show a good agreement with in-situ data with a slight over-estimation of the water levels at stations closer to the coastline (about 10 cm).

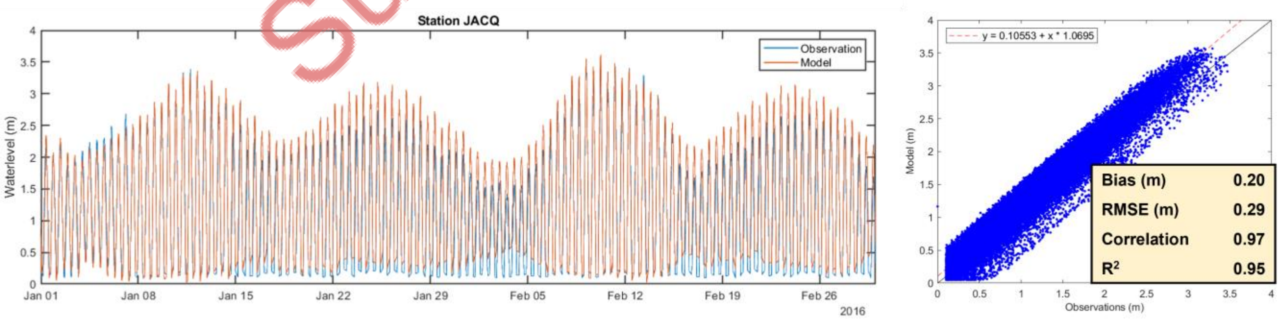

Figure 6.3.4: Water levels (m) for JACQ station over months Jan. and Feb. 2016 (left). Regression diagram comparing observations of the 9 sampling stations within the lagoon, and model results for the entire period of simulation (right). The equation of the linear regression is indicated.

With respect to the wave characteristics, the model results are compared to in-situ observations at 3 sampling stations. Observations of significant wave heights (H_s), wave period at peak (T_p) and spectra are compared to model results (Figure 6.3.5). Waves within the Arcachon lagoon are mainly induced by wind processes. Therefore, meteorological forcing schematization and good representation of wind processes in the model are very important to assess waves characteristics within the bay. The applied meteorological forcings are hourly estimates from ERA5 products, although over-estimation of wind velocities has been noticed (Molina et al. 2021), leading to discrepancies in wave characteristics estimations. Furthermore, spectral analysis of waves components from in-situ observations hold some uncertainties. Still, taking into account those uncertainties, the model results show good agreement with in-situ observations. The determination coefficient reaches 0.6 for GARR station, located within the Arcachon Bay, near intertidal areas. The wave heights are thus under-estimated by the model with gaps between observations and model results increasing with higher values of H_s. With hourly forcing for winds, it is acceptable not to catch every peaks measured at observation stations but this should be taken into account in assessing coastal flooding hazard.

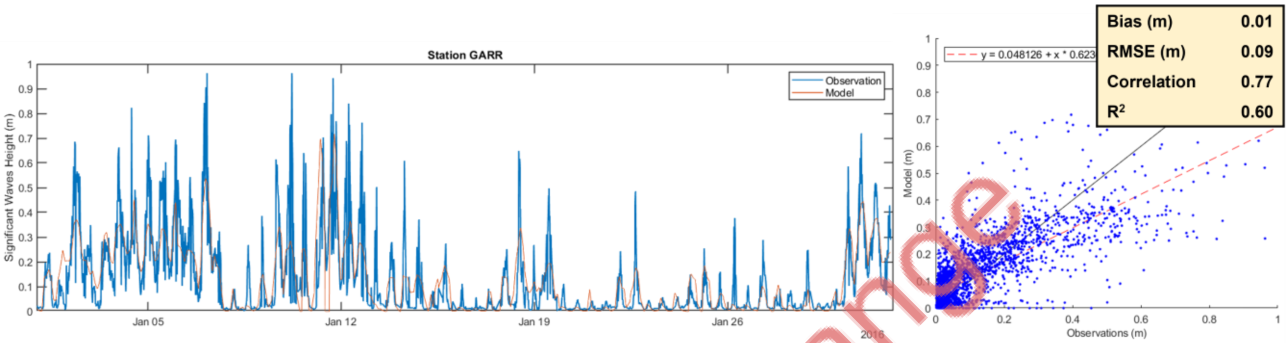

Figure 6.3.5: Significant waves height (m) for GARR station over the period 2015-2016. Regression diagram for the entire period of simulation (right). The equation of the linear regression is indicated.

In terms of current velocities, no in situ observations were available over the studied period. However, the validated modelling platform MARS3D, implemented by Ifremer on the Arcachon Bay (Lazure and Dumas, 2008 ; Ganthy, 2011 ; Kombiadou et al. 2014 ; Cognat, 2019), provides current velocities estimates for the 2015-2016 period. Results obtained with the D-FM coupled model are then compared to MARS3D results over an entire tidal cycle (Figure 6.3.6). Within the Arcachon Bay, the currents are shown to be very close to those calculated by MARS3D. The highest discrepancies between the two models are located around the entry of the Bay, in the channels, still at locations where MARS3D model has not been calibrated.

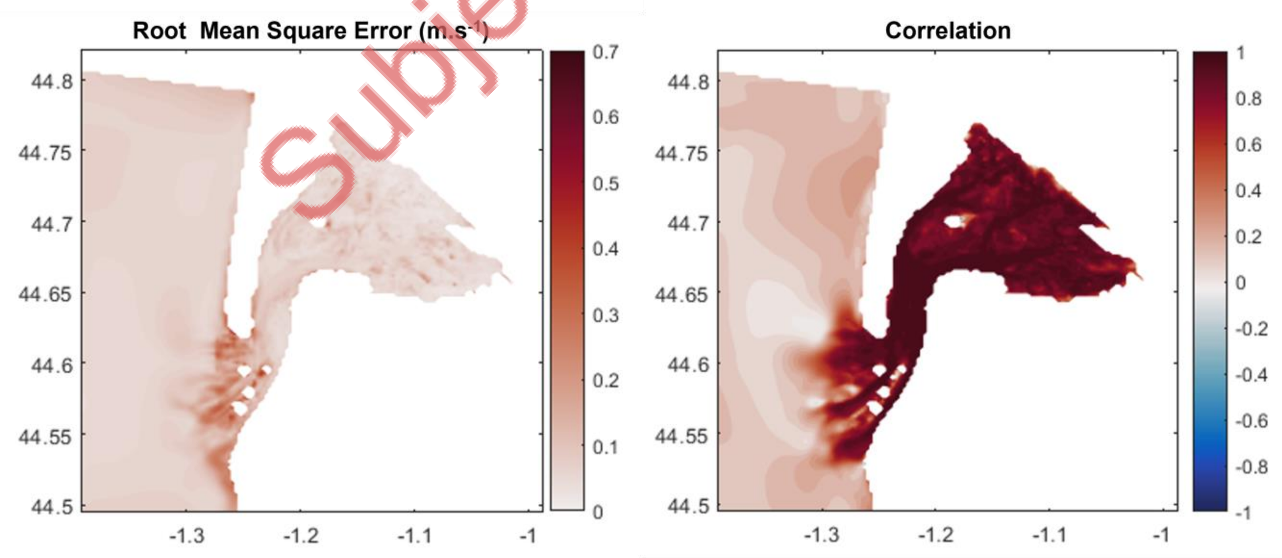

Figure 6.3.6: Map of Root Mean Square Error (m/s), averaged over one tidal cycle, between the coupled DFM model results and MARS3D results (left). Map of correlation coefficient, averaged over one tidal cycle, between the two models results (right).

In addition to hydrodynamics parameters detailed above, sediment characteristics were also available on the 2015-2016 period. The aim of the WP2 at Arcachon Bay is also to work on erosion/sedimentation and water quality linked to sediment dynamics. To ensure addressing these objectives, the CEH model is validated against sediment concentrations collected in 2016 and morphological changes occurring between 2016 and 2019 (from new bathymetric surveys made by SIBA). On the 2015-2016 period, bi-monthly sediment concentration measurements were available within the Arcachon Bay. Figure 6.3.7 shows the comparison between model results and in situ observations.

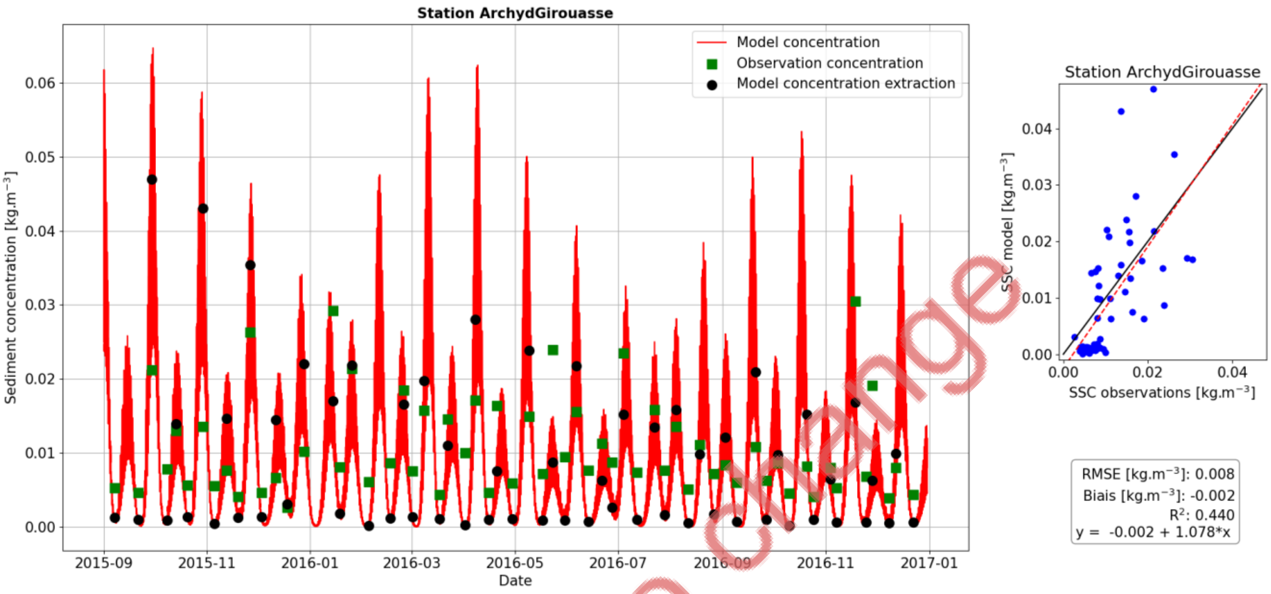

Figure 6.3.7: Suspended sediment concentration (kg.m-3) for Girouasse station over 2015-2016 period. Regression diagram for the entire period of simulation (right). The equation of the linear regression is indicated.

Model results are in the same order of magnitude than in-situ observations. For low sediment concentrations, model results tend to under-estimate the observed concentrations. The determination coefficient remains satisfactory with 0.44 at the Girouasse station.

The validated coupled model enables to : (1) include wave generation and propagation from wind forcing; (2) correctly represent hydrodynamics due to meteorological forcing, tidal processes and with wave coupling; (3) adequately represent sediment transport and resuspension, including 3 types of sediments; (4) include the effect of vegetation on waves, hydrodynamics and erosion/sedimentation patterns.

6.4. Target operational period for testing the EWS nested into CMEMS products

In the context of assessing coastal flooding and erosion hazards for present climatic conditions, and in order to test the developed coupled model, including sediment morphodynamics, operational periods are defined.

After the implementation, development and calibration of the sediment transport and morphodynamics module, the concept of morphological factors is applied aiming at: (1) reducing the computational time of coupled simulations, and then (2) applying the coupled model to simulate longer period of time. A morphological factor is an acceleration factor for morphological changes that should occur during an interval of time (called 'Morfac'; Roelvink, 2006). For example, if one month is simulated, and Morfac is set to 12, then the obtained morphological changes correspond to a one-year evolution. To do that, representative

forcings of the entire considered period are determined and reduced to the simulated period. Only tidal forcing is considered given the tide is the main process for sediment transport in the Arcachon Bay.
A model calibration is currently ongoing with aim at defining the appropriate tidal forcing reduction and associated morphological factor. To do so, a sensitivity analysis is carried out for assessing the influence on these two aspects (work in progress).

To validate the implementation of the morphological module in the coupled DFM model, a simulation will be then conducted over the period 2016 to 2019 (work in progress), given that two bathymetric surveys of the Arcachon Bay are available in 2016 and 2019. The results obtained using the morphological factor approach will be additionally compared to the results obtained based on a real-time simulation and covering the 3-years period.

The assessment of coastal erosion hazard will then follow, with new possibilities in terms of long-term morphological application. For instance, the consideration of several scenarios of future bathymetric changes due to sea level rise could be envisioned.

6.5. Hazard reduction from ESS as a function of restoration scale.

The aim of this study is to assess coastal flood and erosion hazards for the Arcachon Bay, considering potential restoration scenarios, for present climatic conditions.

6.5.1.Definition of restoration scenarios

In this study, two restoration scenarios (S0 and S1) are considered. Two additional scenarios (S2 and S3) are envisioned but the delimitation of potential restored vegetation extent is still a work in progress (WP1). S0 corresponds to the present state of vegetation, considering that restoration actions will maintain the actual extent. S1 corresponds to the pre-regression state, defined from observations made in 1989. S2 and S3 correspond to two strategies of deployment of Roselière devices within the Arcachon Bay. This device aims at reducing flow velocities, recreating favorable hydro-sedimentary conditions for the spontaneous recovery of vegetated areas. The first considered deployment consists of settling Roseliere devices along the secondary channels, around the intertidal areas, limiting strong currents that could possibly affect vegetated areas. The second deployment consists of iterated actions: place Roseliere near vegetated areas, wait for a natural recolonization of vegetation towards Roseliere devices, move the devices further away from re-vegetated areas and then start a new iteration. The second one will certainly need more maintenance and tracking than the first one. Figure 6.5.1 shows the normalized cover for scenarios S0 and S1.

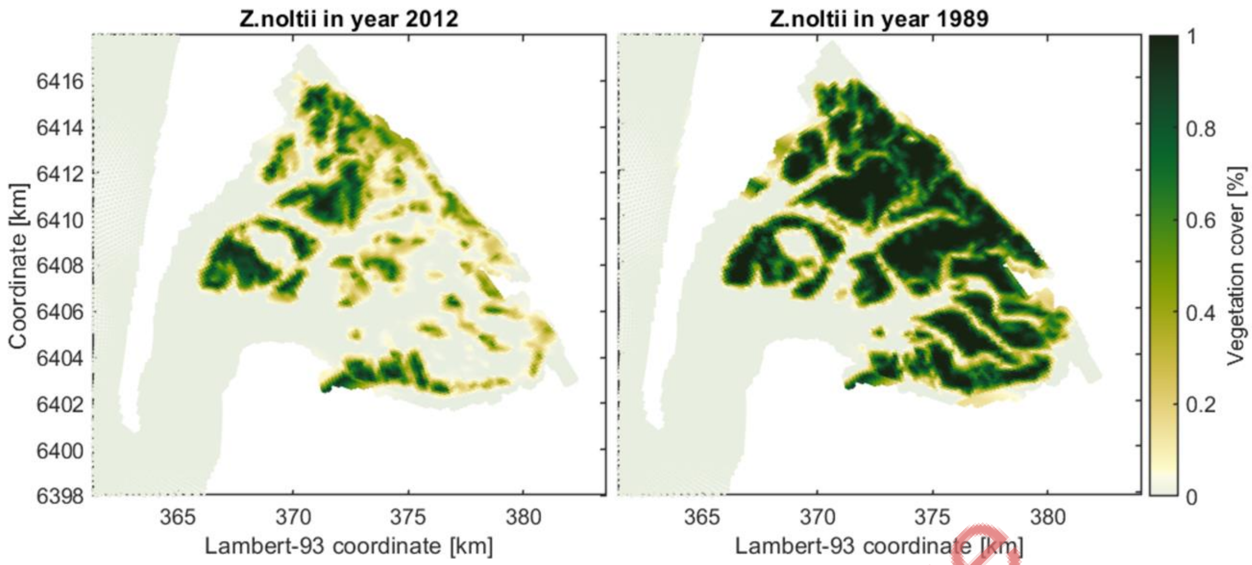

Figure 6.5.1: Map of vegetation cover for present state scenario (S0, left) and pre-regression state scenario (S1, right).

6.5.2. Coastal flooding hazards

The coastal flooding hazard refers to the coastal inundation extent in areas bordering the Arcachon Bay with impacts on population and infrastructures. To assess this hazard, the model outputs targeted are the water levels reaching the coastal areas inside the Bay and the corresponding current velocity components.

In order to define different flooding scenarios, a statistical analysis of environmental forcings is carried out. The water levels inside the Arcachon Bay are influenced by tidal processes, waves, and meteorological components such as atmospheric pressure during storm events. Inside the Bay, prevailing waves are wind-induced waves (Parisot et al. 2008). Then, the definition of flooding scenarios has been led by the analysis of wind forcings, more than offshore waves. Figure 6.5.2 shows the results from statistical analysis on wind data coming from Météo-France observations in Cap Ferret meteorological station. An extreme values analysis has been followed, determining extreme values using block maxima on 1-year window. On the right panel, wind speed values can be linked with return period. The theorical Gumbel distribution is correctly fitting extreme values selected.

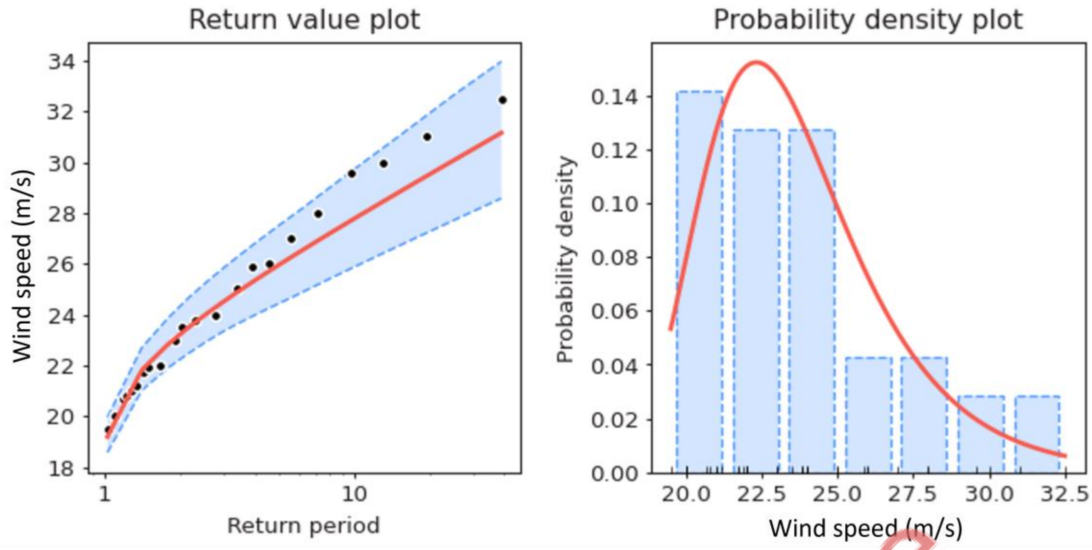

Figure 6.5.2: Return value plot (left) and probability density plot (right) for wind velocity extreme values (m.s-1), determined by block maxima method on one year window. Météo-France observations in Cap Ferret station over 1985-2022 period are used.

The same approach was followed for water levels measured by SHOM (Service Hydrographique et Océanographique de la Marine) at the Eyrac station, located in the Arcachon habor. The Gumbel distribution is also used for assessing return values (Figure 6.5.3; location = 2.46 and scale = 0.14).

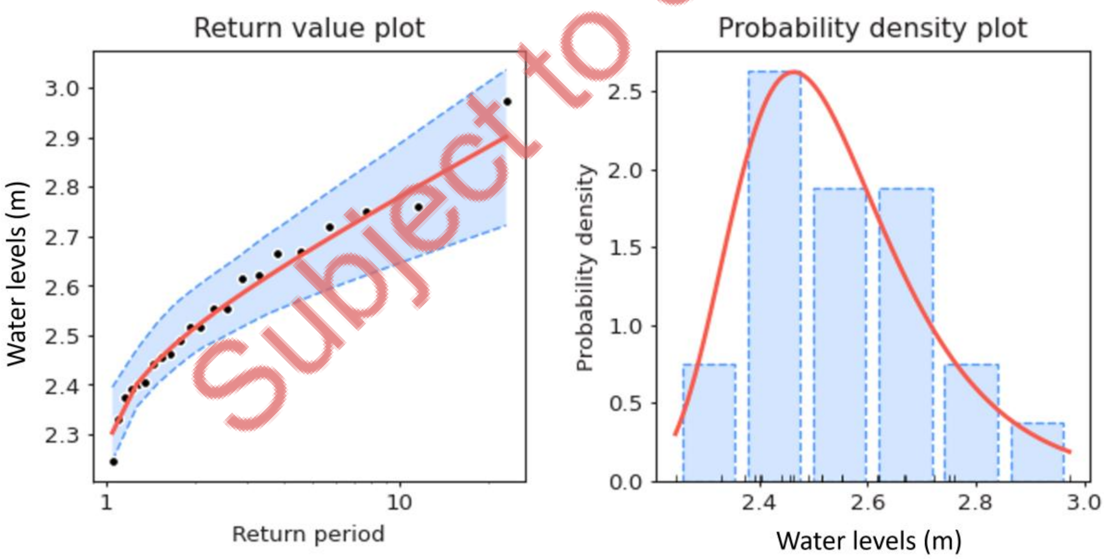

Figure 6.5.3: Return value plot (left) and probability density plot (right) for water levels extreme values (m.s-1), determined by block maxima method on one year window. SHOM observations in Eyrac station over 2001-2023 period are used.

The univariate statistical analysis is a first step in defining conditions for flooding scenarios. A multi-variate analysis is needed to take into account the possibility of having concomitant events of extreme water levels (1 value) and extreme winds (speed and direction, 2 values). Following the JOIN-SEA approach, Mugica et al. (2014) assessed 100-year return period of concomitant events for the Arcachon Bay. The same approach is followed here and the results are presented in Table 6.5.1. Directions of wind follow the results of Mugica et al. (2014) and are considered as the most unfavorable in terms of coastal flooding.

Table 6.5.1: Definition of flooding events for different return periods, based on joint analysis of water levels and wind characteristics.

Return period (year)	Water level (m MSL)	Wind speed (m.s-1)	Wind direction (°N)
1	1.92	10.6	[270°, 215°]
5	2.18	12.4	[270°, 215°]
10	2.42	16.6	[270°, 215°]
100	2.65	22.6	[270°, 215°]

6.6. Conclusions

A D-FM coupled wave-hydro-morpho-eco model is developed for the Arcachon Bay. It includes the effect of the vegetation on wave propagation, hydrodynamics, and morphodynamics. Using in-situ observations available within the Bay over the 2015-2016 period, the coupled model is calibrated and validated, leading to an optimized parameterization of the vegetation module, based on a sensitivity analysis of key parameter settings. Furthermore, the development and implementation of the sediment transport and morphodynamics module offer good perspectives for application under current and climatic forcing for testing various seagrass restoration scenarios. Consolidated modelling results will be presented in the following deliverable.

7. Integrated conclusions

This section presents the integrated conclusions for modelling supported risk reduction, focusing on multi-hazard assessments. These conclusions, supported by modelling from the inital set of Pilots with more mature simulation tools, will be the basis to entend the modelling approach to other Pilots. Therefore, Pilots at earlier stages in risk assessments, not reported here, are following these advances to support their work in developing adaptation pathways and governance transformation supported by these tools.

Contribution of the Ebro Delta Pilot

The partners are validating a 2-D river solid transport model to analyse sediment fluxes in the Ebro river and the benefits and tradeoffs of controlled floods to overcome barriers that currently prevent implementing large scale projects to by-pass sediments in the Ebro reservoirs. The results include, as presented in the Coastal Sediments 2023 conference, an assessment of the potential sediment carrying-capacity under different hydrological regimes. The model validation is based on permanent river networks (SAIH discharge and level measurements) and an intensive campaign during the controlled flood in the Ebro river in May 2022 (turbidity and velocities). These controlled floods have been stopped last fall and spring due to the present drought crisis in Spain.

River discharges are combined with coastal hydro-morpho models, initially validated with field data from the Gloria storm in January 2020 (largest registered event).

The suite of nested codes achieved a reduction of RMSE compared to previous experiences (e.g. down to 0.3 m for significant wave height at the peak of the storm). The modelling strategy, for an easy evolution towards an operational EWS, downscales from CMEMS to COAWST, nd from COAWSTto XBeach, using the MPI modules of the models to reduce the computational expense and the post-processing using Python/Matlab. The models are now being used for validation under storm events based on Satellite, LiDAR and ortophotos provided by ICGC, covering extreme events from 2020 till 2023 that include the Gloria storm. The 2023 storms are used to assess the performance of the implemented NbS under energetic conditions, by simulating coastal erosion/flooding with/without the NbS.

Contribution of the Wadden Sea Pilot

The partners are simulating sediment transport and morphological changes under different sea level conditions (up to 1.5 m), using the Delft 3D model to project the behaviour of the Ems-Dollard estuary under future scenarios. These simulations are being used to assess the enhancement of hydrodynamics (i.e., water level, current and wave height), sediment transport (i.e., focussed ESS herein) and morphodynamics due to the increase of SLR and considering the sediment supply from the North Sea, coastal islands and ebb-tidal delta. Predicted flood velocities increase with SLR, with higher intensities from deep to shallow areas in the basin. Wave heights increase with SLR, more significantly in the shallow parts of the basin. Sediment transport is enhanced by SLR, and areas close to the mainland are subject to sedimentation. The work also addressed residual flows together with sediment sources and sinks, considering sediment transport for different sediment fractions, which required the implementation of new functionalities in Delft3D (allowing the user to decide whether individual sediment fractions are computed in morphostatic or morphodynamic mode).

The analysis of NbS based on coastal vegetation has required a specific validation of the coupled hydro-morphodynamics in the German Bight, parameterizing seagrass effects (vegetation module within the SCHISM modelling framework) based on observations and incorporating the Weser River and Jade Bay.

Erosion and flooding risk reduction is being investigated by comparing simulations with present-day seagrass coverage (from observations) against a scenario without seagrass and three additional expansion scenarios for coastal seagrass restoration. The simulations are applying the same downscaled climate scenarios agreed upon in REST-COAST, and selected extreme events from the recent past, such as the October 2017 storm, including Xbeach in the modelling suite for exploring seagrass as a nature-based storm buffer to mitigate beach erosion. Preliminary results show that expanded seagrass areas can effectively reduce currents and waves (reduction of more than 30%). To optimise the location and size of seagrass meadows it is necessary to consider local hydrodynamics, meadow size, stem height and plant density, using baroclinic 3D simulations of the southern North Sea and Pilot estuaries to account for realistic internal variability under future sea level rise scenarios. The performed simulations derived the bandwidth of sea level variability due to sea level change and internal variability, providing unprecedented data for estuarine management and city planners.

Contribution of the Venice Lagoon Pilot

The partners have designed the best set-up for the modelling suite, using unstructured-grid variable-resolution circulation (SHYFEM) and wave (WW3) models that have been implemented for the area of Venice Lagoon, including high-resolution bathymetric and topographic Lidar datasets merged with EMODNET bathymetry. Regarding CMEMS downscaling, a number of sensitivity experiments on the location of boundary conditions have been performed, based on improved descriptions of coastline, marshland and channels in the Pilot. The models have now been advanced to include NbS, in particular the effects of vegetation (seagrass meadows) and marshes ('barene') in the attenuation of circulation and wave hydrodynamics.

The hydro-morpho-eco modelling with interactions is supporting the design of observation campaigns to assess restoration performance based on an improved validation of coupled models and the interactions stemming from vegetation and distributed marshes and channels, including the type and density of margins. The target is a comprehensive assessment of erosion and flooding risks under future climate scenarios and for different types of management of the MOSE barriers.

Contribution of the Rhone Delta Pilot

The partners'work has supposed the hydrodynamic validation of an improved coupled hydro-morpho model (X-Beach + Tomawac + TELEMAC-2D) that now includes capabilities to simulate the overwash and breaching potentials to define innovative criteria for water management that favour restoration. The reduction of erosion risks was addressed with a statistical analysis of historical storms, combining observations with simulations to estimate the potential for overwash at this site, creating new beach areas, as well as the potential for the creation of new connections of the southern part of the Pilot with the sea to assess the role of enhanced connectivity.

The ESS related to water quality purification through hydro-saline regulation are being addressed with the same modelling tools plus additional data for coastal lagoons with beaches, halophilous scrubs and Salicornia and other annuals colonising mud and sand. Thanks to the airborne LIDAR topo-bathymetric measurement campaign carried out in October 2022 within REST-COAST, the partners were able to update the topo-bathymetry of the hydro-saline model (TELEMAC-2D) for the main coastal wetlands of the Rhone delta, specially the area around the Pilot Site targeted for the larger scale restoration (“Vaccarès Lagoon System”). The new model suite and settings therefore take into account the geomorphological evolution of the site since the choice of not maintaining the historical protection dykes based on XBeach simulations.

To estimate the differences in flooding and hydro-saline dynamics induced by the non-maintenance of historical dykes, a mesh for the TELEMAC-2D model with the historical dykes was also created (scenario with dike maintenance). For each habitat type considered for restoration, hydro-saline conditions were simulated for the various management options. The work on the food provisioning ESS (fish) was initiated by talks with those monitoring and collecting historical data on fish dynamics at the Pilot, to identify the ranges of hydro-saline conditions to be targeted to favour the presence of the different fish species considered in the restoration strategies, conditions that can be then simulated with the prepared modelling suite.

Contribution of the Arcachon Bay Pilot

The partners’work here deals with risk reduction and recovery potential associated to seagrass beds conveniently parameterized in the modelling suites that combine the flexible mesh DElft 3D with Dwaves (SWAN + Dflow) for the hydrodynamics. The main ESS targeted in the restoration analysis are the reduction of coastal flooding and coastal erosion risks, considering also the improvement of water quality, carbon sequestration and food production.

Coastal flooding and erosion hazards directly affect food provisioning activities and tourism that are a main source of revenue for the cities around the Arcachon bay. Reduction of hydrodynamics by seagrass is now implemented in the coupled modelling suite, separating the effect of vegetation on flow resistance by a specific trachytopes formulation, where a quadratic term is included in the momentum equation to parametrically represent the flow resistance by vegetation. This avoids that the increase of the bed roughness leads to higher bed shear stress and larger sediment transport rates, which is opposite to the expected morphological behaviour.

Using in situ observations of water levels, wave parameters and sediment parameters, the hydro-morphodynamics have been validated for present conditions. The sampling sites are located within the Arcachon bay and further data will lead to additional improvements in the modelling suite, being considered in close cooperation with the Wadden Sea Pilot team and their sediment dynamics application on the Ems Dollard estuary.

References

Anderson, R.S. (2002). Modeling the tor-dotted crests, bedrock edges, and parabolic profiles of high alpine surfaces of the Wind River Range, Wyoming. Geomorphology, 46, 35–58.

Ardhuin, F., Accensi, M., Roland, A., Girard, F., Filipot, J. F., Leckler, F., & Le Roux, J. F. (2014). Numerical wave modeling in PREVIMER: multi-scale and multi-parameter demonstrations. Editorial–Apr 2014–The Pre-operational PREVIMER system, 2017.

Ardhuin, F., O'Reilly, W.C., Herbers, T.H.C., Jessen, P.F., 2003. Swell transformation across the continental shelf. Part I: attenuation and directional broadening. J. Phys. Oceanogr. 33 (9), 1921–1939.

Ardhuin, F.; Rogers, E.; Babanin, A.V.; Filipot, J.F.; Magne, R.; Roland, A.; Collard, F. Semiempirical dissipation source functions for ocean waves. Part I: Definition, calibration, and validation. J. Phys. Oceanogr. 2010, 40, 1917–1941.

Ballé-Béganton, J., J. Herry, M. Philippe, R. Pasco, B. Angst, M. Urien, D. Bailly, M. Cassé. Les services écosystémiques en soutien à la gestion des herbiers de zostères du golfe du Morbihan, Projet Interreg IVA Manche VALMER, 14p, 2015.

Baptist, M.J., van der Wal, J.T., Folmer, E.O., Gräwe, U., Elschot, K., 2019. An ecotope map of the trilateral Wadden Sea, Journal of Sea Research 152, 101761.

Battjes, J.A., Janssen, J.P.F.M., 1978. Energy loss and set-up due to breaking of random waves. Proc. 16th Int. Conf. Coastal Eng. ASCE, pp. 569–587.

Baptist, M. J. Modelling floodplain biogeomorphology. 2005.

Bellafiore, D., Umgiesser, G., 2010. Hydrodynamic coastal processes in the north Adriatic investigated with a 3D finite element model, Ocean Dynam., 60, 255–273.

Beudin, A., Kalra, T. S., Ganju, N. K., & Warner, J. C. Development of a coupled wave-flow-vegetation interaction model. Computers & Geosciences, 100, pp. 76-8, 2017.

Bidlot, J, S Abdalla, and PAEM Janssen (2005). A revised formulation for ocean wave dissipation in CY25R1. In: Internal Memorandum Research Department

Bidlot, JR (2008). Intercomparison of operational wave forecasting systems against buoys: Data from ECMWF, MetO

Bladé, E.; Cea, L.; Corestein, G.; Escolano, E.; Puertas, J.; Vázquez-Cendón, E.; Dolz, J.; Coll, A. (2014). Iber: Herramienta de simulación numérica del flujo en ríos. Rev. Int. Métodos Numér. Cálc. Diseño Ing., 30, 1–10.

Bouchet, J.-M., J.-P. Deltreil, F. Manaud, D. Maurer, and G. Trut. Etude intégrée du bassin d’arcachon. 1997. L.C. Braat, de Groot, R. The ecosystem services agenda: bridging the worlds of natural science and economics conservation and development, and public and private policy. Ecosyst. Serv. 1, 4–15, 2012.

Burchard, H., Bolding, K., Villarreal, M.R., 1999. GOTM—a general ocean turbulence model. Theory, applications and test cases. Technical Report EUR 18745 EN, European Commission.

Carniello L., Defina, A., & D'Alpaos, L. (2009). Morphological evolution of the Venice lagoon: Evidence from the past and trend for the future. *Journal of Geophysical Research: Earth Surface*, *114*(F4), 4002. https://doi.org/10.1029/2008JF001157

Cavazzoni, S. 1973. Acque dolci in laguna di Venezia. Rapporto No. 64. Laboratorio per lo Studio della Dinamica delle Grandi Masse, Venezia.

Cayocca, F Modélisation morphodynamique d'une embouchure tidale: Application aux passes d'entrée du Bassin d'Arcachon. PhD thesis, Bordeaux 1, 1996.

Cea, L.; Puertas, J.; Vázquez-Cendón, M.E. (2007). Depth Averaged Modelling of Turbulent Shallow Water Flow with Wet-Dry Fronts. Arch. Comput. Methods Eng., 14, 303–341.

Chalikov, D. V., and M. Y. Belevich (1993), One-dimensional theory of the wave boundary layer, Bound. Layer Meteor., 63, 65–96.

Cognat, M. Rôles des facteurs environnementaux et des interactions biomorphodynamiques sur l'évolution spatio-temporelle des herbiers de zostères dans une lagune mésotidale. PhD thesis, Université de Bordeaux, 2019.

Convention on Biological Diversity. COP Decision X/2, 2010.

Costanza, R., Kubiszewski, I. The authorship structure of ecosystem services as a transdisciplinary field of scholarship. Ecosyst. Serv. 1, 16–25, 2012.

Cressman, G.P., 1959. An operational objective analysis scheme, Mon. Weather Rev., 87, 367–374.

Dalrymple, R.A., Kirby, J.T., Hwang, P.A., 1984. Wave diffraction due to areas of energy dis- sipation. ASCEJ. Waterw. Port Coast. Ocean Eng. 110 (1), 67–79.

Den Hartog, C. 1977. Structure, function and classification in seagrass communities. In: (C.P. McRoy and C. Helfferich, eds) Marine Science Volume 4: Seagrass Ecosystems, A Scientific Perspective. Marcel Dekker, Inc., New York, U.S.A. pp. 89-122.

Dissanayake, P., & Wurpts, A. (2013). Modelling an anthropogenic effect of a tidal basin evolution applying tidal and wave boundary forcings: Ley Bay, East Frisian Wadden Sea. *Coastal engineering*, *82*, 9-24.

Dobricic, S., Pinardi, N., 2008. An oceanographic three-dimensional variational data assimilation scheme, Ocean Model., 22, 89–105.

Donatelli, C., Ganju, N.K., Kalra, T.S., Fagherazzi, S., Leonardi, N., 2019. Changes in hydrody- namics and wave energy as a result of seagrass decline along the shoreline of a microtidal back-barrier estuary. Adv. Water Resour. 128, 183–192.

Egoh, B., Drakou, E.G., Dunbar, M.B., Maes, J., Willemen, L. Indicators for Mapping Ecosystem Services: A Review. Publications Office of the European Union, Luxembourg. 2012.

Eldeberky, Y. (1996), Nonlinear transformations of wave spectra in the nearshore zone, Ph.D. thesis, Delft University of Technology, Delft, The Netherlands, 203 pp.

Escudier, R., Clementi, E., Cipollone, A., Pistoia, J., Drudi, M., Grandi, A., Lyubartsev, V., Lecci, R., Aydogdu, A., Delrosso, D., Omar, M., Masina, S., Coppini G., Pinardi, N. (2021). A High Resolution Reanalysis for the Mediterranean Sea. Frontiers in Earth Science, 9, 1060,

Ferrarin, C., Roland, A., Bajo, M., Umgiesser, G., Cucco, A., Davolio, S., Buzzi, A., Malguzzi, P., Drofa, O., 2013. Tide-surge-wave modelling and forecasting in the Mediterranean Sea with focus on the Italian coast, Ocean Model., 61, 38–48.

Ferrarin C, Maicu F, Umgiesser G., 2017. The effect of lagoons on Adriatic Sea tidal dynamics. Ocean Model., 119:57–71.

Fonseca, M.S., Fisher, J.S., 1986. A comparison of canopy friction and seagrass movement be- tween four species of seagrass with reference to their ecological restoration. Mar. Ecol. 29, 15–22.

Ganthy, F. Rôle des herbiers de zostères (Zostera noltii) sur la dynamique sédimentaire du Bassin d'Arcachon. PhD thesis, Universté de Bordeaux 1, 2011.

Gómez Martín, E., Costa, M.M., Egerer, S., Schneider, U.W., 2021. Assessing the long-term ef- fectiveness of nature-based solutions under different climate change scenarios. Sci. Total Environ. 794, 148515.

Gorria, H. (1877). Desecación de las marismas y terrenos pantanosos denominados de Los Alfaques. Techical Report. Ministerio de Agricultura, Madrid, España.

Günther, H., Hasselmann, S., & Janssen, P. A. E. M. (1992). The WAM model Cycle 4 (revised version). Klim. Rechenzentrum. Techn. Rep, (4), 23-40.

Hanley, M.E., Bouma, T.J., Mossman, H.L., 2020. The gathering storm: optimizing management of coastal ecosystems in the face of a climate-driven threat. Ann. Bot. 125 (2), 197–212.

Hasselmann, D.; Bösenberg, J.; Dunckel, M.; Richter, K.; Grünewald, M.; Carlson, C. Measurements of wave-induced pressure over surface gravity waves. In Wave Dynamics and Radio Probing of the Ocean Surface; Springer: Boston, MA, USA, 1986; pp. 353–368.

Hasselmann, S.; Hasselmann, K.; Allender, J.K.; Barnett, T.P. Computations and parameterizations of the nonlinear energy transfer in a gravity-wave specturm. Part II: Parameterizations of the nonlinear energy transfer for application in wave models. J. Phys. Oceanogr. 1985, 15, 1378–1391.

Hellermann, S., Rosenstein, M., 1983. Normal wind stress over the world ocean with error estimates, J. Phys. Oceanogr., 13, 1093–1104.

Ibàñez, C., Prat, N., Canicio, A. (1996). Changes in the hydrology and sediment transport produced by large dams on the lower Ebro river and its estuary. Regulated Rivers: Research & Management, 12(1), 51-62.

IPBES. Global assessment report on biodiversity and ecosystem services of the Intergovernmental Science-Policy Platform on Biodiversity and Ecosystem Services (Version 1). 2019.

James, C. S., A. L. Birkhead, A. A. Jordanova & J. J. O'Sullivan. Flow resistance of emergent vegetation, Journal of Hydraulic Research, 42:4, 390-398, 2004.

Janssen, P. A. E. M. (1991), Quasi-linear theory of of wind wave generation applied to wave forecasting, J. Phys. Oceanogr., 21, 1,631–1,642.

Kambiadou, K., Ganthy F., Verney R., Plus M., Sottolichio A. Modelling the effects of Zostera noltei meadows on sediment dynamics: application to the Arcachon lagoon. Ocean Dynamics 64, pp. 1499-1516, 2014.

Kara, B. A., Wallcraft, A. J., Hurlburt, H. E., 2007. A Correction for Land Contamination of Atmospheric Variables near Land–Sea Boundaries, *J. Phys. Oceanogr.*, 37, 803–818.

Koch, E.W., Gust, G., 1999. Water flow in tide and wave dominated beds of the seagrass Thalassia testudinum. Mar. Ecol. Prog. Ser. 184, 63–72.

Korres, G., Ravdas, M., Zacharioudaki, A., Denaxa, D., & Sotiropoulou, M. (2021). Mediterranean Sea Waves Analysis and Forecast (CMEMS MED-Waves, MedWAM3 system) (Version 1) set. Copernicus Monitoring Environment Marine Service (CMEMS). https://doi.org/10.25423/CMCC/MEDSEA_ANALYSISFORECAST_WAV_006_017_MEDWAM3

Kumar, P., Debele, S.E., Sahani, J., Aragão, L., Barisani, F., Basu, B., Bucchignani, E., et al., 2020. Towards an operationalisation of nature-based solutions for natural hazards. Sci. Total Environ. 731, 138855.

La Notte, A., D'Amato D., Mäkinen H., Paracchini M.L., Liquete C., Egoh B., Geneletti D., Crossman N.D. Ecosystem services classification: A systems ecology perspective of the cascade framework. Ecological indicators 74, pp. 392-402, 2017.

Lazure, P., Jegou, A.-M. 3D modelling of seasonal evolution of Loire and Gironde plumes on Biscay Bay continental shelf. Oceanologica Acta 21, 165–177, 1998.

Lazure, P. and Dumas, F. An external-internal mode coupling for a 3D hydrodynamical model for application at regional scale (MARS). Advances in Water Ressources, 31: 233-250, 2008.

Lobeto, H., Menendez, M., Losada, I.J., 2021. Future behavior of wind wave extremes due to climate change. Sci. Rep. 11, 7869.

Longuet-Higgins, M., and R. Stewart (1964), Radiation stresses in water waves; a physical discussion, with applications, Deep Sea Res. Oceanogr. Abstr., 11, 529–562

MA. Millennium Ecosystem Assessment. World Resources Institute, Washington, DC, 2005.

Maes, J., Teller, A., Erhard, M., Murphy, P., Paracchini, M., Barredo, J., Grizzetti, B., Cardoso, A., Somma, F., Petersen, J. Mapping and Assessment of Ecosystems and Their Services—Indicators for Ecosystem Assessments Under Action 5 of the EU Biodiversity Strategy to 2020. European Commission, ISBN, pp. 978–992, 2014.

Mazzella, L., Guidetti, P., Lorenti, M., Buja, M.C., Zupo, V., Scipione, M.B., Rismondo, A., Curiel, D., 1998. Biomass partioning in Adriatic Seagrass ecosystems (Posidonia Oceanica, Cymodoces Nodosa, Zostera Marina). Rapp. Comm. Int. Mer Medit. 35, 562–563.

McKenzie, L.J., Nordlund, L.M., Jones, B.L., Cullen-Unsworth, L.C., Roelfsema, C., Unsworth, R.K.F., 2020. The global distribution of seagrass meadows. Environ. Res. Lett. 15, 074041.

Méndez, F.J., Losada, I.J., 2004. An empirical model to estimate the propagation of random breaking and nonbreaking waves over vegetation fields. Coast. Eng. 51, 103–118.

Mudd, S.M.; Furbish, D.J. (2004). Influence of chemical denudation on hillslope morphology. J. Geophys. Res. Earth Surf., 109.

Mugica, J., Bulteau T., Paris F. et Pedreros R., avec la collaboration de Delvallee E. Caractérisation de l'aléa submersion marine dans le cadre des PPRL du Bassin d'Arcachon (Gironde), Détermination de l'évènement naturel de référence. Rapport intermédiaire BRGM/RP-61408-FR, 73 p., 2014.

Munaretto, S., & Huitema, D. (2012). Adaptive comanagement in the Venice lagoon? An analysis of current water and environmental management practices and prospects for change. *Ecology and Society*, *17*(2). https://doi.org/10.5751/ES-04772-170219

Mütterlein, S., Ganthy F., Sottolichio A. Effect of small seagrass Zostera noltei on tidal asymmetry in a semi-enclosed shallow lagoon: the Arcachon Bay (SW France). International Coastal Symposium, 6-11 March 2016.

Nesshöver, C., Assmuth, T., Irvine, K.N., Rusch, G.M., Waylen, K.A., Delbaere, B., et al., 2017. The science, policy and practice of nature-based solutions: an interdisciplinary perspective. Sci. Total Environ. 579, 1215–1227.

Paola, C.; Voller, V.R. (2005). A generalized Exner equation for sediment mass balance. J. Geophys. Res. Earth Surf., 110

Parisot,J.-P., J. Diet-Davancens, A. Sottolichio, E. Crosland, C. Drillon, and R. Verney. Modélisation des agitations dans le bassin d'arcachon. Xèmes Journées Sophia Antip, pages 435–444, 2008.

Paul, M., Amos, C.L., 2011. Spatial and seasonal variation in wave attenuation over Zostera noltii. J. Geophys. Res. 116, C08019.

Pettenuzzo, D., Large, W. G., and Pinardi, N., 2010. On the corrections of ERA40 surface flux products consistent with the Mediterranean heat and water budgets and the connection between basin surface total heat flux and NAO, J. Geophys. Res., 115, C06022

Pirazzoli, P. 1974. Dati storici sul medio mare a Venezia. Atti Acc. Sci. Istituto Bologna 13(1): 125-148.

Plus, M., D. Maurer, J.-Y. Stanisiere, and F. Dumas. Caractérisation des composantes hydrodynamiques d'une lagune mésotidale, le bassin d'arcachon. 2006.

Potschin, M., Haines-Young, R., 2016. Defining and measuring ecosystem services. In: Potschin, M., Haines-Young, R., Fish, R., Turner, R.K. (Eds.), Routledge Handbook of Ecosystem Services. Routledge, Taylor & Francis Group, London; New York, p. 2016.

Pranavam Ayyappan Pillai, U., Pinardi, N., Federico, I., Causio, S., Trotta, F., Unguendoli, S., & Valentini, A. (2022). Wind-wave characteristics and extremes along the Emilia-Romagna coast. Natural Hazards and Earth System Sciences, 22(10), 3413-3433.

Proveditorato for the Public Works of Veneto, Trentino Alto Adige and Friuli Venezia Giulia, n.d. Progetto Venezia2021.

Puillat, I., Lazure, P., Jégou, A.-M., Lampert, L., Miller, P. Mesoscale hydrological variability induced by north-westerly wind on the French continental shelf of the Bay of Biscay. Scientia Marina 70S1, 15–26, 2006.

Roelvink, J.A. Coastal morphodynamic evolution techniques. Coastal Engineering, 53(2), 277–287, 2006.
C. Rhodes. National ecosystem services classification system. 2015.

Roland, A., Zhang, Y. J., Wang, H. V., Meng, Y., Teng, Y. C., Maderich, V., ... & Zanke, U. (2012). A fully coupled 3D wave-current interaction model on unstructured grids. *Journal of Geophysical Research: Oceans*, *117*(C11).

Santillán, D., Cueto-Felgueroso, L., Sordo-Ward, A., Garrote, L. (2020). Influence of Erodible Beds on Shallow Water Hydrodynamics during Flood Events. Water, 12(12), 3340.

Secretariat, C. W. S. (2008). Nomination of the Dutch-German Wadden Sea as world heritage site. *Wadden Sea Ecosystem*, *24*, 200.

Seppelt, R., Dormann, C.F., Eppink, F.V., Lautenbach, S., Schmidt, S. A quantitative review of ecosystem service studies: approaches, shortcomings and the road ahead. J. Appl. Ecol. 48, 630–636, 2011.

Sfriso, A., C. Facca and M. Tibaldo. 2005. Macrophyte biomass updating in the lagoon of Venice. In: Lagoons and Coastal Wetlands in the Global Change Context: Impacts and Management Issues. IOC Integrated Coastal Area Management (ICAM), Dossier N° 3. UNESCO. Cap. 29, pp. 224-231.

Sfriso, A., C. Facca and S. Ceoldo. 2004. Growth and production of Cymodocea nodosa (Ucria) Ascherson in the Venice Lagoon. In: (P. Campostrini, ed.) Scientific Research and Safeguarding of Venice. CoRiLa. Research Programme 2001-2003. 2002 Results. Multigraf, Spinea. Vol II. pp. 229-236.

Shields, A. (1936) Anwendung Der Aehnlichkeitsmechanik Und Der Turbulenzforschung Auf Die Geschiebebewegung. Ph.D. Thesis, Technical University Berlin, Berlin, Germany.

Soulsby, R.L., Whitehouse, R.J.S. (1997). Threshold of sediment motion in coastal environments. In Pacific Coasts and Ports' 97: Proceedings of the 13th Australasian Coastal and Ocean Engineering Conference and the 6th Australasian Port and Harbour Conference; Volume 1 (pp. 145-150). Christchurch, NZ: Centre for Advanced Engineering, University of Canterbury.

Stanev, E. V., Jacob, B., & Pein, J. (2019). German Bight estuaries: An inter-comparison on the basis of numerical modeling. *Continental Shelf Research*, *174*, 48-65.

Stankovic, M., Ambo-Rappe, R., Carly, F., Dangan-Galon, F., Fortes, M.D., et al., 2021. Quan- tification of blue carbon in seagrass ecosystems of Southeast Asia and their potential for climate change mitigation. Sci. Total Environ. 783, 146858.

Suzuki, T., Zijlema, M., Burger, B., Meijer, M. C., & Narayan, S. Wave dissipation by vegetation with layer schematization in SWAN. Coastal Engineering, 59(1), 64-71, 2012.

Tagliapietra, D., Baldan, D., Barausse, A., Buosi, A., Curiel, D., Guarneri, I., Pessa, G., Rismondo, A., Sfriso, A., Smania, D., & Volpi Ghirardini, A. (2018). *Protecting and restoring the salt marshes and seagrasses in the lagoon of Venice*. http://journal.um-surabaya.ac.id/index.php/JKM/article/view/2203

Tolman, H.; Accensi, M.; Alves, J.H.; Ardhuin, F.; Bidlot, J.; Booij, N.; Bennis, A.C.; Campbell, T.; Chalikov, D.; Chawla, A. Usermanual and System Documentation of WAVEWATCH III R Version; NOAA/NWS/NCEP/MMAB: Baltimore, MD, USA, 2019; 465p.

Tommasini, L., Carniello, L., Ghinassi, M., Roner, M., & D'Alpaos, A. (2019). Changes in the wind-wave field and related salt-marsh lateral erosion: inferences from the evolution of the Venice Lagoon in the last four centuries. *Earth Surface Processes and Landforms*, *44*(8), 1633–1646. https://doi.org/10.1002/esp.4599

Van Ledden, M.. Sand-mud segregation in estuaries and tidal basins. University of Technology Sydney, 2003.

Van Ledden, M., Wang, Z. B., Winterwerp, H., & Vriend, H. D. (2004). Sand–mud morphodynamics in a short tidal basin. *Ocean Dynamics*, *54*, 385-391.

Van Leer, B. (1979). Towards the Ultimate Conservative Difference Scheme, V. A Second Order Sequel to Godunov's Method. J. Comput. Phys., 32, 101–136.

Van Rijn, L.C. (1984a). Sediment Transport, Part I: Bed Load Transport. J. Hydraul. Eng., 110, 1431–1456

Van Rijn, L.C. (1984b). Sediment Transport, Part II: Suspended Load Transport. J. Hydraul. Eng., 110, 1613–1641

Van Rijn, L.C. (1987). Mathematical modelling of morphological processes in the case of suspended sediment transport. Delft: Delft Hydraulics Communications #382.

Van Rijn, L. C., Nieuwjaar, M. W., van der Kaay, T., Nap, E., & van Kampen, A. Transport of fine sands by currents and waves. Journal of waterway, port, coastal, and ocean engineering, 119(2), 123-143, 1993.

Vanoni, V. A., Brooks, N. H. (1987). Laboratory Studies of the Roughness and Suspended Load of Alluvial Streams, Sedimentation Laboratory, California Institute of Technology, Report E-68, Pasadena, CA, USA.

Warner, J. C., Sherwood, C. R., Signell, R. P., Harris, C. K., & Arango, H. G. (2008). Development of a three-dimensional, regional, coupled wave, current, and sediment-transport model. *Computers & geosciences*, *34*(10), 1284-1306.

Waycott, M., Duarte, C.M., Curruthers, T.J.B., Orth, R.J., Dennsion, W.C., Olyarnik, S., Callandine, A., Fourqurean, J.W., Heck Jr., K.L., Hughes, A.R., Kendrick, G.A., Kenworthy, W.J., Short, F.T., Williams, S.L., 2009. Accelerating loss of seagrass across the globe threatens coastal ecosystems. Proc. Natl. Acad. Sci. 106 (30), 12377–12381.

Umgiesser, G., Canu, D. M., Cucco, A., Solidoro, C., 2004. A finite element model for the Venice lagoon: Development, set up, calibration and validation, J. Marine Syst., 51, 123–145.

Yamaguchi, M. (1984). Approximate expressions for integral properties of the JONSWAP spectrum. Doboku Gakkai Ronbunshu, 1984(345), 149-152.

Zhang, Y. J., Gerdts, N., Ateljevich, E., & Nam, K. (2020). Simulating vegetation effects on flows in 3D using an unstructured grid model: model development and validation. *Ocean Dynamics*, *70*, 213-230.

Zhang, Y., Nepf, H., 2019. Wave-driven sediment resuspension within a model eelgrass meadow. J. Geophys. Res. Earth Surf. 124 (4), 1035–1053.

Zhang, Y. J., Ye, F., Stanev, E. V., & Grashorn, S. (2016). Seamless cross-scale modeling with SCHISM. *Ocean Modelling*, *102*, 64-81.

Zuliani, A., L. Zaggia, F. Collavini and R. Zonta 2005. Freshwater discharge from the drainage basin to the Venice Lagoon (Italy). Environ. Int. 31: 929-938.